



A University of Sussex PhD thesis

Available online via Sussex Research Online:

<http://sro.sussex.ac.uk/>

This thesis is protected by copyright which belongs to the author.

This thesis cannot be reproduced or quoted extensively from without first obtaining permission in writing from the Author

The content must not be changed in any way or sold commercially in any format or medium without the formal permission of the Author

When referring to this work, full bibliographic details including the author, title, awarding institution and date of the thesis must be given

Please visit Sussex Research Online for more information and further details

**RECONSTRUCTION OF MULTIPLE
POINT SOURCES BY EMPLOYING A
MODIFIED GERCHBERG-SAXTON
ITERATIVE ALGORITHM**

By

MAITHAM, HABOOL AL-SHAMERY

*Submitted For the Degree Of
Doctor of Philosophy*

**DEPARTMENT OF ENGINEERING &
DESIGN
SCHOOL OF ENGINEERING AND
INFORMATICS
UNIVERSITY OF SUSSEX
BRIGHTON
UK**

June, 2018

DECLARATION AND STATEMENT OF ORIGINALITY
DEPARTMENT OF ENGINEERING AND DESIGN,
SCHOOL OF ENGINEERING AND INFORMATICS,
UNIVERSITY OF SUSSEX,
BRIGHTON
4th June, 2018

I hereby declare that this thesis has not been and will not be, submitted in whole or in part to another University for the award of any other degree.

It is the original work of Maitham Habool Al-Shamery with results from experiments performed in United Kingdom.

Signature:

DEDICATION

This thesis I dedicate to:

My father, who never stops giving of himself in countless ways.

My late Mother, I remember your prayers and they are with me all my life.

My Wife, you are my everything, so thankful to have you in my life.

My beloved Brother and Sisters, thank you seems hardly enough for all you have done for me, without you this work would not been achieved.

SUMMARY

Digital holograms has been developed and used in many applications. They are a technique by which a wavefront can be recorded and then reconstructed, often even in the absence of the original object. In this project, we use digital holography methods in which the original object amplitude and phase are recorded numerically, which would allow these data be downloaded to a spatial light modulator (SLM). This provides digital holography with capabilities that are not available using optical holographic methods. The digital holographically reconstructed image can be refocused to different depths depending on the reconstruction distance. This remarkable aspect of digital holography as can be useful in many applications and one of the most beneficial applications is when it is used for the biological cell studies. In this research, point source digital in-line and off-axis digital holography with a numerical reconstruction has been studied. The point source hologram can be used in many biological applications. As the original object we use the binary amplitude Fresnel zone plate which is made by rings with an alternating opaque and transparent transmittance. The in-line hologram of a spherical wave of wavelength, λ , emanating from the point source is initially employed in the project. Also, we subsequently employ an off-axis point source in which the original point-source object is translated away from original on-axis location. Firstly, we create the binary amplitude Fresnel zone plate (FZP) which is considered the hologram of the point source. We determine a phase-only digital hologram calculation technique for the single point source object. We have used a modified Gerchberg-Saxton algorithm (MGSA) instead of the non-iterative algorithm employed in classical analogue holography. The first complex amplitude distribution, $f_i(x, y)$, is the result of the Fourier transform of the point source phase combined with a random phase. This complex filed distribution is the input of the iteration process. Secondly, we propagate this light field by using the Fourier transform method. Next we apply the first constraint by modifying the amplitude distribution, that is by replacing it with the measured modulus and keeping the phase distribution unchanged. We use the root mean square error (RMSE) criterion between the reconstructed field and the target field to control the iteration process. The RMSE decreases at each iteration, giving rise to an error-reduction in the reconstructed wavefront. We then extend this method to the reconstruction of multiple points sources. Thus the overall aim of this thesis has been to create an algorithm that is able to reconstruct

the multi-point source objects from only their modulus. The method could then be used for biological microscopy applications in which it is necessary to determine the position of a fluorescing source from within a volume of biological tissue.

ACKNOWLEDGEMENTS

I am lucky enough to have been given supportive, kind, and amazing people in my life. I am grateful to people who worked with me from the beginning until the completion of this project, particularly my supervisor Dr. Rupert Young, for the guidance, encouragement and advice. I have been very lucky to have a supervisor who cared so much about my work, and who respond to my questions and queries so promptly. I also would like to extend my thanks to my supervisor Prof. Chris Chatwin for his help and support.

I also would like to express my sincere appreciation to Prof. John Loomis, University of Dayton, Ohio for your help.

I would like to take this opportunity to say warm thanks to all my colleagues in the Engineering Department, Yeovil College: Simon, Charles, Mal, Stephen, Dr. Ike Dike, Sharon Curtis and the rest who have been so supportive. Also, I'd like to thank Esther Dobbs and IT team at Yeovil college.

My sincere thanks also goes to Mr. Ali Danbos and Mr. Mohamod Danbos for their help and support.

Sincere thanks are also to all my friends particularly Marco, for your help and support.

Finally, and without hesitation, I would like to thank my family, Ektab, Rahamn, Hatam, Kadhem, Daddi, my Father and Mother in law, Auday, Hanan, Ahmed Al-Soufi, and my cousins (Ali and Wisam).

CONTENTS

DEDICATION	ii
SUMMARY	iii
ACKNOWLEDGEMENTS	v
CONTENTS	vi
LIST OF FIGURES	ix
LIST OF TABLES	xv
LIST OF ACRONYMS	xvi
LIST OF PRINCIPAL SYMBOLS	xvii
1 CHAPTER 1	1
1.1 Introduction	1
1.2 Thesis Objectives	2
1.3 Methodology	3
1.4 Achievements	4
1.5 Related Research	4
1.6 Thesis Outline	5
2 CHAPTER 2	8
2.1 Background	8
2.2 Optical Holography	9
2.2.1 Basic Principle of Holography	9
2.2.2 Methods in Optical Holography	12
2.3 Optical Holography Applications	19
2.4 Conclusion	20
3 CHAPTER 3	21
3.1 Computer Generated Holography	21
Introduction	21
3.2 The Detour - Phase	22
3.2.1 The Detour - Phase Hologram with Random Mask	24
3.2.2 The Detour - Phase Hologram without a Random Phase Mask	28
3.3 The Kinoform	30

3.4	The Gerchberg-Saxton Algorithm.....	35
3.5	Applications of Computer-Generated Holograms.....	38
3.5.1	Basic Concept of the HOE.....	39
3.6	The Iterative Fourier Transform Hologram	39
3.7	Conclusion.....	45
4	CHAPTER 4.....	46
4.1	Reconstruction the Quadratic Phase from the Modulus of its Fourier Transform	46
	Introduction	46
4.2	Light Point Source.....	47
4.2.1	In-Line Hologram	48
4.2.2	Off-Axis Hologram.....	50
4.3	The MGSA algorithm and the random phase effect	51
4.4	Error – Reduction Algorithm	56
4.5	The Iterative Method.....	56
4.6	Results of Applying the Iterative Reconstruction	58
4.7	The Iterative Method.....	60
4.8	Image Enhancement	65
4.8.1	Mean Filter.....	65
4.8.2	Median Filter.....	66
4.9	Propagation of a Point Source	67
4.10	Grey-Level Fresnel Zone Plate (FZP).....	68
4.11	Conclusion.....	82
5	CHAPTER 5.....	83
5.1	Multiple-Point Source Locations	83
	Introduction	83
5.2	Digital Holographic Microscopy for 3D Imaging.....	84
5.3	Resolution and Depth of Field in Digital In-Line Holographic Microscopy	84
5.4	Pinhole Size.....	84
5.5	Distance between the Point Source and the Hologram	86
5.6	Hologram as a Collection of Fresnel Zone Plates	92
5.7	Two-Source Interference.....	94
5.8	Reconstruction of Two Point Source Objects	95

5.9	Thesis Project	95
5.10	In-Line Digital Hologram Microscopy	96
5.11	Off-Axis Hologram	98
5.12	Modified Error-Reduction Algorithm	103
5.13	Simulation Results.....	103
5.14	Conclusion.....	129
6	CHAPTER 6.....	131
6.1	Conclusion and Future Work	131
	Conclusion.....	131
6.2	Future work	134
	List of Published Papers	135
	REFERENCES	136
	APPENDICES	150
	APPENDIX A.....	150
	A.1 Fresnel Diffraction for a Circule Aperture	150
	A.1.2 Fresnel Diffraction	150
	A.1.3 Fresnel Zones	151
	A.2 Rayleigh-Sommerfeld Solution.....	153
	A.3 Fresnel Approximation.....	154
	A.4 Fraunhofer Approximation.....	155
	A.4.1 Fraunhofer Diffraction Example	155
	A.5 Propagation Simulation	158
	A.5.1 Fresnel Transfer Function Propagator.....	158
	A.5.2 Circle Beam Example.....	159
	A.5.3 Sample Interval.....	160
	A.5.4 Coordinates.....	161
	A.5.5 Indexing, Centering and Shifting	162
	APPENDIX B	178
	APPENDIX C	181
	APPENDIX D.....	183
	APPENDIX E	189

LIST OF FIGURES

Figure 1.1: Schematic diagram of the optical system	2
Figure 2.1: Recording stage of the optical hologram [35]	9
Figure 2.2: Reconstruction stage of the optical hologram [35]	10
Figure 2.3: In-Line holography: recording stage	13
Figure 2.4: In-Line holography: reconstruction stage.....	14
Figure 2.5: Off-axis holography: recording stage.....	15
Figure 2.6: Off-axis holography: reconstruction stage	16
Figure 2.7: Optical system to implement Fourier holography: recording	18
Figure 2.8: Optical system to implement Fourier holography: reconstruction.....	19
Figure 3.1: (a) the detour-phase binary hologram; (b) the cell description	23
Figure 3.2: The Detour-Phase hologram with random phase: (a) the original object; (b) the object spectrum.....	25
Figure 3.3: The Detour-Phase hologram with random phase: the detour phase CGH	26
Figure 3.4: The Detour-Phase hologram with random phase: the reconstructed image.	27
Figure 3.5: The Detour - Phase hologram without random phase: the original object.....	28
Figure 3.6: The Detour - Phase hologram without random phase: (a); the object spectrum; and (b) the reconstructed image.	29
Figure 3.7: The kinoform hologram with a random phase mask (a) the original object; and (b) the spectrum modulus	32
Figure 3.8: The kinoform hologram with a random phase mask: (a) the spectrum phase; and (b) the reconstructed image.	33
Figure 3.9: The kinoform hologram without a random phase mask: (a) the original object; (b) the spectrum modulus	34
Figure 3.10: The kinoform hologram without a random phase mask: (a) the spectrum phase; and (b) the reconstructed image.....	35
Figure 3.11: The Gerchberg-Saxton Algorithm [56]	36

Figure 3.12: The Gerchberg-Saxton algorithm result: (a) the original object; (b) the spectrum phase	37
Figure 3.13: The Gerchberg-Saxton algorithm result: the reconstructed image.....	38
Figure 3.14: Iterative Fourier transform hologram (number of iterations = 100): the original object.....	41
Figure 3.15: Iterative Fourier transform hologram (number of iterations = 100): the RMSE with number of iterations	42
Figure 3.16: Iterative Fourier transform hologram (number of iterations = 100): the reconstructed image.....	43
Figure 3.17: Iterative Fourier transform hologram (number of iterations = 10): the original object	43
Figure 3.18: Iterative Fourier transform hologram (number of iterations = 10): (a) the RMSE with number of iterations; and (b) the reconstructed image.	44
Figure 4.1: Recording stage of off-axis hologram	47
Figure 4.2: Recording stage of in-line hologram	48
Figure 4.3: On-axis Fresnel zone plate as a function of point source distance, z_0 : a) $z_0 = 2mm$, b) $z_0 = 5mm$, c) $z_0 = 8mm$, and d) $z_0 = 10mm$	49
Figure 4.4: Off-axis Fresnel zone plate as a function of point source location, z_0 : a) $z_0 = 2mm$, b) $z_0 = 5mm$, c) $z_0 = 8mm$, and d) $z_0 = 10mm$	50
Figure 4.5: Intensity at z_0 for the random phase: $random\ phase = \exp(-j\pi * random())$	53
Figure 4.6: Intensity at z_0 for the random phase: $random\ phase = \exp(-j\pi * random()/256)$	54
Figure 4.7: General calculation algorithm of a MGSA in the Fourier domain.....	55
Figure 4.8: Binary FZP, $z = 0.5 mm$	58
Figure 4.9: The original object Fourier plane phase	58
Figure 4.10: Example random phase function	59
Figure 4.11: Phase distribution (represented as a grey-level) of the Fourier transform of the Fresnel pattern plus random phase distribution	59

Figure 4.12: The intensity distribution of Figure 4.11	60
Figure 4.13: RMSE as a function of the number of iterations: 10 iterations	61
Figure 4.14: RMSE as a function of the number of iterations: 50 iterations	62
Figure 4.15: RMSE as a function of the number of iterations: 100 iterations	63
Figure 4.16: Phase produced after a number of iterations: (a) 3, (b) 10 iterations	64
Figure 4.17: Phase produced after a number of iterations: (a) 50, (b) 100 iterations	64
Figure 4.18: reconstructed phase	65
Figure 4.19: enhanced image by applying mean 3×3 filter	66
Figure 4.20: enhanced image by applying a median filter of size 256×256	66
Figure 4.21: Flowchart of the general MGSA	69
Figure 4.22: Reconstructed point sources for different distances: (a) 0.05mm, (b) 0.1 mm	71
Figure 4.23: Reconstructed point source intensity for different distances: (a) 20mm, (b) 100 mm.	72
Figure 4.24: Reconstructed point source intensity for distance 0.05mm.....	73
Figure 4.25: Reconstructed point source intensity for different distance: 0.1 mm.....	74
Figure 4.26: Reconstructed point source intensity for different distance: 20mm.....	75
Figure 4.27: Reconstructed point source intensity for different distance: 100mm	76
Figure 4.28: Reconstructed point source intensity for different distance: 0.05mm.....	77
Figure 4.29: Reconstructed point source intensity for different distance: 0.1mm.....	78
Figure 4.30: Reconstructed point source intensity for different distance: 20mm.....	79
Figure 4.31: Reconstructed point source intensity for different distance: 100mm.....	80
Figure 4.32: Reconstructed point source intensity for different distance: 5000mm	81
Figure 5.1: FZP for different pinhole size: for d=180nm	85
Figure 5.2: FZP for different pinhole size for 220nm	86

Figure 5.3: Off axis Fresnel zone plate (a hologram of two point sources, two point sources located side by side and separated by a distance z): for $z=3\text{mm}$,	87
Figure 5.4: Off axis Fresnel zone plate (a hologram of two point sources, two point sources located side by side and separated by a distance z): (a) for $z=5\text{mm}$,.....	88
Figure 5.5: Off axis Fresnel zone plate (a hologram of two point sources, two point sources located side by side and separated by a distance z): for $z = 10\text{m}$	89
Figure 5.6: On-axis Fresnel zone plate (a hologram of two point sources are located at same coordinates): for $z=3\text{mm}$,.....	90
Figure 5.7: On-axis Fresnel zone plate (a hologram of two point sources are located at same coordinates): for $z=5\text{mm}$,.....	91
Figure 5.8: On-axis Fresnel zone plate (a hologram of two point sources are located at same coordinates): for $z = 10\text{mm}$	92
Figure 5.9: Holographic recording and reconstruction of a three-point object.....	94
Figure 5.10: Zone plate with two point sources.....	96
Figure 5.11: On-axis Fresnel zone plate as a function of depth, z_0 : a) $z_0 = 2\text{mm}$, b) $z_0 = 5\text{mm}$, c) $z_0 = 8\text{mm}$, and d) $z_0 = 10\text{mm}$	97
Figure 5.12: Off-axis Fresnel zone plate as a function of depth, z_0 : a) $z_0 = 2\text{mm}$, b) $z_0 = 5\text{mm}$, c) $z_0 = 8\text{mm}$, and d) $z_0 = 10\text{mm}$	99
Figure 5.13: Intensity at z_0 for the random phase: $\text{phase}=\exp(-j\pi*\text{random}())$	101
Figure 5.14: Intensity at z_0 for the random phase: $\text{random phase} = \exp(-j\pi * \text{random}()/256)$	102
Figure 5.15: Reconstructed original point sources for different propagation distance: for - $z_0=0.05\text{mm}$	105
Figure 5.16: Reconstructed original point sources for different propagation distance: for - $z_0=5\text{mm}$	106
Figure 5.17: Reconstructed original point sources for different propagation distance: for - $z_0=10\text{mm}$	107
Figure 5.18: Reconstructed original point sources for different propagation distance: for - $z_0=50\text{mm}$	108

Figure 5.19: Reconstructed original point sources for different propagation distance: for $-z_0 = 150mm$	109
Figure 5.20: In- line FZPs for a 2mm propagation distance (distance between the point sources and the hologram)	110
Figure 5.21: Reconstructed point sources for different propagation distance: $z=50mm$	111
Figure 5.22: Reconstructed point sources for different propagation distance: $z=75mm$	112
Figure 5.23: Reconstructed point sources for different propagation distance: $z=100mm$	113
Figure 5.24: Reconstructed point sources for different propagation distance: $z=110mm$	114
Figure 5.25: Reconstructed point sources for different propagation distances: $z = 150mm$...	115
Figure 5.26: Reconstructed point sources intensity for different propagation distances (distance between the point sources and the FZPs): (a) $z=50mm$	116
Figure 5.27: Reconstructed point sources intensity for different propagation distances (distance between the point sources and the FZPs): $z=75mm$	117
Figure 5.28: Reconstructed point sources intensity for different propagation distances (distance between the point sources and the FZPs): $z=100mm$	118
Figure 5.29: Reconstructed point sources intensity for different propagation distances (distance between the point sources and the FZPs): $z=110mm$	119
Figure 5.30: Reconstructed point sources intensity for different propagation distances (distance between the point sources and the FZPs): $z = 150mm$	120
Figure 5.31: Reconstructed point sources intensity for different propagation distances (distance between the hologram and the screen): $-z=0.05mm$	121
Figure 5.32: Reconstructed point sources intensity for different propagation distances (distance between the hologram and the screen): $-z=5mm$	122
Figure 5.33: Reconstructed point sources intensity for different propagation distances (distance between the hologram and the screen): $-z=50mm$	123
Figure 5.34: Reconstructed point sources intensity for different propagation distances (distance between the hologram and the screen): $-z = 100mm$	124
Figure 5.35: Isometric views of the reconstructed two point sources intensity for different distances between the FZP centres: $x=1mm$	125

Figure 5.36: Isometric views of the reconstructed two point sources intensity for different distances between the FZP centres: $x=5\text{mm}$	126
Figure 5.37: Isometric views of the reconstructed two point sources intensity for different distances between the FZP centres: $x=50\text{mm}$	127
Figure 5.38: Isometric views of the reconstructed two point sources intensity for different distances between the FZP centres: $x = \mathbf{150mm}$	128

LIST OF TABLES

Table 4.1: Random Phase	52
-------------------------------	----

LIST OF ACRONYMS

Spatial Light Modulator	SLM
Fresnel Zone Plate	FZP
Modified Gerchberg-Saxton algorithm	MGSA
Root Mean Square Error	RMSE
Fast Fourier transform	FFT
Iterative Fourier Transform Algorithm	IFTA
detour phase hologram	DPH
Gerchberg - Saxton algorithm	GS
Three Dimensional	3D
Holographic optical elements	HOEs
Diffractive Optical Elements	DOE
Digital In-Line Holographic Microscopy	DIHM
Digital Holographic Microscopy	DHM
Digital Off-Axis Hologram Microscopy	DOHM
Two Dimensional	2D
Inverse Fourier transform	IFFT

LIST OF PRINCIPAL SYMBOLS

$f_i(x, y)$	complex amplitude distribution,
λ	wavelength of the light
$U_o(x, y)$	Object wave
$U_r(x, y)$	Reference wave
$A_o(x, y)$	Amplitude of the object wave
$e^{i\phi(x, y)}$	Phase of the object wave
$A_r(x, y)$	Amplitude of the reference wave
$e^{i\psi(x, y)}$	Phase of the reference wave
$I(x, y)$	Intensity on the hologram
$t(x, y)$	Transmission function
q	The spatial carrier frequency
$N \times N$	Object cells on the hologram
$p_{mn} \times q_{mn}$	Detour phase hologram -the open aperture size
a_{mn}	Detour phase hologram -the open aperture shifting distance
$H(x, y)$	The kinoform hologram
abs	The modulus of the complex field
$g_i(u, v)$	The Fourier transform of $f_i(x, y)$
$f'_i(x, y)$	Computed signal
$ f_i(x, y) $	Modulus of the original object distribution
k_o	A wave number $k_o = 2\pi/\lambda_o$
$\delta(x, y)$	A delta function
SEF	Fourier transform of the combination of the original phase and the known random phase
z	The propagation distance
$-z$	The propagation distance between the hologram and the screen

1 CHAPTER 1

1.1 Introduction

Digital holograms have been developed and used in many applications since it is a technique that allows a wavefront to be recorded and then reconstructed even in the absence of the original object. Thus the digital holography shows capabilities are not available in the optical holography. In this project, we employ digital holography for this reason. The original object amplitude and phase are recorded numerically, therefore the resulting data can easily be sent to a spatial light modulator (SLM) [1]. Digital holographically reconstructed image can be refocused at different depths depending on the reconstruction distance. This is the remarkable aspect of digital holography that can be useful in many applications, one of the most beneficial being its use for the biological cell studies [2, 3]. In this research, point source digital in-line and off-axis holography with a numerical reconstruction has been studied. The point source hologram can be used in many biological applications [4, 5]. As the original object we use the binary amplitude Fresnel zone plate which is made by rings with an alternating opaque and transparent pattern [6-8]. For the in-line holography a spherical wave of wavelength (λ) emanating from the point source is used in the project. Also we use an off-axis point source in which the original object is located away from original. Firstly, we create a binary amplitude Fresnel zone plate (FZP) which is considered the hologram of the point source of the original object.

We implement a phase-only Computer-Generated Hologram (CGH) calculation technique for the point source object. We use the modified Gerchberg Saxton algorithm (MGSA) instead of the non-iterative recording methods used in classical holography. A schematic diagram of our proposed design technique is shown in Figure 1.1.

Firstly, the complex amplitude distribution, $f_i(x, y)$, which is the result of the Fourier transform of the point source phase is combined with a random phase and is the input of the iteration process. Second, this wavefront is transformed to the frequency plane by using a two dimensional fast Fourier transform (FFT). We apply the first constraint by removing the amplitude distribution directly calculated and replace it with the measured modulus but keep the phase distribution unchanged. We use the root mean square error (RMSE) measure to control the iteration process. The RMSE decreases at each iteration [9], giving rise to the name error-reduction approach.

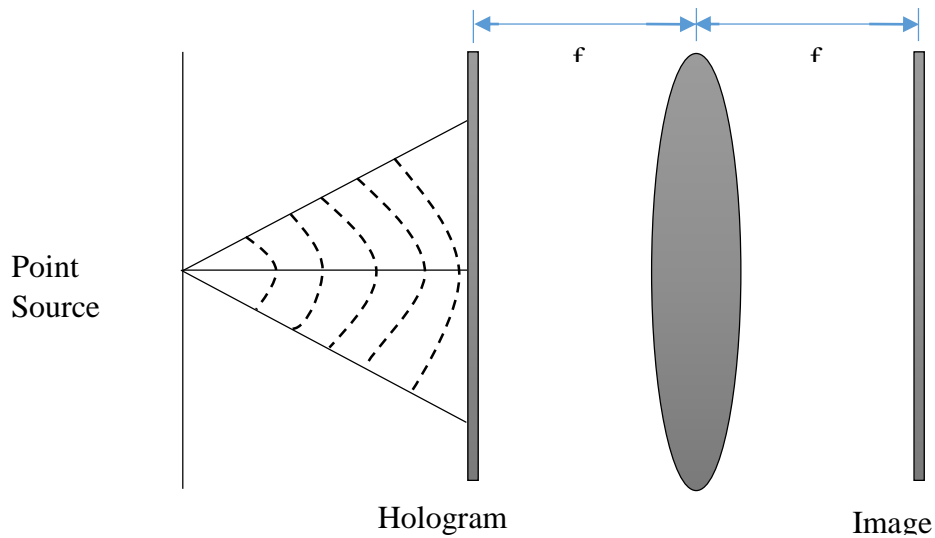


Figure 1.1: Schematic diagram of the optical system

1.2 Thesis Objectives

The aim of this thesis is to create an algorithm that is able to reconstruct multi point source objects. The method could then be used for biological microscopy applications in which it is required to locate point scattering sources from within the volume of a cell cytoplasm. These practical applications are briefly discussed in Chapter 3. The major tasks to be solved in this thesis are:

- Reconstruct a point source of light when the phase information is not known..
- The use of a random initial phase to control the quality of the final reconstructed image.
- Modifying the Gerchberg-Saxton algorithm iteration and able to use it to solve the specific project problem.

1.3 Methodology

The method used in this project is to be applied in microscopy applications (for biological cells, for instance) [10-17]. The digital hologram can be recorded by more than one technique such as: a detour phase method; a kinoform; and an iterative Fourier transform. In this project we manage to create a good quality reconstructed hologram image using the kinoform technique. Our research started with creating a detour phase hologram and then the kinoform hologram. From the outcomes of both methods we analysed the quality of their reconstructed images and the kinoform image shows a better quality and high efficiency. We also applied a mask when we use the kinoform technique and studied the quality of the reconstructed image.

Our project is to deal with the microscopy object and with only the intensity is known [18] and its phase needs to be reconstructed. The two techniques above (the detour phase and the kinoform) are not suitable to this task. We searched for other options to manipulate this project problem and the Iterative Fourier Transform Algorithm (IFTA) [19-21] is a highly efficient method to use. We modified this algorithm as we have only the intensity information of the original object (in combination with a random phase). The IFTA is based on using a Fourier transform between the hologram and the reconstruction plane for which constraints are imposed in each domain. Such iteration will continue to converge even if in some cases we find it is very slow [22, 23]. When the constraints are enforced strictly then we are able to generate a reconstructed image with low errors. In this project, we describe the iterative method and show results of computer experiments applying the technique to reconstruct the quadratic phase of a Fresnel Zone Plate (FZP). The iterative technique we use in Chapters 4 and 5 are very effective in solving the problem of reconstructing the quadratic phase of the FZP from only known modulus information of its Fourier transform.

The results obtained by the iterative method could not have been achieved by any other practical technique. The results of the reconstruction of the point source object are particularly significant: they indicate the ability to obtain clear images of the original point source object and thus this technique should prove an important tool in a number of areas of optics and related fields.

1.4 Achievements

The major contributions of this research are:

- Using the modified Gerchberg-Saxton algorithm to reconstruct the binary amplitude Fresnel zone plate (FZP). MATLABTM code was developed and used to calculate the optical fields for different distances between the point source and the hologram. The FZP thus has different features for each distance and the reconstructed images change accordingly.
- Adding a random phase to the original object. As a first attempt, we add a random phase and we determine that the quality of the final hologram and reconstructed image depend on which initial phase we use.
- We adapt the iterative Fourier transform algorithm (IFTA) and the error reduction algorithm to reconstruct the point source from only the known modulus. The original object is a grey-scale FZP which is assessed for many different propagation distances to show its effect on the final reconstructed image.
- We use the root mean squared metric to measure the convergence of the algorithm to a solution which is the Fourier transform pair satisfying all the constraints in both domains.

1.5 Related Research

There are number of techniques have been used for digital holography and most of these techniques are based on a Fourier transform approach. Fourier holography is a good method to acquire an image reconstruction through Fourier transformation. The reconstructed images are not ideal due to noise and missing information.

Since the invention of digital holography, many algorithms have been suggested to solve the problem of transforming a given light distribution into another desired light distribution. One of the best methods for this challenge is the iterative Fourier transform algorithm (IFTA). This algorithm is based on the process of iterating back and forth between two spatial planes related by a Fourier transform. The IFTA which is thus an error- reduction algorithm, was used by Gerchberg and Saxton for phase retrieval [24].

We modified the IFTA to solve the problem set for this project by containing only the intensity of the original point source object at the plane of the hologram. Also, there is another iterative algorithm which is due to Fienup [25-27]. This iterative algorithm, is mainly used to speed up the

convergence, so that the deviation between the obtained and desired amplitude can be made small enough.

There is another technique to calculate a phase only hologram which is able to reconstruct a 3D object with higher image quality. This technique is based on IFTA which is employed between the hologram and a virtual intermediate plane [28-33]. The main advantage of using this technique is the computation time can be greatly decreased as compared to the conventional method.

1.6 Thesis Outline

The thesis is divided into six chapters. After the introduction and problem formulation, Chapter 2 surveys major lines of research in the field of optical holography and different types of hologram recording techniques which includes in-line and off-axis holograms. Also, in this chapter we consider the Fourier plane hologram. Chapter 2 reviews the science of digital holography and covers in detail its practical implementation. We start by describing the first stage of any digital holographic process which is the recording stage. We study different recording techniques available and compare their strengths and weaknesses. We then examine the second stage of the digital holographic process, the different methods for identifying and removing of error terms inherent in digital holograms, which involve the in-line and off-axis digital holographic techniques used to record the holograms in this thesis. We then examine in this chapter the third stage of the digital holographic process, the reconstruction stage. There is more than one reconstruction algorithm available for digital holography and we review three of them. The last section of this chapter we review some applications of digital holography.

In Chapter 3 we further reviews different types of the digital hologram. We review some of the classic techniques of generating Computer Generated Holograms i.e. the Detour-Phase hologram and the Kinoform techniques, and then study some more modern methods of generating CGHs such as the Iterative Fourier Transform Algorithm (IFTA). Also, we examine the coded mask technique for an example object (Lena image), considering different sizes of random masks that have been used.

In Chapter 3 we detail the fundamental theory of digital holography and examine the first method of recording a computer-generated hologram (CGH) that was proposed by Lohmann and his collaborators that required only amplitude binary media. In this technique, an elementary cell of the medium is allocated for reproducing the amplitude and phase of each sample of a discretely

sampled hologram. The modulus of the complex number can be represented by the size of the opening in the aperture in the cell and the phase can be represented by the position of the opening within the cell (the so-called detour phase technique).

The second technique we present in this chapter is the kinoform method which is a special hologram encoding technique where only phase information can be recorded. The kinoform is thus a CGH in which the phase data are recorded in a phase-only medium while the amplitude data are ignored.

Although, we ignore the amplitude in the recording stage, this results in hologram reconstructions with substantial distortions such as the appearance of speckle noise in the reconstructed image. The main advantage of using the kinoform hologram is the saving of energy of the reconstruction wave light without it being absorbed in the hologram plate.

Also in this chapter we detail the iterative Fourier transform algorithm (IFTA) which is the technique we use to implement the method described in this thesis which is the reconstruction of the phase of an original object from only the known modulus.

The IFTA has been used in computer holography to smooth the power spectrum and to reduce the influence of speckle noise in the reconstructed holographic image. The main application of the IFTA is for its use for phase retrieval. For this, it has been applied in many fields such as astronomy and electron microscopy. We also describe digital hologram applications such as for three dimensional displays, spatial filters and optical testing.

In Chapter 4 we develop the technique of reconstructing a point source object from only its modulus information by using the modified GS algorithm. We apply the modified GS algorithm for the case where there are two point sources to be reconstructed from knowledge only of their intensity at the output plane of the system.

Chapter 4 then describes how the IFTA can be used to reconstruct the original phase of the point sources at the plane of the hologram from only modulus information available in the output plane of the system. In this chapter, we present the binary Fresnel zone plate (FZP) which are optical diffractive elements that focus a beam in a similar manner as in a conventional refractive lens. The FZP consists of several radially symmetric rings which called zones. Zones interchange between opaque and transparent. Also, we examine the use the sinusoidal zone plates. These FZPs differ from the traditional binary zone plates in that the transparency of the sinusoidal FZP varies sinusoidally from the center of the zone plate, unlike the binary FZP which are either fully

transparent or opaque. We examine use the sinusoidal FZP in Chapter 4 and 5 as test objects to determine how effectively the ITFA can reconstruct the unknown phase distribution.

In Chapter 4 we present the method of reconstruction of the quadratic phase FZP from only the known modulus of its Fourier transform. The problem is to find an object that is non-negative with the modulus of its Fourier transform equal to the measured modulus.

We use the modified iterative Fourier transform to match this problem by setting a new set of object constraints, and designate this as the error-reduction approach. We summarise this approach in a diagram showing all separate stages comprising the algorithm.

In Chapter 5 we introduce multiple point sources and apply a similar method to that described in Chapter 4 in to determine their locations.

Chapter 6 concludes by summarising the results of the thesis and considering some directions for future work.

2 CHAPTER 2

2.1 Background

Introduction

Holography is a technique that has been used in many fields in the world as it is able to generate a 3D image of any object without requiring complex optical devices for the reconstruction to be generated.

Holography was initiated in 1947 by the British/Hungarian scientist Dennis Gabor who developed the theory of holography while working to improve the resolution of an electron microscope. The term Hologram comes from the Greek words Holo, meaning “whole” and gramma meaning “message” [34].

The art of holography has undergone many changes since its invention. The methods and principles of holography have been modified and improved through the years to realise better efficiency and quality. Everyone will encounter holography very soon as it will be applied in everyday life and in many fields.

In general, holography consists of two stages. The first process is the recording stage, and Gabor proposed a method of recording both amplitude and phase information of light diffracted off an object by recording the intensity of the interference pattern between the light and a coherent reference beam. An image of the original object can be obtained from the recorded interference pattern. He called the recorded interference pattern a hologram, meaning total recording.

In the recording stage, the hologram is encoded on a holographic recording medium by using two mutually coherent light beams. Before the invention of the laser (i.e. a powerful coherent light source), holograms were not easy to generate. The invention of the laser was the achievement that made creating and reconstructing holograms much more practically possible.

There are many methods of generating an optical hologram and each one has its own merits and drawbacks. In this chapter the basic theory of optical holography, the techniques and methods available for constructing and reconstructing optical holograms and some holographic applications will be described.

2.2 Optical Holography

Optical holography is the technique that employs laser light for recording and reconstructing information using a high resolution photographic plate. This was the first and the most popular technique for making holograms which requires the presence of a real object with a further restriction that the real object should be highly stable. The reconstruction stage can be done by using either laser light or white light depending on the exact nature of the recording. This technique can create a good quality hologram which reconstructs an image that is very close to the original object. There were no electronic devices that were employed in the construction and reconstruction using this technique and that is the reason this method is called the optical holography.

2.2.1 Basic Principle of Holography

Figure 2.1 shows a schematic of holographic recording. This process consists of the light source, original object, and the film (the recording device). The light source should be of sufficient coherence. Before the invention of the laser (i.e. a coherent light source), holograms were difficult to create. The invention of the laser was the event that made creating and observing holograms more easily achievable. Using a thermal light source, certain conditions are required to observe the hologram.

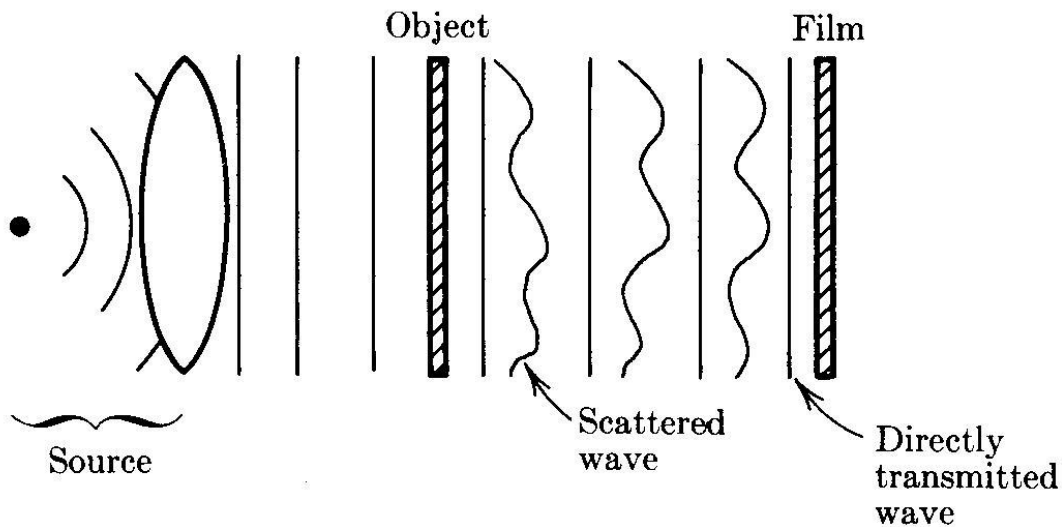


Figure 2.1: Recording stage of the optical hologram [35]

The lack of light with a good coherence (i.e. monochromatic, from a single spatial point) in the early years of holography was the most restricting factor in producing a hologram of any depth of

focus. The mercury lamp was the most coherent light source available for making holograms at that time in the 1950's. Figure 2.1 illustrates that the light can be considered as splitting into two waves. The first wave is the object wave which is scattered from the object and propagates to the recording medium. The second wave is called the reference wave. This undiffracted wave illuminates the film (recording medium) directly. The two waves will interfere on the film to create the recorded interference pattern. The film (photographic plate) is then developed chemically to generate the recorded interference pattern. This interference pattern is now called the hologram. The hologram records all the information in the light field which was diffracted from the object, i.e. the phase and amplitude of the diffracted field is recorded.

The second stage of the optical holography process is called the reconstruction. In this stage, the hologram is illuminated with only the reference beam. Figure 2.2 shows a schematic of the reconstruction of an optical hologram.

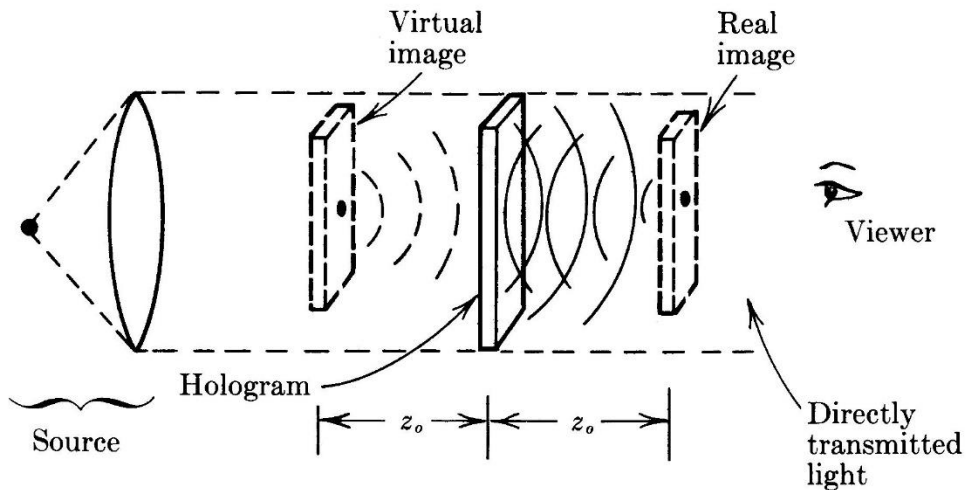


Figure 2.2: Reconstruction stage of the optical hologram [35]

The Figure 2.2 shows the hologram illuminated with only the reference beam. A viewer looking through the hologram observes two images. The first image is the virtual image of the object which looks like the original object. Another image is the real image of the object. The two images and the other wavefronts reconstructed by the hologram will be described further shortly. The reconstructed image shows all effects of variable view angle and depth of focus. Now, we can explain the recording and reconstruction stages mathematically, as follows.

The light passing through a semi-transparent object consists of the scattered wave $U_o(x, y)$, which is the object wave and the unscattered reference wave with field $U_r(x, y)$.

The complex amplitude of the object is given by:

$$U_o(x, y) = A_o(x, y)e^{i\phi(x, y)} \quad (2.1)$$

where $A_o(x, y)$ is the amplitude, and $e^{i\phi(x, y)}$ is the phase.

The reference wave is given by:

$$U_r(x, y) = A_r(x, y)e^{i\psi(x, y)} \quad (2.2)$$

where $A_r(x, y)$ is the amplitude, and $e^{i\psi(x, y)}$ is the phase.

At a distance z behind the object, the detector (a photographic film during Gabor's time) records an intensity distribution generated by the interference of these two fields [36-37]:

$$I(x, y) = |U_o(x, y) + U_r(x, y)|^2 \quad (2.3)$$

which, when expanded, becomes:

$$I(x, y) = |U_o(x, y)|^2 + |U_r(x, y)|^2 + U_o(x, y) \cdot U_r^*(x, y) + U_o^*(x, y) \cdot U_r(x, y) \quad (2.4)$$

If we assume a linear response to intensity associated with the photographic film, then we will find that its transmission function has the form:

$$t(x, y) = a + bI(x, y)$$

(2.5) where a and b are constants. Thus all information about the object is in the transmission function $t(x, y)$.

Reconstructing the hologram requires illuminating the hologram with a wave similar to the reference beam. The field scattered from the hologram derives from the product between the illuminating plane wave $U_r(x, y)$ and the transmission function $t(x, y)$. Thus we obtain:

$$U(x, y) = U_r(x, y) \cdot t(x, y) \quad (2.6)$$

$$= (a + b[|A_o(x, y)|^2 + |A_r(x, y)|^2 + U_r(x, y) \cdot U_o(x, y) + U_r(x, y) \cdot U_o^*(x, y)]). U_r(x, y) \quad (2.7)$$

The first term of Eq. 2.7 is spatially constant. The second term can be neglected, since if we compare it with the third and fourth terms we can see that for the hologram (transparent object) the scattered field is much weaker than the unscattered field i.e. $|U_r(x, y)| \gg |U_o(x, y)|$.

The third term in Eq. 2.7 represents the virtual image. The virtual image will appear at the same position of the original object. The fourth term represents the real image which appears at the opposite side of the hologram. Both images together are called the twin images. The virtual image is the most important part of Eq. 2.7 which is called virtual because the waves that create this image are divergent from the hologram. The virtual image appears to originate at a distance z in front of the film. The reconstructed image will move if we use a different wavelength in the reconstruction stage to the wavelength used in the recording stage.

2.2.2 Methods in Optical Holography

There are many techniques that are available to produce the holographic image. Each technique has its own advantages and disadvantages. This section will discuss ‘in-line’, and ‘off-axis’ techniques.

2.2.2.1 The In-Line Hologram

In 1948 Gabor developed the theory of holography while working to improve the resolution of electron microscopy. As stated above, the term holography indicates that we record the intensity and phase of the object, not only the intensity as in case of photography. The Gabor hologram has inherent distortion and creates twin images. Also, Gabor’s holography used a mercury arc lamp as the light source and so was limited to reconstructing transparencies.

Figure 2.3 shows the original set up for the recording stage of Gabor’s in-line hologram. In this technique, the illumination beam doubles as the reference beam. The light passing through a partially transparent object consists of the scattered and unscattered field. At a distance z behind the object, the detector (photographic film during Gabor’s time) records an intensity distribution generated by the interference of these two fields [38].

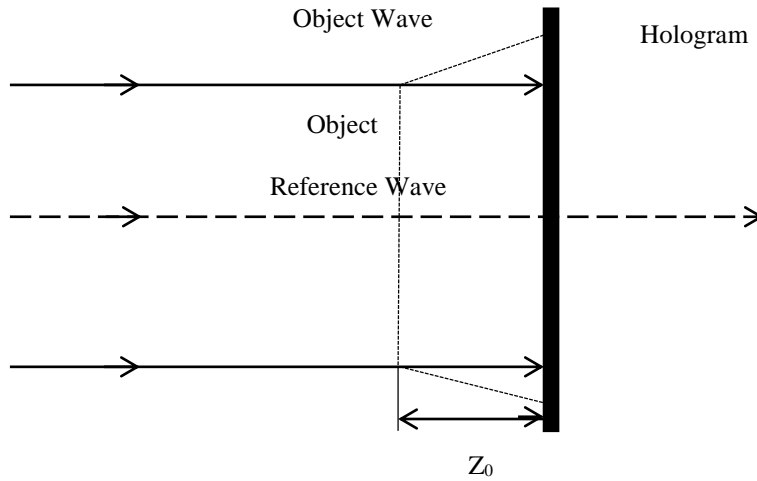


Figure 2.3: In-Line holography: recording stage

The second process, known as the reconstructing stage is shown in Figure 2.4. After the recording medium has been developed, Gabor illuminated the hologram with the reference beam which is similar to that used in the recording stage. The field scattered from the hologram originates from the product between the illuminating plane wave and the transmission function (t). Then we obtain:

$$U(x, y) = U_r \cdot t(x, y)$$

$$U(x, y) = U_o(a + b|U_o|^2 + bU_o \cdot |U_1(x, y)|^2 + b|U_o|^2 \cdot U_1(x, y) + bU_o^2 \cdot U_1^*(x, y)) \quad (2.8)$$

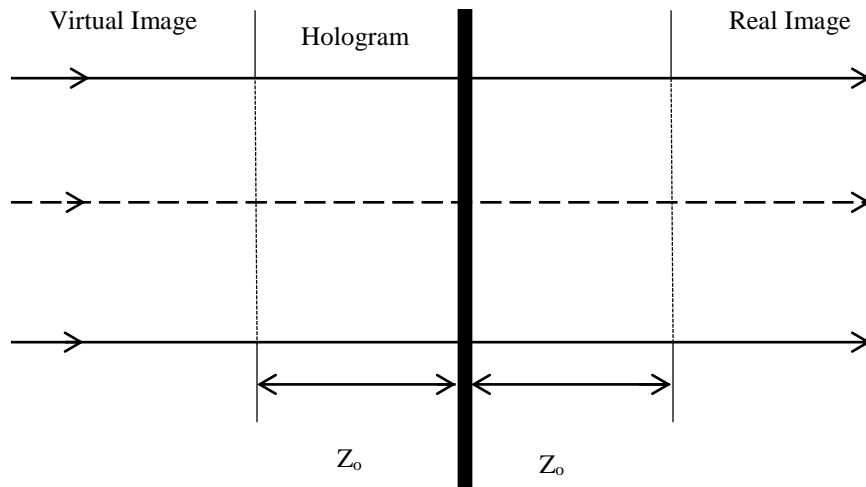


Figure 2.4: In-Line holography: reconstruction stage

If the original object is simply an axial point which emits a spherical wave, using a plane reference wave will result in a hologram which is a Fresnel zone lens. There are two images that will be generated in the reconstruction stage which are the virtual and real images. The virtual image will appear to be formed at the original object position and the real image will be formed at the opposite side of the hologram at the same distance.

This technique has some disadvantages. The virtual and real images are located on the same axis and so interfere. Thus the blurred and twin image overlap in the reconstruction, all the light beams travelling together in the same direction since there is no angle between the object and the reference beams. The twin image problem cannot be solved using this technique. Thus the in-line technique cannot be applied to highly reflective objects. The problem can be solved by using an independent reference beam. Also, there is a safety issue in using the in-line technique as the observer during the reconstruction stage looks directly into the reconstruction light which can be harmful if too bright.

The main advantage of this technique is that the setup needed is very simple and the light required to achieve the holographic image can be low in coherence. Also, we can use only a single beam for the recording and reconstruction stages.

2.2.2.2 The off-Axis Hologram

The setup of the recording and reconstruction for off-axis holography is shown in the Figure 2.5 and Figure 2.6, respectively.

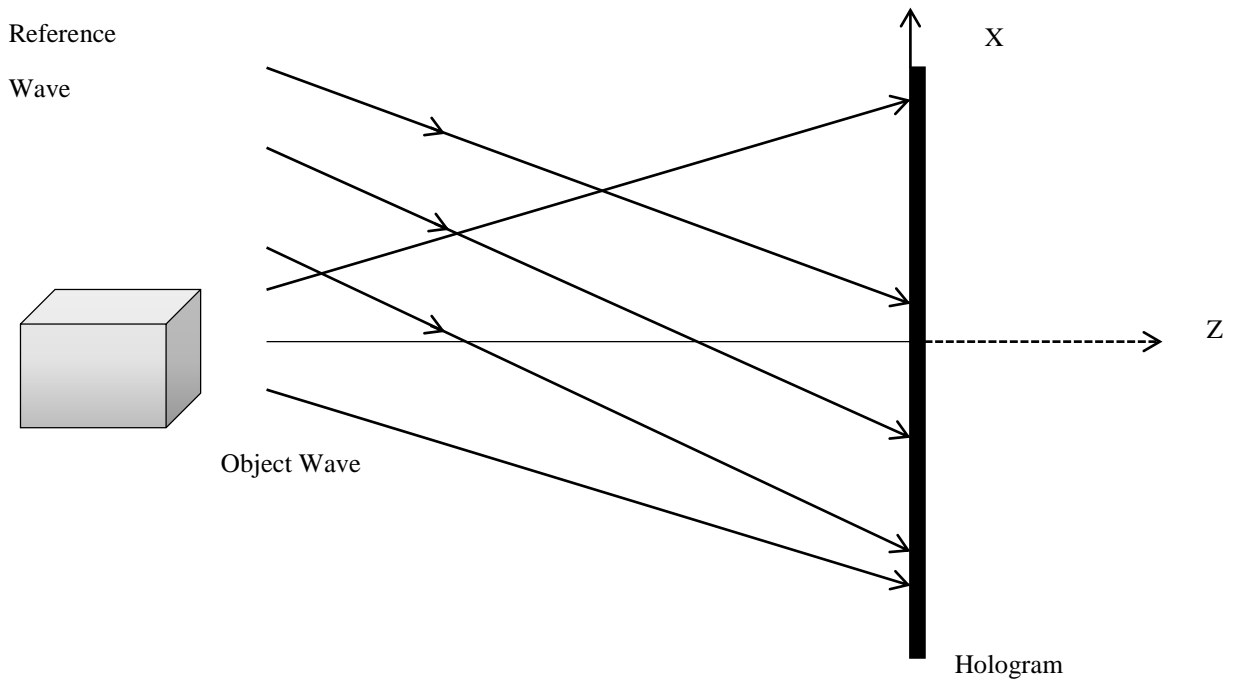


Figure 2.5: Off-axis holography: recording stage

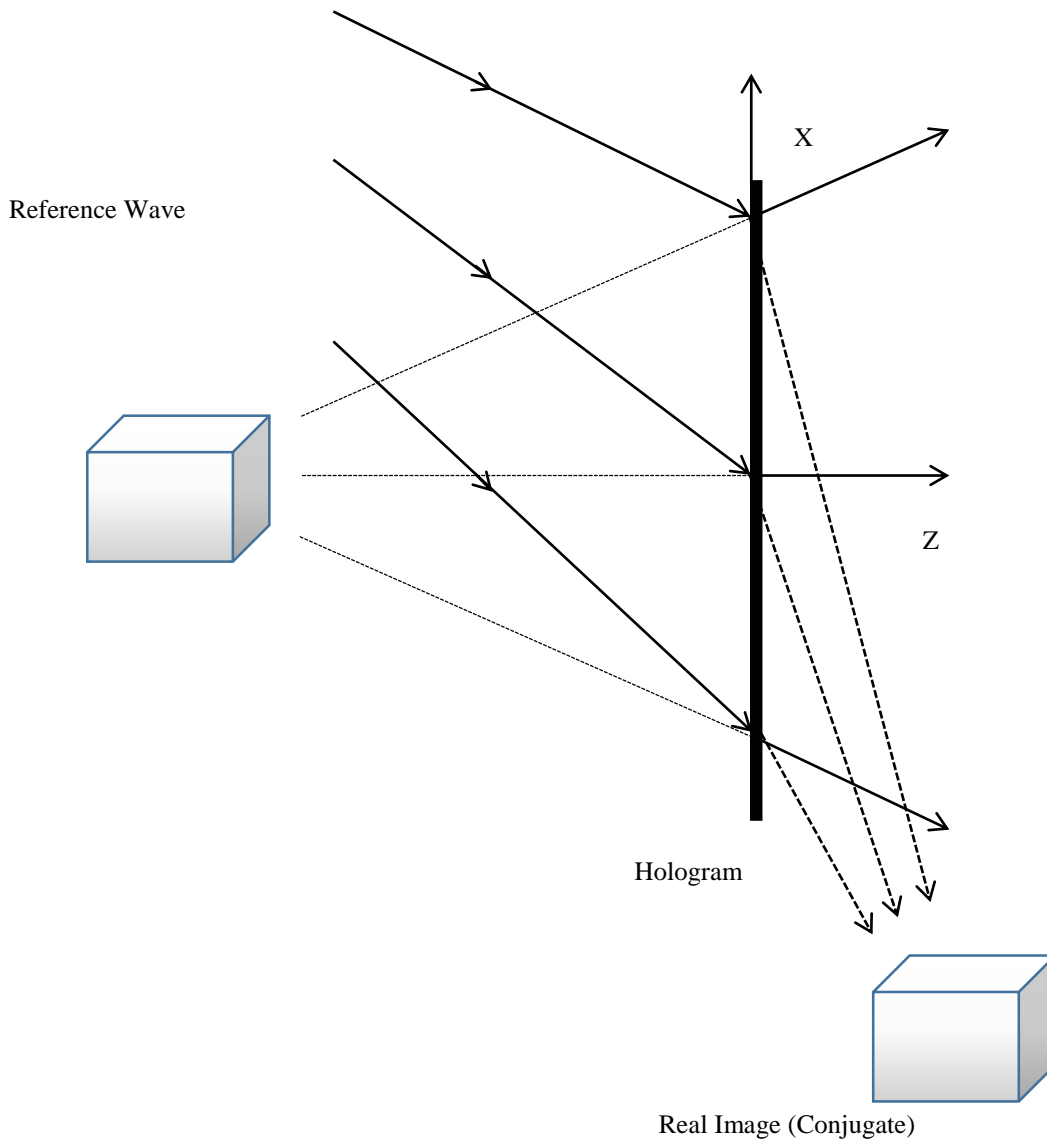


Figure 2.6: Off-axis holography: reconstruction stage

Gabor was tied to the use of the in-line technique due to the lack of coherence of the light sources at that time. There was no significant development of holography in the next decade (i.e. the 1950s) because the light sources available at that time were of very limited temporal coherence. However, this problem was overcome in 1960 with the invention of the laser which soon provided a fully coherent light source which it was possible to concentrate into a narrow beam of intense light which was ideal for recording holograms.

In 1962, Emmett Leith and Juris Upatnieks recognised that the holographic method could be used to create a three dimensional visual medium. They duplicated Gabor's technique using a laser source and an "off-axis" technique which resulted in the production of images with clarity and realistic depth [39].

The main difference between the in-line and off-axis methods of producing the holographic image is that a reference beam is split from the laser source and arranged at an angle to the recording medium rather than along the direction of the object beam as in the in-line technique. The benefit of having the angle between the two light beams is that it provides a carrier frequency to the signal and this leads to resolving the twin image overlap problem that occurs with the in-line technique:

$$I(x, y) = |U_o|^2 + |U_r|^2 + U_o^*U_r + U_oU_r^* \quad (2.9)$$

$$I(x, y) = |U_o|^2 + |U_r|^2 + \exp\left(\frac{i\pi}{2}\right)U_o^*U_r + \exp\left(-\frac{i\pi}{2}\right)U_oU_r^* \quad (2.10)$$

where, $U_o(x, y)$ and $U_r(x, y) = A_r \exp(i2\pi qx)$ represent the object and reference beam complex amplitudes respectively. q denotes the spatial carrier frequency introduced by the angle between the object and the reference waves.

The only disadvantage of this technique is that it is difficult to use it directly in digital holography as the density of fringes increases with the angle between the object and reference beams which in turn leads to the requirement to increase the sampling rate in the digital hologram resulting in time consuming calculation of the diffraction pattern. Digital holograms, particularly early realisations, thus generally used the in-line holographic arrangement.

Figure 2.5 and Figure 2.6 illustrate the off-axis arrangement. In the construction stage, as shown in the Figure 2.5, the incident beam is diffracted from the object and interferes with the reference beam in the recording medium. The incident beam is split into two beams before reaching to the object, one of which illuminates the object and the other forms the reference beam. The reference beam is directed at an angle with the object beam as discussed earlier. In the reconstruction process, as shown in Figure 2.6, the hologram is illuminated by a reconstruction beam which is arranged to be in the same direction of the reference beam in the recording stage.

2.2.2.3 The Fourier hologram

Figure 2.7 and Figure 2.8 show the recording and reconstruction configurations of the Fourier holographic arrangement. In the recording stage, the object wave is positioned in the first focal plane of the converging lens, and the reference wave is emitted from a point light source which is in the same plane. The recording medium (photographic plate) is placed at the other side of the lens in its back focal plane. When the recording of the hologram is completed, the reconstruction is implemented using the setup in Figure 2.8, in which the hologram is illuminated with a plane wave which results in the generation of two images in the back focal plane of the lens. Also, an undiffracted portion of the reference wave produces a zeroth diffraction order on-axis.

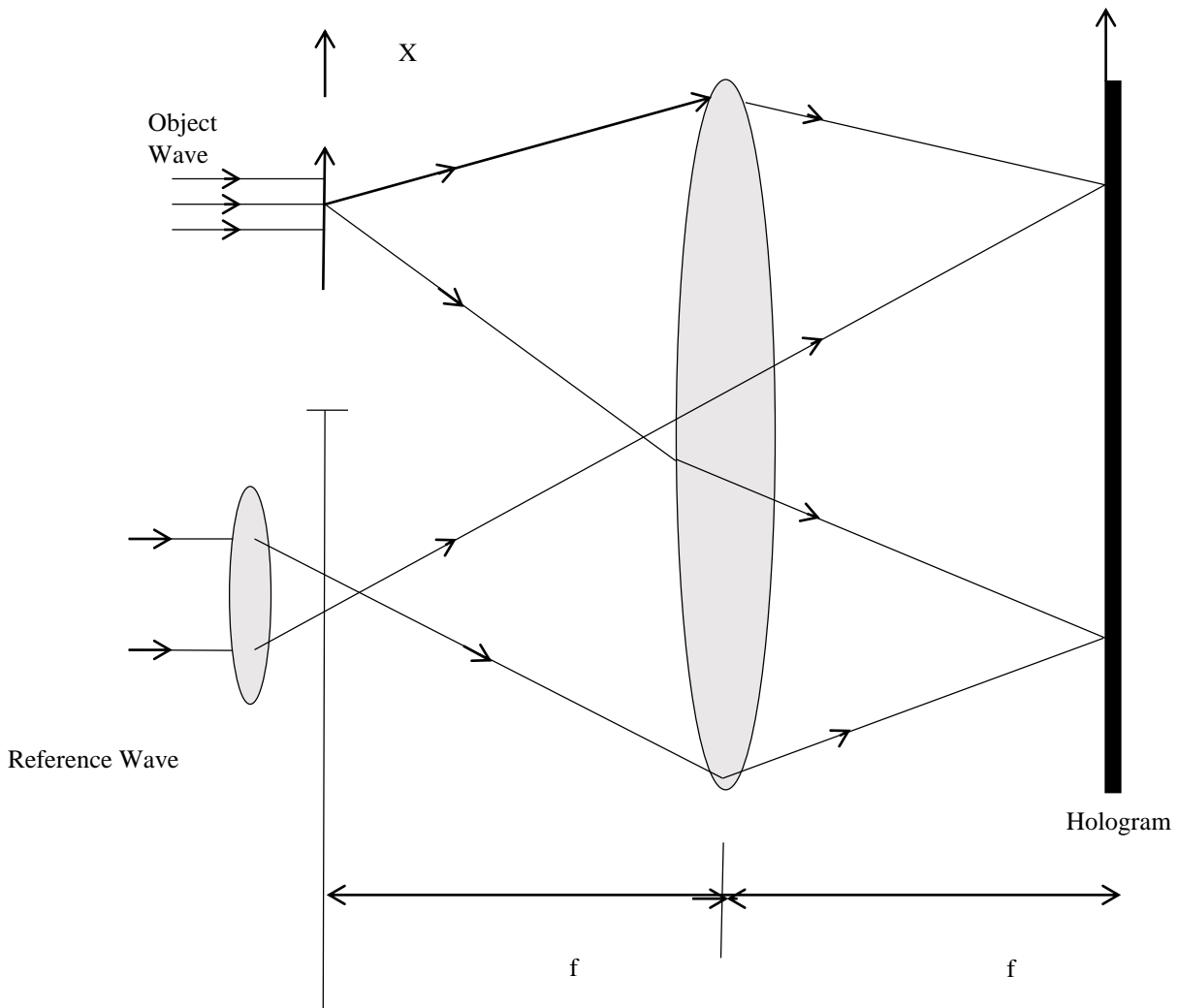


Figure 2.7: Optical system to implement Fourier holography: recording

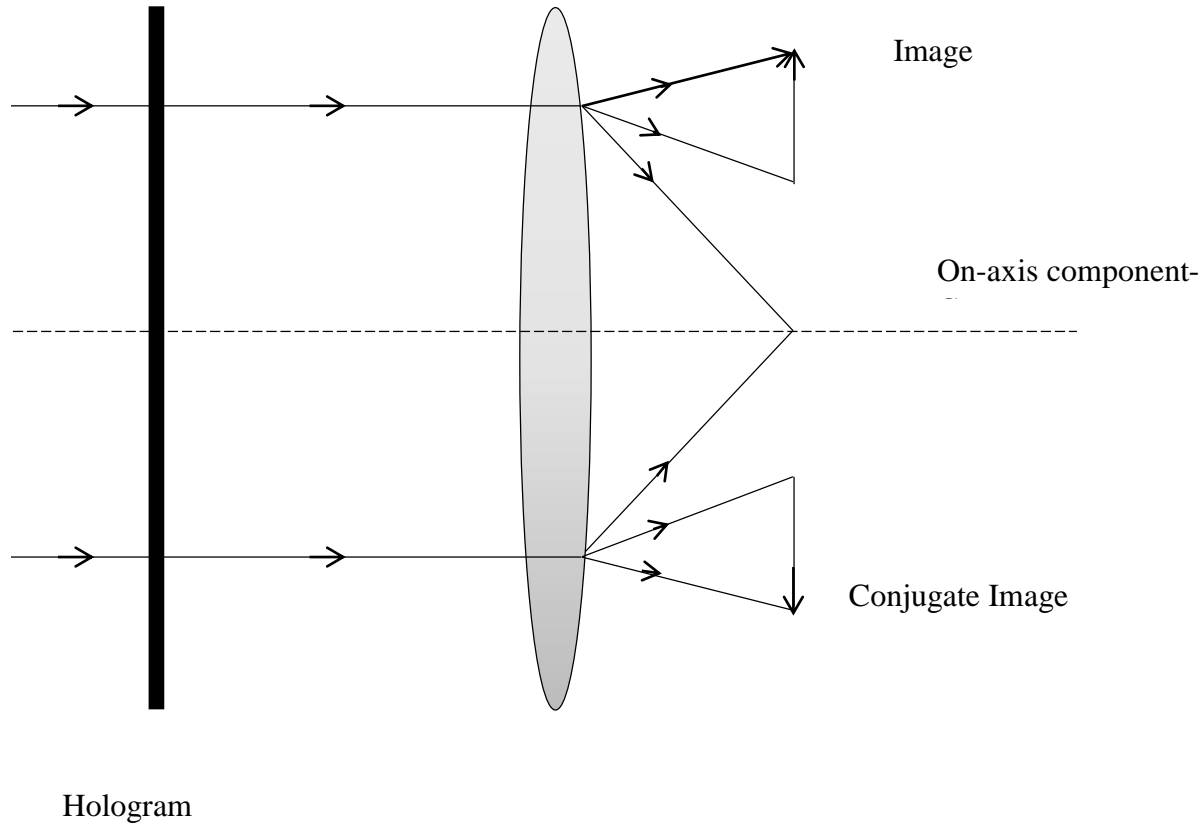


Figure 2.8: Optical system to implement Fourier holography: reconstruction

The main advantage of using the Fourier hologram is that the reconstructed image does not translate when the hologram is translated in its own plane.

2.3 Optical Holography Applications

The technological applications of optical holography since its invention include:

- (1) The Holographic approach improves heads-up displays for aircraft and cars. Head-up displays are transparent devices that can be used to provide information e.g. flight data and driving directions. The data and directions display on the windshield. The optical hologram approach make heads-up displays easier to use and increase the range of the view [40].
- (2) Holography and credit card security. This technique is implemented by printing a plastic card which has multi-layer images that are arranged to be alternately visible at different viewing angles [41].

(3) High resolution imaging based on X-ray holography. The basic principle is that of in-line holography in combination with X-rays which produce a clear image at an atomic scale for the imaging of structures in the micrometre range. X-ray holography used at the atomic scale was proven by research by producing a hologram of atoms in the bulk of crystals [42, 43].

2.4 Conclusion

This chapter has briefly described the major types of optically recorded hologram i.e. in-line and off-axis, their mathematical description and some of the applications to which the technique can be applied. Chapter 3 will discuss the computer generated holography (CGH). We will present the detour phase and the kinoform techniques of generating the hologram digitally. Also, will study the Gerchberg- Saxton algorithm and some of the CGH applications. The last part of the chapter will illustrate the iterative Fourier transform hologram and we able to run the MATLAB™ code reconstruct the origin image and controlling its quality by applying different number of iterations.

3 CHAPTER 3

3.1 Computer Generated Holography

Introduction

In 1965, Lohmann and Brown coded a hologram by using the computer [44], which they later called a Computer Generated Hologram (CGH). The first application was in applying the CGH as spatial filter. There is great motivation for producing a CGH. For instance, the CGH technique can be applied as the interferometric prototype for testing a complex optical surface during its manufacture. The recording process is made by computer and this will resolve any problem in the optical recording process such as: illumination coherence; vibration; or air turbulence. However, the main advantage for synthesising holograms is the fact that the object no longer needs to be physically present. As already mentioned, computer generated holograms have been used in spatial filtering experiments. Optically, there is always a problem to produce a reliable spatial filter with a high function efficiency. The CGH solved most of these difficulties which arise from complex division and other mathematical operations difficult to perform by optical and photographic methods. A binary transmittance pattern has been used instead of the sinusoidal fringe pattern of a classical hologram (i.e. an optically recorded hologram).

For producing the CGH, we need four steps. First, we calculate the complex amplitude that results from the wavefront propagation from the object to the hologram plane. We have to consider the computer limitations and thus the calculated amplitude should be computed at a finite number of sampling points. Secondly, we encode the interference pattern as a simulation of the interference pattern made by interaction of the reference and object beams, as in the case of the conventional holograms.

The last two steps are just to make the artwork and to change the hologram to the right size and lastly to just printing or displaying the hologram image. The CGH created from the sampled computed data would then allow reconstruction of the optical wavefront.

Computer Generated Holography (CGH) deals with the technique that we use for producing the hologram digitally. In the holographic reconstruction, the recording hologram can be printed on a film or loaded onto a Spatial Light Modulator (SLM) [45].

The CGH is a very flexible technique. First, a physical object is not needed. Thus the three-dimensional objects do not have to exist in the real world. In other words, for encoding we can use just the mathematical description of the object. Second, there are different encoding techniques that have been developed for fitting various display devices and reconstruction methods. In this chapter, we first discuss some of the classic techniques of generating a CGH (the Detour-Phase hologram and Kinoform techniques) and then we review some modern methods of generating CGHs such as: the Iterative Fourier Transform Algorithm (IFTA) and the Phase Conjugation technique. These have very fast calculation times and a better quality of reconstructed image. Also, we describe the coded mask technique for an object (Lena image), considering different sizes and associated random masks.

3.2 The Detour - Phase

It is possible to use a gray scale output device to produce this type of hologram. However, it is easier to produce the hologram if we change the amplitude transmittance of the hologram to have two levels only i.e. zero or one and the hologram produced is then called a binary hologram. The first hologram created using this technique was called the detour phase hologram (DPH) and constructed without using a reference beam. To construct the detour - phase hologram, we have to apply first the discrete Fourier transform of the complex amplitude in the object plane. The complex amplitude of the object has to be divided into $N \times N$ cells. These cells correspond to the $N \times N$ coefficients of the discrete Fourier transform of the complex amplitude in the object plane. There is a single transparent area within the corresponding cell that represents each complex Fourier coefficient. The size of this transparent area is calculated according to the modulus of the corresponding Fourier coefficient. The position of the area within the cell represents the phase of the Fourier coefficient. Thus the detour - phase technique derives its name from the idea that the transparent area shifts in each cell to record the phase information at that sampled location in the plane of the hologram [46, 47].

The detour - phase method is the simplest technique that we can use to produce a computed hologram. It is based on making the transmittance of the hologram to have only two levels either zero or one. The hologram that is made by this technique known as a binary detour - phase hologram.

We calculate the phase to find the position of the cell, and in each cell we make an aperture with an area proportional to a_{mn} . The principle of the detour-phase hologram is that we can control the phase of the light by slightly shifting the centre of the aperture. Figure 3.1(a) shows the detour - phase binary hologram and Figure 3.1(b) shows the cell description. The open aperture size is $p_{mn} \times q_{mn}$ and is shifted by a_{mn} along the x-direction, as shown in the Figure 3.1 (b). The binary hologram can thus be expressed by:

$$H_b(x, y) = \sum_{m,n} \text{rect}\left(\frac{x-x_m-a_{mn}}{p_{mn}}, \frac{y-y_n}{q_{mn}}\right) \quad (3.1)$$

MATLABTM code was written to generate a detour - phase binary hologram. We use 16×16 pixels to construct each cell and each hologram has 64×64 cells. There are 1024×1024 pixels in this hologram [48]. We have the ability to control the structure of the hologram by using a different number of pixels and a different number of cells. Most of the energy will concentrate on the zeroth-order and that will produce a very poor quality hologram. To avoid this problem, we use a random - phase mask together with the object to flatten the object spectrum.

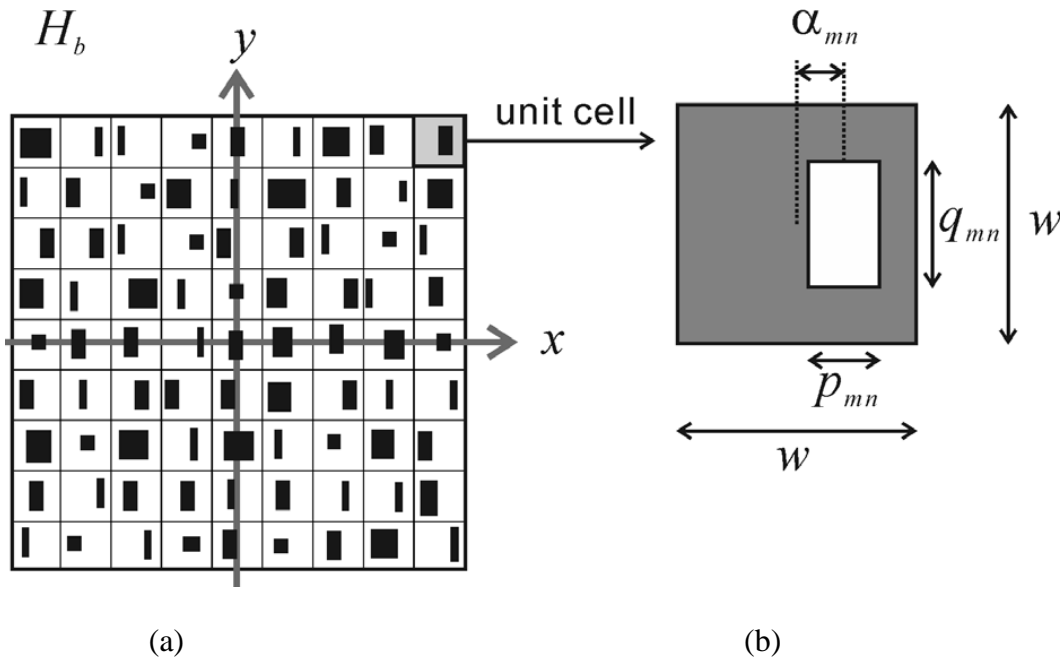


Figure 3.1: (a) the detour-phase binary hologram; (b) the cell description

We generate a detour phase CGH. In this hologram, we construct a cell by employing 16 pixels and each hologram consists of 64 cells. The total pixels in each hologram can thus be found by multiplying the number of the pixels by the number of the cells i.e. the total number of pixels in the hologram generated is 1024×1024 .

3.2.1 The Detour - Phase Hologram with Random Mask

The Figures 3.2, 3.3, and 3.4 illustrate our first attempt at making a detour - phase CGH. In this case we use a random phase mask. To make the image spectrum almost uniform, a solution is to allocate to images an artificial random phase component. In the binary hologram, as previously shown, we have to encode the object wavefront amplitude and phase. Displaying the image will represent only the amplitude of the image, however.

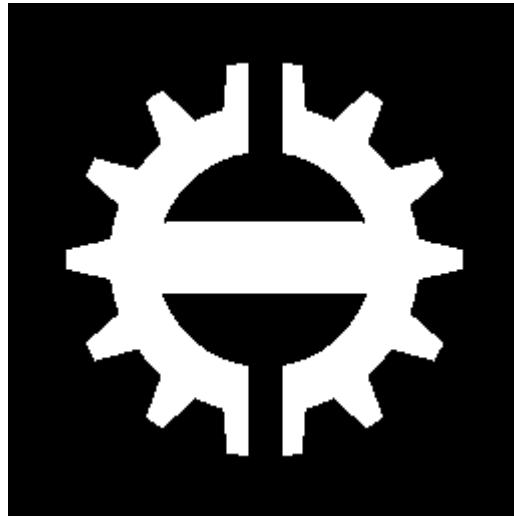
Thus we cannot use visual observation to determine the object wavefront phase component. However, the object wavefront phase affects the object spectrum. There is always distortion of the object's hologram in the recording stage because of the limitation of the hologram dynamic range and the quantisation. Using a random phase mask is the simplest way to distribute the object wavefront phase. This process makes the Fourier spectrum of the object more uniform over all of spatial frequencies. We use MATLABTM code to show how the random phase distribution enhances the reconstructed holographic image. Figures 3.2, 3.3, and 3.4 showing the detour phase CGH with a random phase mask.

In our MATLABTM code, we quantized the modulus of the object wavefront to 16 levels. The phase of the object wavefront was quantized first to 8 levels, shown in Figure 3.4.

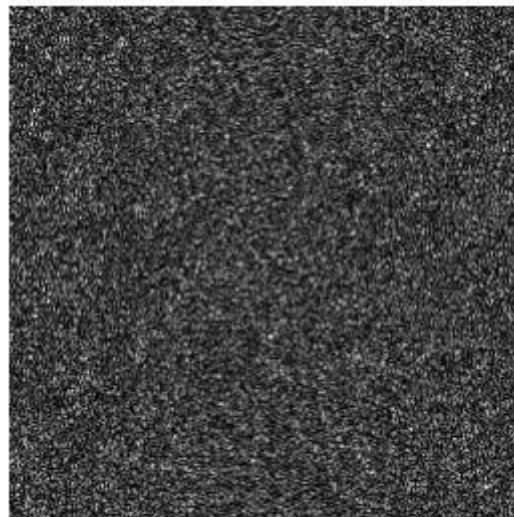
The size of each cell is $p_{mn} = 9$ pixels. To represent the modulus levels we choose the dimension of each aperture as $q_{mn} = 1 \sim 16$ pixels. The 8 levels of the phase in this case is represented by $a_{mn} = -4 \sim 3$ pixels.

Figures 3.2, 3.3, and 3.4 showing the detour phase hologram produced by the MATLABTM code developed. Figure 3.3 shows the hologram and Figure 3.4 illustrates the reconstructed image. The cell grids produce many diffracted orders of light. However, we use only specific diffracted orders of light to match with our calculations. The quality of the reconstructed image is not very high with the basic method. To improve the holographic reconstructed image, improving the diffraction efficiency by using a coding pattern device will be effective in this case.

The main disadvantage of the binary detour phase CGH is that to represent one Fourier coefficient requires a display device with many resolution elements. Even more demanding, three times the display resolution would be required when we record a three-colour separation binary detour phase CGH.



(a)



(b)

Figure 3.2: The Detour-Phase hologram with random phase: (a) the original object; (b) the object spectrum

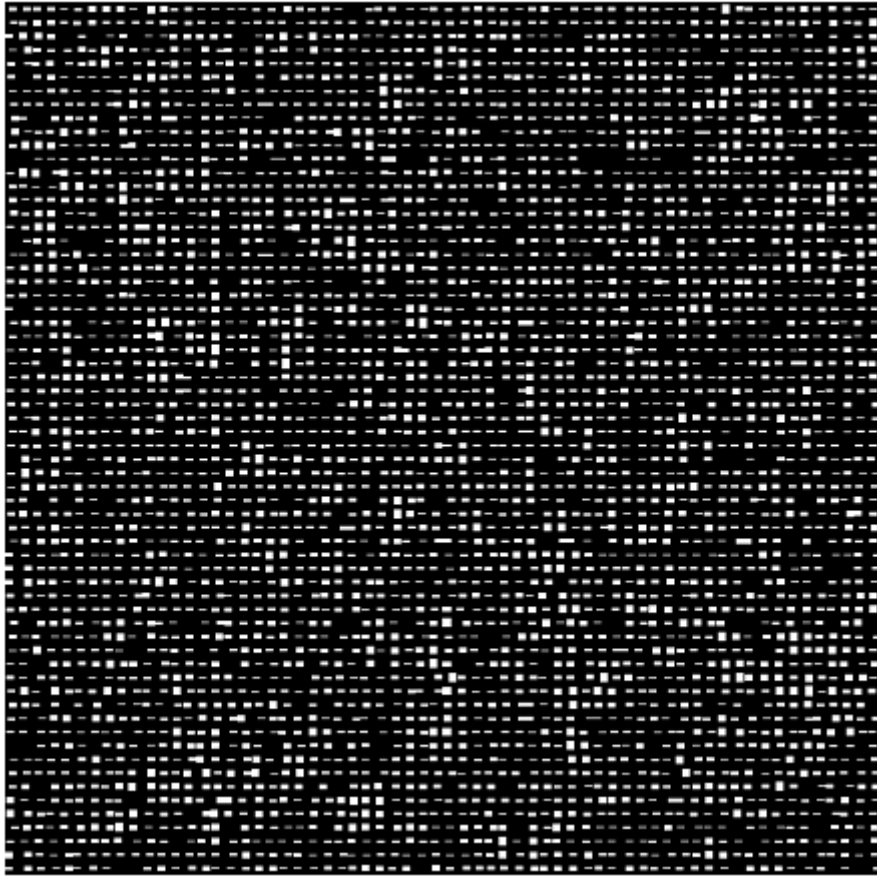


Figure 3.3: The Detour-Phase hologram with random phase: the detour phase CGH

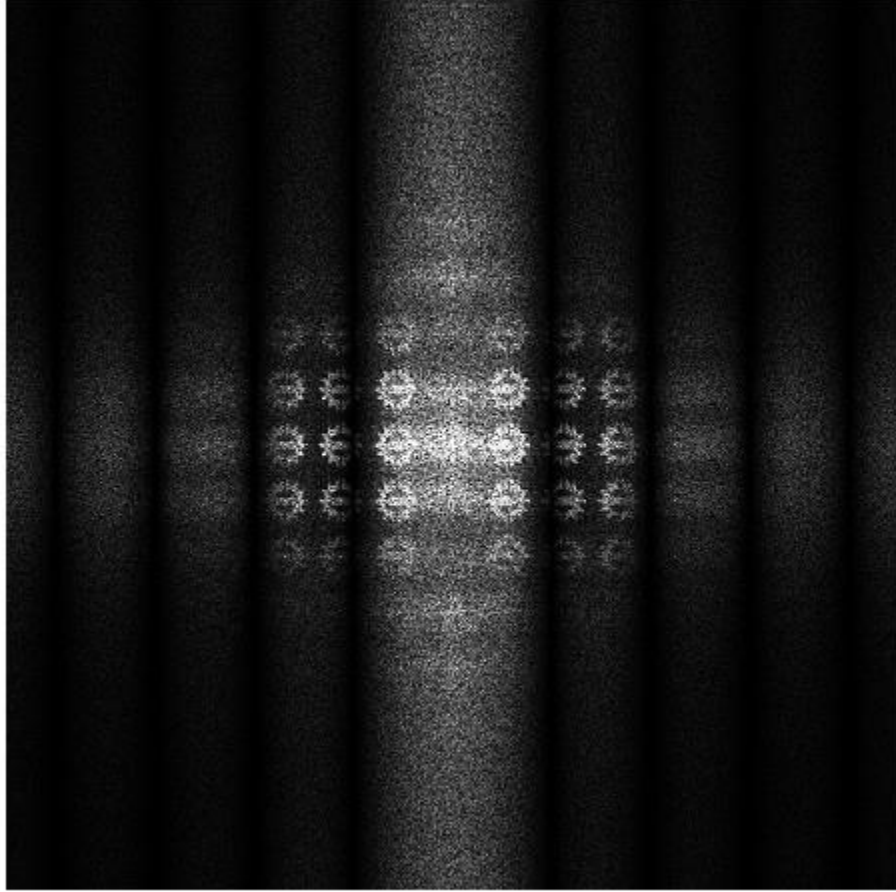


Figure 3.4: The Detour-Phase hologram with random phase: the reconstructed image.

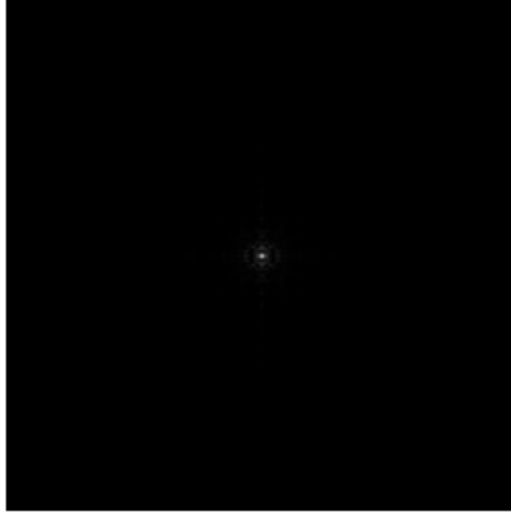
3.2.2 The Detour - Phase Hologram without a Random Phase Mask

Secondly, we attempt to generate the detour phase CGH for the object, i.e. the logo, without a random phase and we have written MATLABTM code to generate the recording process. Also code is used to reconstruct the holographic image. It is easy to notice that the reconstructed image is unclear and distorted because most of the energy is concentrated only in the zeroth - order and the effective dynamic range of the hologram so produced is reduced.

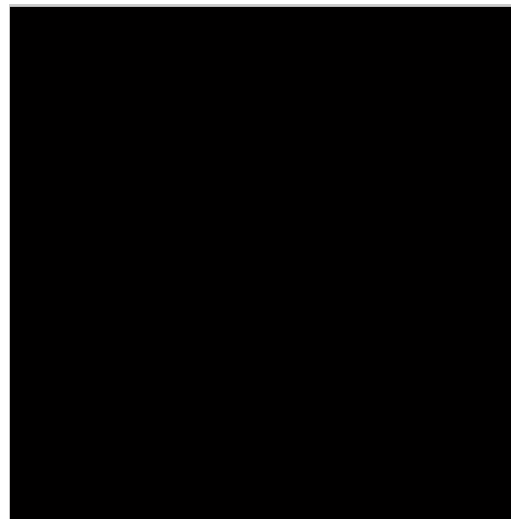
There is not any reconstructed image when we perform the Detour - Phase hologram without using a random phase mask, as most of the energy concentrates into the zeroth-order. We can easily notice that the quality of the reconstructed image shown in Figure 3.4, although not good, is an improvement in comparison with the reconstructed image without a random phase shown in Figure 3.6 (b) which is too weak to be observable.



Figure 3.5: The Detour - Phase hologram without random phase: the original object



(a)



(b)

Figure 3.6: The Detour - Phase hologram without random phase: (a); the object spectrum; and (b) the reconstructed image.

3.3 The Kinoform

As we have seen in the previous section, the detour phase binary hologram technique records a sampled complex hologram and represents the modulus as well as the phase of the original object wavefront which we require to generate a computer generated hologram. The diffraction efficiency is the ratio of the intensities of the desired (usually the plus-first order) diffracted beam and the illuminating beam, measured when both beams are large enough to overfill the area of the detector being used.

The diffraction efficiency of the detour phase technique is relatively low and the quality of the reconstructed image is poor and with a relatively unclear reconstructed image. Thus a new computer generated hologram method is needed to produce a reconstructed image with better quality. The kinoform was next computer generated hologram technique proposed. The kinoform is a computer generated hologram technique in which all the cells are completely transparent. The detour phase hologram technique as well as the kinoform technique are usually based on Fourier transform holography.

The kinoform is a special hologram encoding technique to record a phase-only hologram. It is a computer-generated hologram in which we only record the phase of the object wavefront (the incident wave). The kinoform is computationally faster than the detour-phase and it is unnecessary to introduce the reference beam and consider the image separation calculations when we use the kinoform [49]. The kinoform hologram is classified as a Fourier hologram which we can represent by:

$$H(x, y) = a(x, y) \exp[-i\varphi(x, y)] \quad (3.2)$$

where $a(x, y)$ is the amplitude (i.e. the modulus) of the original object. The modulus should be uniform and so can be ignored in the kinoform technique. The magnitude of the Fourier coefficients are relatively unimportant when the object is diffusely illuminated, and so the object can be reconstructed by using only the values of the phases of the Fourier coefficients.

A random phase mask should be attached to the object pattern to spread the energy across a wide spectrum and thus the modulus of the object wavefront will be uniform and unimportant in making the kinoform CGH. $\varphi(x, y)$ is the object wavefront phase, and is what is used in the kinoform

technique. The phase $\varphi(x, y)$ is thus the only term in Equation (3.2) we need to employ. To display the hologram we generate a gray level representation of the pattern which is proportional directly to the phase function $\varphi(x, y)$. To actually generate the hologram, however, we either employ a phase-only Spatial Light Modulator (SLM) [50, 51] or print the pattern on a photographic film. In the case of the gray-tone which is generated on photographic film, firstly, the pattern should be plotted correctly.

Secondly, the film should be processed by bleaching which is a chemical process that converts an amplitude hologram into a phase hologram. Finally, the phase should be tailored to be between $0 \sim 2\pi$. If we fail to keep the phase in this range, the diffraction efficiency will be reduced and the zeroth order light will appear and this will affect the quality of the reconstructed holographic image.

When not using the random phase mask in kinoform calculation, the reconstructed images from the kinoform are heavily degraded and appear like edge-only preserved images [52]. In addition, the kinoform cannot record a large object that exceeds the kinoform size because the object light does not spread widely. In order to avoid this degradation and to spread the object light more, the random phase mask is applied the kinoform calculation.

In the kinoform hologram, we make a basic assumption by forcing the modulus $a(x, y)$ to a constant value. We can then re-write Equation (3.2) as:

$$H_p(x, y) = \exp[-i\varphi(x, y)] \quad (3.3)$$

The diffraction efficiency of the kinoform hologram can be very close to 100% because there is only one diffraction order from the kinoform hologram (i.e. it diffracts all the illumination it receives into a single diffraction order). In this technique, we do have to however keep phase retardation between 0 and 2ρ radians, as mentioned above.

A MATLABTM code was written to generate a kinoform hologram. To do this, first we have to calculate the complex field of the object, then we extract the phase from the complex field so we can display only the phase. Figures 3.7 and 3.8 showing a kinoform with a random phase mask

and Figures 3.9 and 3.10 showing a kinoform without the random phase mask. In this case, even without random phase mask, we still obtain a reconstructed image.

The main advantage of the kinoform computer generated hologram over the detour phase computer generated hologram is its ability to diffract all the incident light into the final image. However, we have to accurately keep the phase-matching condition.

If we fail to satisfy the phase-matching condition we will end up with light that is diffracted into the zero order which can distort the reconstructed image.

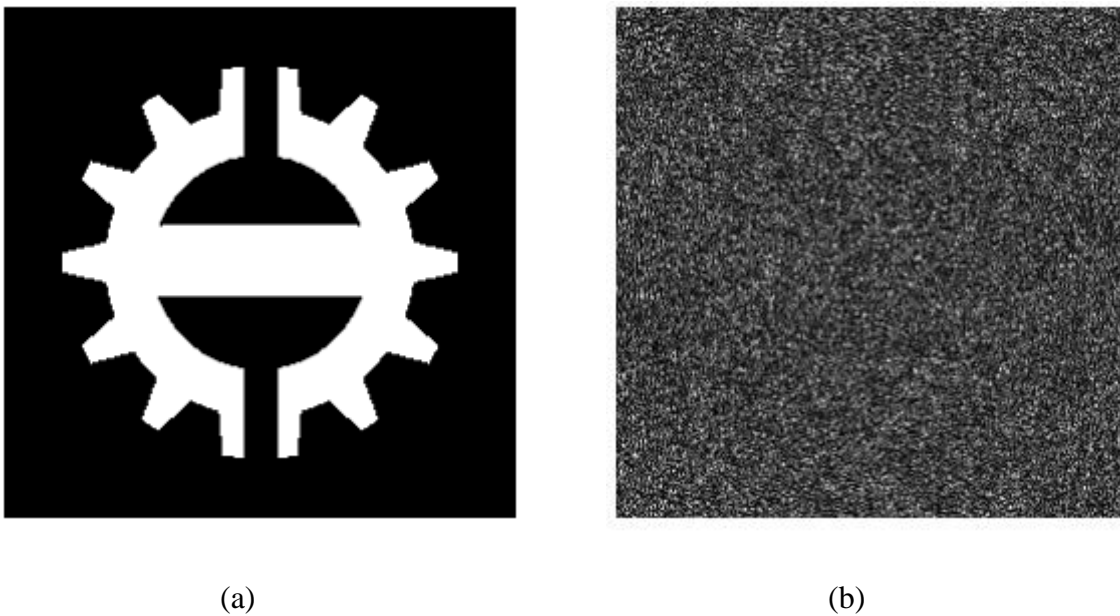
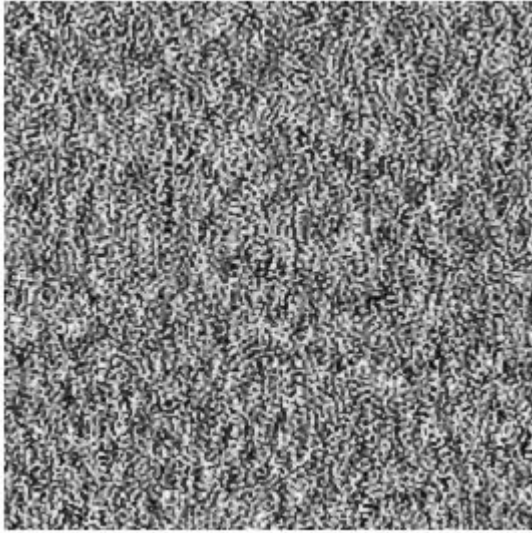
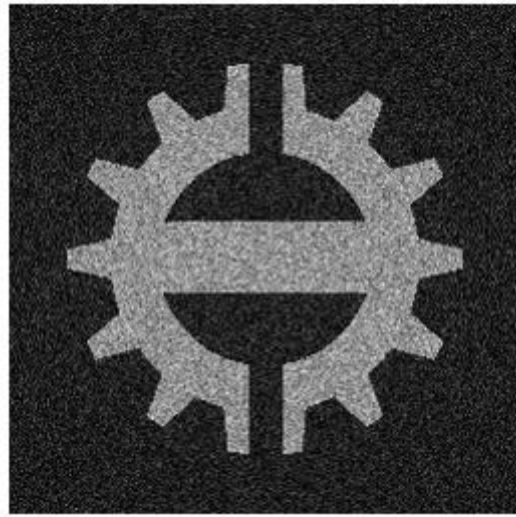


Figure 3.7: The kinoform hologram with a random phase mask (a) the original object; and (b) the spectrum modulus



(a)

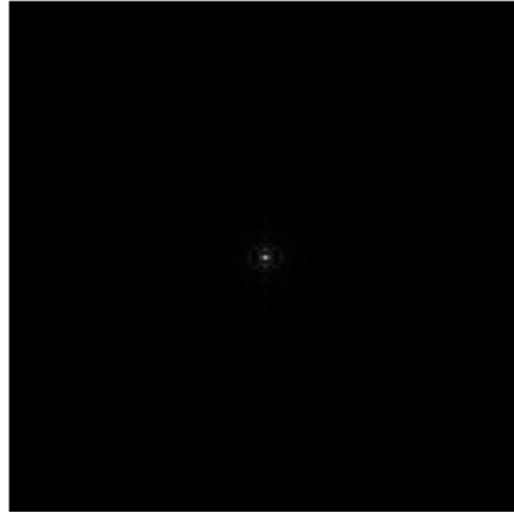


(b)

Figure 3.8: The kinoform hologram with a random phase mask: (a) the spectrum phase; and (b) the reconstructed image.



(a)



(b)

Figure 3.9: The kinoform hologram without a random phase mask: (a) the original object; (b) the spectrum modulus

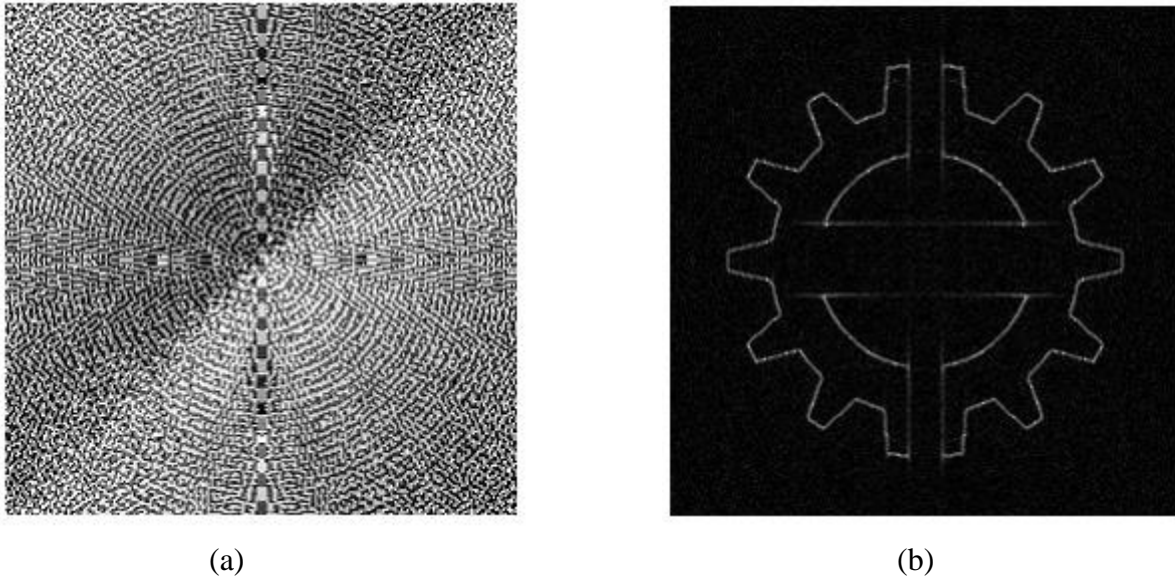


Figure 3.10: The kinoform hologram without a random phase mask: (a) the spectrum phase; and (b) the reconstructed image.

3.4 The Gerchberg-Saxton Algorithm

It is very noticeable that the kinoform reconstructed image has some noise corruption [53]. To optimize the computer-generated phase only Fourier hologram we have to use an iterative Fourier Transform Algorithm (IFTA) and so we use the Gerchberg - Saxton algorithm (GS) to implement the IFTA technique.

The GS algorithm is an iterative algorithm to solve the problem of phase retrieval at two different planes, when at those planes only the field amplitudes are known and given that the fields are related by a Fourier transform [54]. We need to know only the phase distribution from one of the planes, and the phase distribution on the other plane can be found by performing the Fourier transform on the plane at which the phase is known. Figure 3.11 shows the Gerchberg-Saxton algorithm (GS) in diagrammatic form. The GS algorithm is an iterative algorithm [55] and in each iteration cycle the following steps are performed:

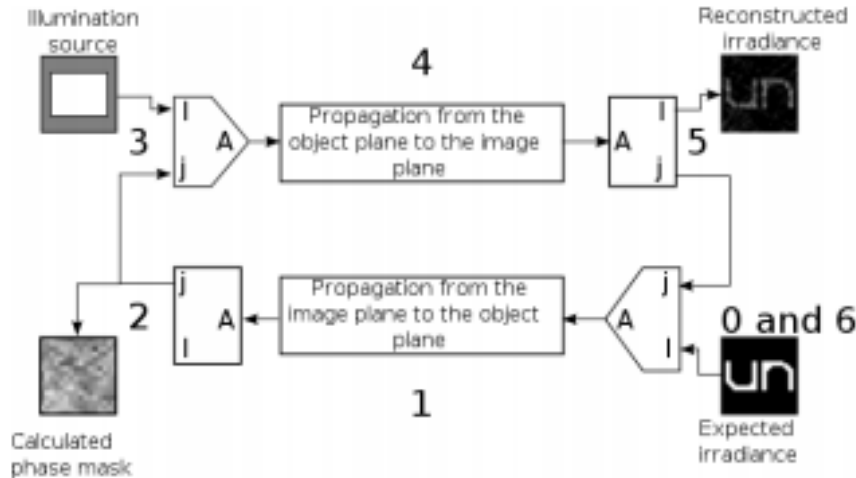


Figure 3.11: The Gerchberg-Saxton Algorithm [56]

0. At the beginning, a field with an amplitude given by the square root of the expected irradiance and a constant phase is taken.
1. The field is propagated from the image-plane to the object-plane.
2. The amplitude information is discarded, leaving only the phase information (for the phase mask).
3. The amplitude and phase of the illumination field are added to the phase information to obtain the resulting object field.
4. The field is propagated from the object plane to the image plane.
5. The resulting reconstructed image (square of the field amplitude) is compared with the expected one. By using the correlation between both images as a criterion, a decision is taken to finish the process or continue iterating.
6. The phase from the reconstructed image is combined with the field amplitude obtained from the expected irradiance, and the process is repeated from step 1

The principle of making a phase-only hologram is that the amplitude of the reconstructed image must be proportional to the desired amplitude distribution which when it produces a small error

represents the condition to stop the iterative process. We use the root mean square error (RMSE) criterion between the reconstructed field and the desired field to control the iteration process. The RMSE decreases at each iteration and will be minimum when both amplitudes are equal.

Figures 3.12 and 3.13 showing the result produced from application of the GS algorithm to the kinoform design.

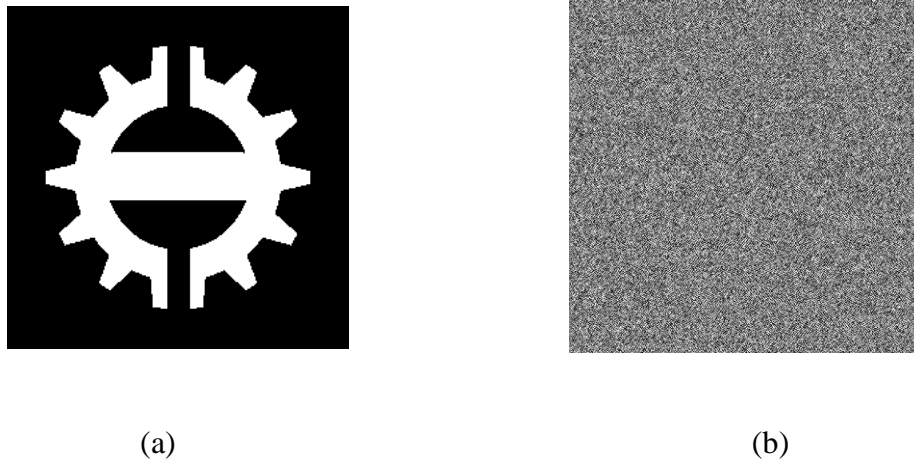


Figure 3.12: The Gerchberg-Saxton algorithm result: (a) the original object; (b) the spectrum phase

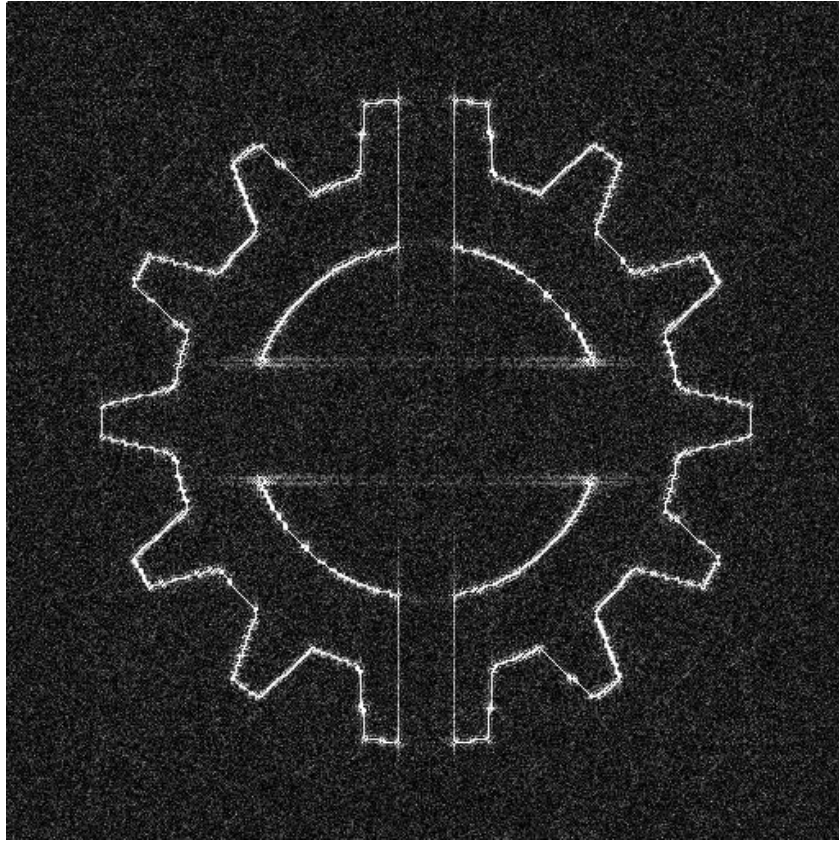


Figure 3.13: The Gerchberg-Saxton algorithm result: the reconstructed image.

3.5 Applications of Computer-Generated Holograms

Holography is a method that is based on interference and diffraction phenomena of visible light. Holography is used to record the 3D information of the object into a hologram and reconstruct the 3D image of the original object. Holographic optical elements (HOEs) are one of a number of very important applications of holography.

The HOE is a holographic mirror which was developed by Denisjuk in 1962. After this Schwar *et al.* in 1967 used the hologram as a lens. The HOE is thus mainly used to replace heavy and complicated optical elements which can be a mirror, lens or directional diffuser. One of the best

advantages of the HOE is that it can perform many functions with a single material. Thus HOEs are used in many fields like holographic projects, holographic memory and holographic printing.

3.5.1 Basic Concept of the HOE

The HOE can be a lens, mirror or filter and is made by using the holographic process. The concept of the HOE is that there are two beams, i.e. the object and reference beams which make an interference pattern in the recording material. The interference pattern of the two beams (object beam and the reference beam) records the information of the original object. In case of the original object as a lens, the interference pattern of the two beams will reconstruct the optical element that has a function of a lens.

HOEs can be classified into two main types: thin and volume HOEs. The efficiency of a thin HOE is very low because the incident light beams are diffracted in different directions. Also, the incident angle affects the diffraction efficiency thus a small change of angle will change the diffraction efficiency. On the other hand, the volume HOEs have a high diffraction efficiency. Also, HOEs can be classified into transmission and reflection types depending on the geometry of the recording.

HOEs have many advantages for use in current real life applications. The main application of HOEs is in constructing an optical system that is more efficient and lighter than a conventional optical system. This feature is making diffractive optics to be commonly used in many industrial fields. The large improvements in computing power in recent years is making computer generated holograms and the binary optics very interesting subjects for further research.

3.6 The Iterative Fourier Transform Hologram

When we reconstructed the image of the kinoform hologram there was still some noise even though the kinoform hologram image is better than the detour-phase hologram [57]. We used the Gerchberg-Saxton algorithm to improve the image reconstructed by the kinoform hologram. First we load an object (e.g. a camera acquired image), which has an amplitude distribution $A(x,y)$. The amplitude of the reconstructed image must be proportional to the desired amplitude distribution $A(x,y)$ which we can summarise by [58-60]:

$$F\{H_p(x,y)\} = F\{e^{-j\tilde{f}(x,y)}\} = A(x,y)e^{-jq(x,y)} \quad (3.4)$$

where $\tilde{f}(x,y)$ is the phase of the hologram, and $q(x,y)$ is the phase of the reconstructed light which expresses the hologram as a phase-only hologram. To improve the quality of the reconstructed image we apply a phase mask to the input pattern to widen the spectrum of the object. We thus apply the Fourier transform to the initial field (input pattern) which will be transformed to the spectral domain.

In this hologram technique we have two constraints. The first one is that the spectrum modulus after Fourier transform should be uniform. We make the spectrum modulus unity without affecting its phase. After this we apply the inverse Fourier transform to the modified spectrum to take it back to the space domain. Then we apply the second constraint in the spatial (space) domain by making the modulus of the field equal to $A(x,y)$ without altering its phase. The next iteration will take this field $A(x,y)$ as the initial field. After we take the FFT and we will get a new modulus and we apply the constraints. The iteration process will stop when we achieve the goal of making the amplitude $A(x,y)$ the modulus of the field without changing its phase.

A MATLABTM code was written to enhance the kinoform hologram, Appendix C. Figure 3.14 as the initial field, the Lena image, and Figure 3.15 shows using the root-mean square error (RMSE) to show the relation between the RMSE and the number of iterations. In this code, we use a total number iterations of 100. From the Figure 3.15 we can see that the RMSE becomes very small with an increasing number of iterations.

Figure 3.16 shows the reconstructed image when the number of iterations is equal to 100. Figure 3.17 and Figure 3.18 showing same procedure when the number of iterations is only 10. We can easily see the difference between Figure 3.14 and Figure 3.18 (b). The image reconstructed by using 100 iterations appears clearer and has less noise.



Figure 3.14: Iterative Fourier transform hologram (number of iterations = 100): the original object

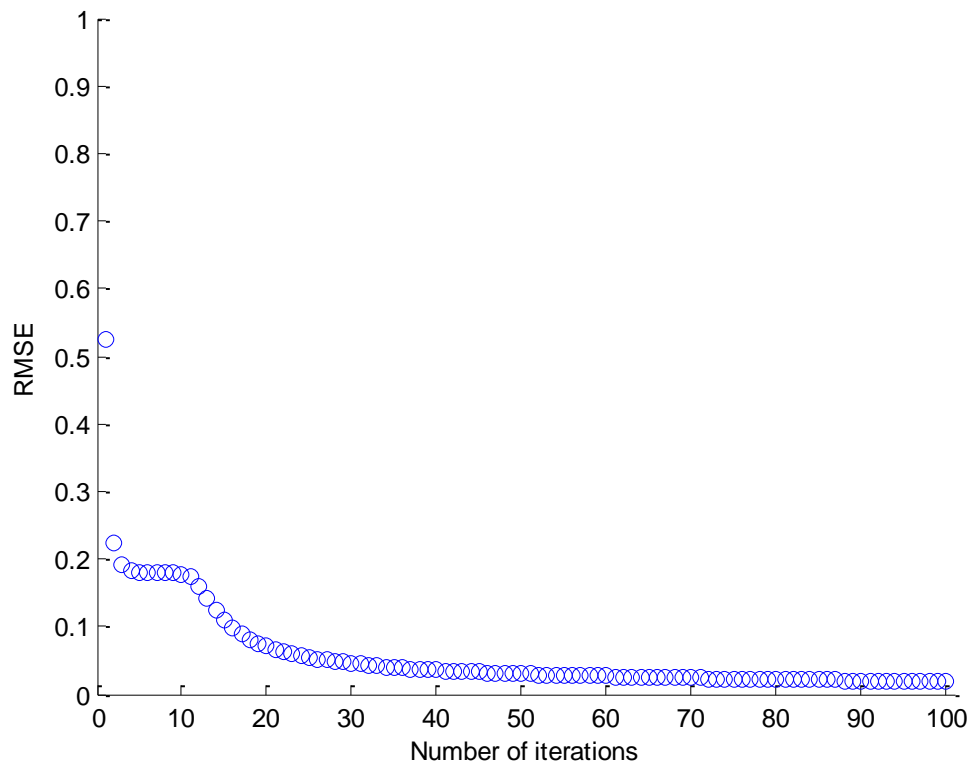


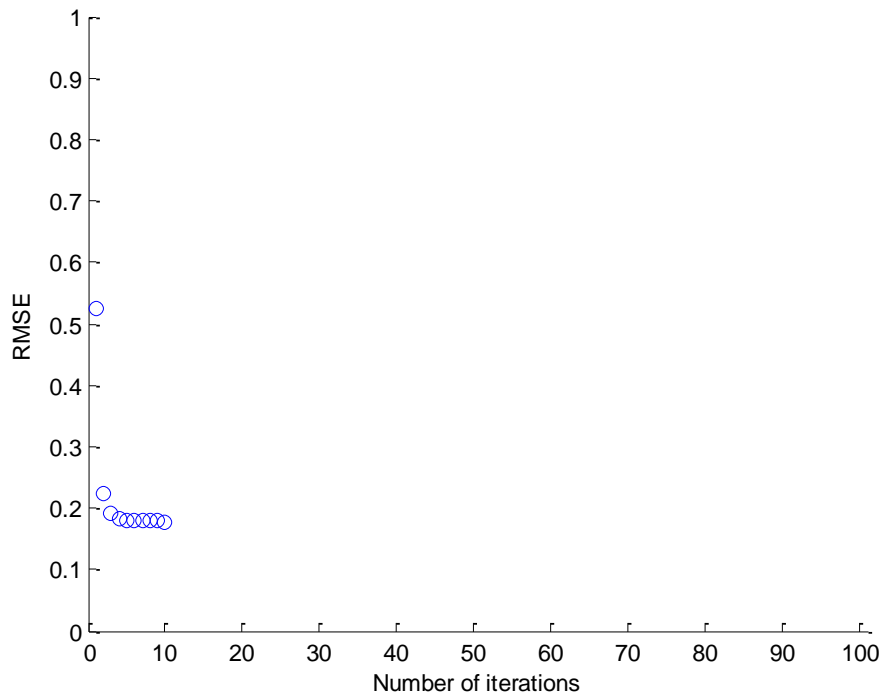
Figure 3.15: Iterative Fourier transform hologram (number of iterations = 100): the RMSE with number of iterations



Figure 3.16: Iterative Fourier transform hologram (number of iterations = 100): the reconstructed image.



Figure 3.17: Iterative Fourier transform hologram (number of iterations = 10): the original object



(a)



(b)

Figure 3.18: Iterative Fourier transform hologram (number of iterations = 10): (a) the RMSE with number of iterations; and (b) the reconstructed image.

3.7 Conclusion

CGHs are used in optics and can be applied in many fields such as: 3D television; diffractive optical elements; projection and encryption. The CGH can be classified into three types: complex amplitude CGHs; amplitude CGHs; and kinoforms. The kinoform CGH also called a phase-only CGH. The complex amplitude CGH reconstructs a high quality image but always needs an extra device which is enable to display the real and imaginary parts of the object beam. In the case of the amplitude CGH and kinoform CGH we take only either the real part or the argument part of the object light and so therefore there is no need for a special display device (SLM phase only) capable of full complex modulation of the wavefront.

The light efficiency of the kinoform CGH is as high as 100% and always better than the light efficiency of the amplitude CGH. This explains why the image reconstructed by the kinoform CGH is a brighter image as compared to the amplitude CGH. Furthermore, the kinoform reconstructed image has no conjugate reconstructed wavefront, which can cause a problem in the amplitude CGH reconstruction.

The kinoform CGH usually has a random phase applied to the original objected random phase diffuses the object light widely and this is very important in the recording stage of the kinoform CGH. The reconstructed image will be very degraded if we ignore using the random phase. The main disadvantage of using the kinoform technique is the size of the original object should not exceed the kinoform size. If the object is larger than the kinoform it will not be fully recorded as some its beam will spread outside of the recording area.

Despite using the random phase to solve the two problems, i.e. the edge enhancement of the reconstructed image and the narrow spreading of light, the reconstructed image will still suffer from speckle noise. There are many iterative techniques to improve the speckle noise of the reconstructed image such as the Gerchberg-Saxton (GS) algorithm, multi-random phase technique, one step phase retrieval technique and the pixel separation technique. The main disadvantage of using these techniques is their time-consuming nature because they involve many diffraction calculations. The random phase mask is a very useful technique to enable the reconstruction of a clear image. However, this technique cannot be used for a large object and three dimensional display as the reconstructed image should not exceed the kinoform size.

4 CHAPTER 4

4.1 Reconstruction the Quadratic Phase from the Modulus of its Fourier Transform

Introduction

We can reconstruct the original object, including the Fourier phase when only the Fourier modulus is given, provided we have known constraints on the area of support in the reciprocal domain. In a Computer Generated Hologram (CGH) we can record almost any wanted phase distribution, contrary to optical holographic recording. We can use the iterative Gershbarg-Saxton (GS) technique to recover unknown phase distributions and the iterative Fourier transform algorithm (IFTA) is also used to reduce the noise in the reconstructed image.

One of the most important applications in digital holography is the synthesis of diffractive optical elements which are used to transform a given distribution of the light from one field distribution into another with the desired features. In the case where both the amplitude and the phase of the output distribution are of interest, the diffractive optical elements (DOE) must be capable of full amplitude and phase control. However, in the case where only the intensity of the output is required, the DOE can be constructed as a pure phase structure of the kinoform type.

The iterative FT algorithm (IFTA) is a technique which is used to improve the reconstructed holographic image. Recently, double constraint IFTA has been developed [61, 62]. In this algorithm, the desired phase and amplitude distribution are constrained in the image field in each iteration [63-67]. The main benefit of using the IFTA is to eliminate speckle noise. The reconstructed image will be affected by a speckle noise [68-71] because of the phase fluctuation between adjacent sampling points [72].

The process of the IFTA involves light distribution being propagated between two planes. For a 3D object reconstruction, this must thus be sliced first into many layers. The IFTA is thus applied between the hologram plane and each layer of the object. This will be time consuming and the iterations may not converge to reconstruct the original object.

In this chapter, we apply an iterative Fourier transform algorithm (IFTA) to generate digital holograms from an initial digital image using intensity information only. The algorithm is implemented with our own MATLAB™ code. We discuss an iterative computer method that can

be used to solve many problems in optics. This technique we use can be applied to two types of problems: (1) we use the Fourier transform pair having desirable properties in both domains, and (2) reconstruction of a point source object when there is only partial information available in any one domain. The benefit of the first method is to reduce the quantisation noise in the reconstructed image. A reconstruction problem appears when only partial information is measured or certain constraints are known *a priori*. The information available in any one domain is insufficient to reconstruct the object or its complex Fourier transform. Both the synthesis and the reconstruction problem can be expressed as follows when there is a set of constraints placed on an object and another set of constraints placed on its Fourier transform. We can then find the Fourier transform pair that satisfies both sets of constraints.

4.2 Light Point Source

The setup of recording a point source [73-77] hologram is shown in Figure 4.1 and Figure 4.2 from which we can observe that the holographic recording can be extended for an object by recording multiple point objects since any object can be considered as a collection of points.

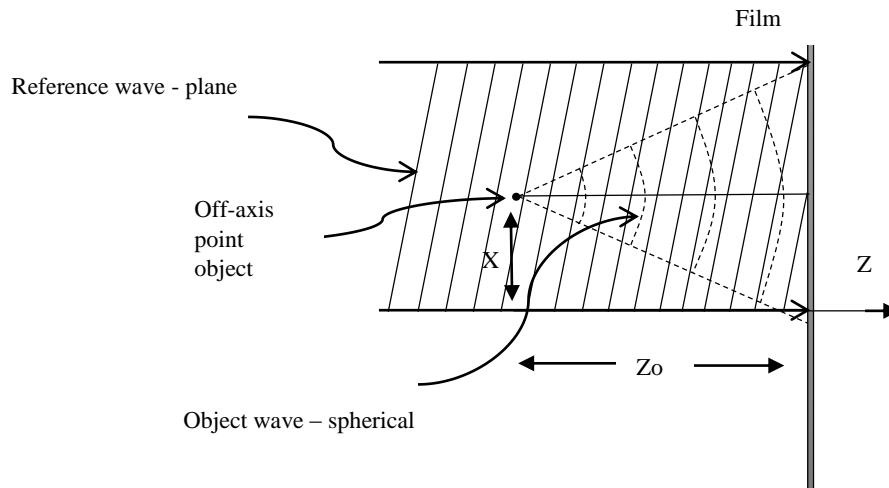


Figure 4.1: Recording stage of off-axis hologram

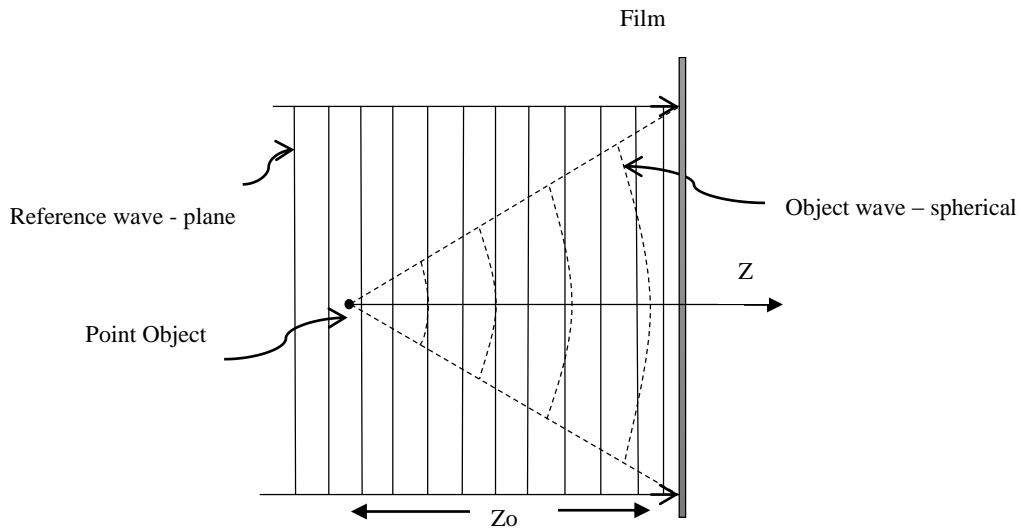


Figure 4.2: Recording stage of in-line hologram

To generate the Fresnel zone plate (FZP) [78], the point source hologram, the distance between each pixel of the FZP and the point source need to be considered. We calculate the phase of the wavefront according to the distance between the point source (the original object) and the hologram.

The phase on the hologram is the combination of both phases; the object origin phase and the reference plane wave phase. The phase of the object wave varies periodically within a range between $0 - 2\pi$ with the distance between the point source and the hologram. In the reconstruction stage, the object wave interferes with the reference plane wave. The plane wave is a normal wave which is constant across the plane of the hologram, therefore we only consider the phase of the object's wave.

4.2.1 In-Line Hologram

We start development of our code by constructing the Fresnel Zone plate (FZP) as shown in Figure 4.3. We construct many examples of the FZP by choosing different distances z_0 between our object (the point source) and the hologram (the photographic plate). In these figures a 0 to 2π phase shift is represented as a grey-level value, zero to black.

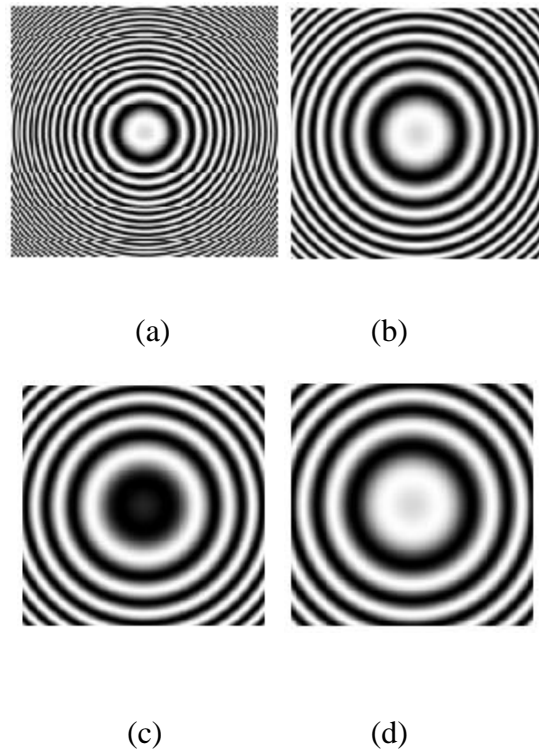


Figure 4.3: On-axis Fresnel zone plate as a function of point source distance, z_o : a) $z_o = 2mm$, b) $z_o = 5mm$, c) $z_o = 8mm$, and d) $z_o = 10mm$

4.2.2 Off-Axis Hologram

Now the point source moves to a new place which is shifted from the (x_o, y_o) location and the centre of the zone plate translates accordingly. Therefore the FZP contains the complete 3D information of the point source. Figure 4.4 shows the off-axis FZP which represents the hologram of the point source.

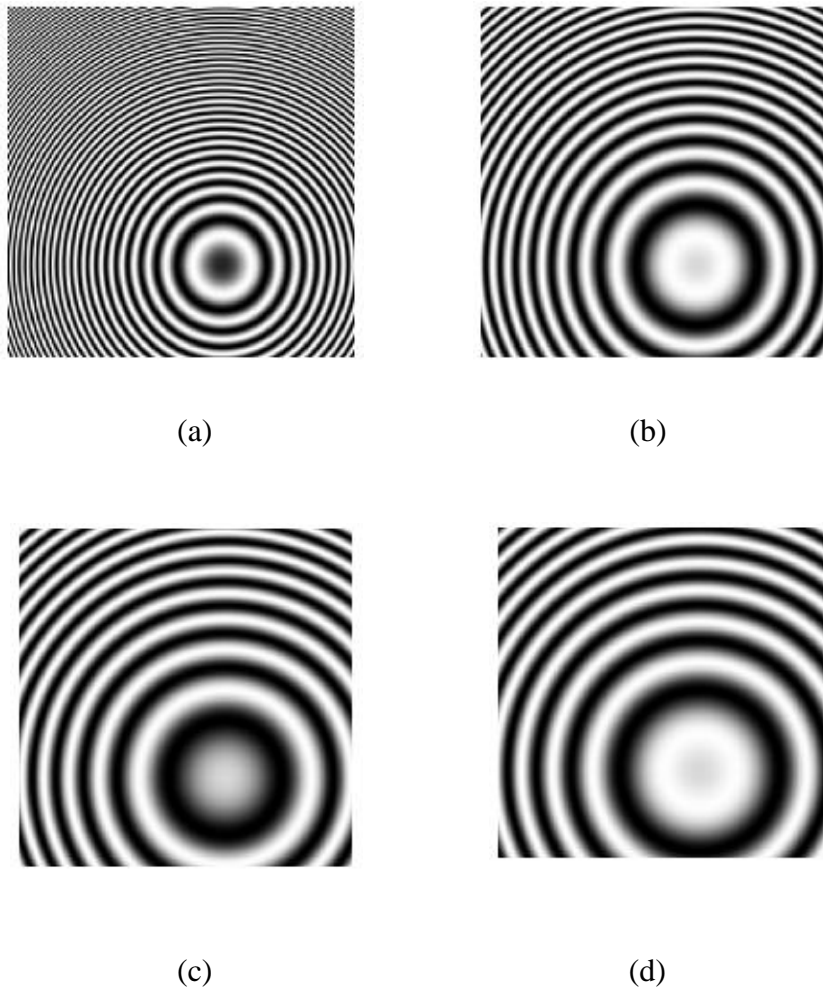


Figure 4.4: Off-axis Fresnel zone plate as a function of point source location, z_o : a) $z_o = 2mm$, b) $z_o = 5mm$, c) $z_o = 8mm$, and d) $z_o = 10mm$

4.3 The MGSA algorithm and the random phase effect

Thus far we have covered the process of transformation of the point source object into a zone plate and this step is identified with the recording stage of the hologram.

We then take the Fourier transform of the diffraction pattern recorded on the hologram to produce a complex spectrum.

We sample the input image, as part of the sampling Fourier transform procedure. The number of frequencies in the Fourier domain corresponds to the number of pixels in the image domain, i.e. the array in both domains has the same size. We thus sampled the image in two dimensions as, $M=256$, and $N=256$ pixels.

As the image is relatively large we use the fast Fourier transform (FFT) [79-81] to compute the spectrum efficiently. The spectrum is a complex array. It can be displayed as real and imaginary arrays, or as magnitude and phase. We are only interested in the phase information i.e.:

$$phase = angle(I(x, y)) \quad (4.1)$$

where $I(x, y)$ represents the FZP (point source hologram) array, and $angle$ is the phase of the array elements. We use a random phase [82-86] to reduce the dynamic range in the image intensity. We use different random phases which are listed in Table 4.1 and we show the results of using only the first two.

Table 4.1: Random Phase

Type	Expression
Random phase	$random\ phase \exp(-j\pi * random())$
Random phase	$random\ phase = \exp(-j\pi * \frac{random()}{256})$
Random phase	$random\ phase = \exp(-j\pi * \frac{random()}{2512})$
Random phase	$random\ phase = \exp(-j\pi * \frac{10*random()}{512})$
Random phase	$random\ phase = \exp(-j\pi * \frac{50*random()}{512})$
Random phase	$random\ phase = \exp(-j\pi * \frac{1000*random()}{512})$

The first random phase we use is:

$random\ phase = \exp(-j\pi * random())$ and the reconstructed intensity distribution is shown in the Figure 4.5. Figures 4.5 and 4.6 show the intensity of the original point source. The difference between the two figures is because we use initially different random phases and even if we subtract the random phases they still have an effect on the reconstructed intensity of the original point source.

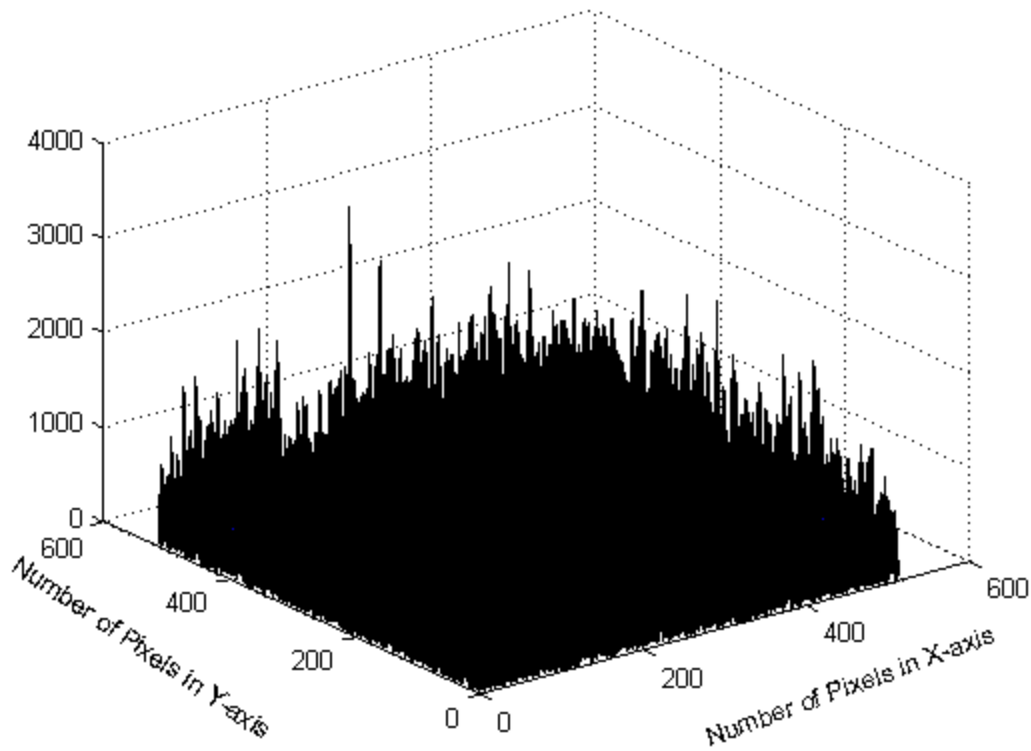


Figure 4.5: Intensity at z_0 for the random phase: $random\ phase = \exp(-j\pi * random())$

Where we use the second uniform random phase with uniform distribution which is $random\ phase = \exp(-j\pi * random()/256)$, the reconstructed image intensity is altered as shown in Figure 4.6.

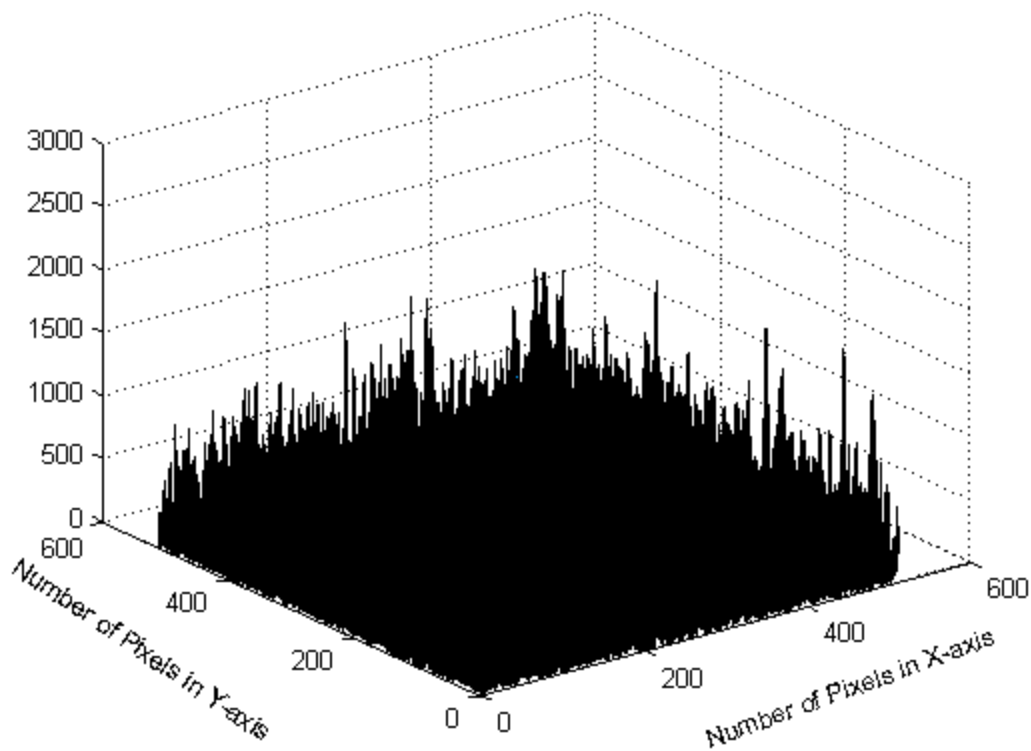


Figure 4.6: Intensity at z_0 for the random phase: $random\ phase = \exp(-j\pi * random()/256)$

In the next step we add the initial phase to the original image phase i.e.: ($phase + random\ phase$). During our simulations with the MATLABTM code, we determined that the quality of the final hologram and the reconstructed image depend on which the initial phase we use.

A random phase is added to the binary object before calculating its 2D FFT, in order to achieve uniform amplitude in the Fourier plane. This random phase has no impact on the reconstructed image, as the human eye and a camera (along with any other optical detector) are sensitive to the squared modulus of the wave, not its phase. The idea for this particular method, like others, comes from what we normally think of as holograms, and it does not work for objects with low light scattering. The wave from the object has to be spread across a large area of the hologram, so

experimentally we would place a finely ground glass plate in its trajectory, just in front of the object plane.

We then apply the Fourier transform (FFT) for the sum of the two phases i.e: $SEF = \mathcal{F}(\text{phase} + \text{random phase})$.

The propagation algorithm we used in this project is a fast Fourier transform (FFT) propagation. It is based on the Gerchberg-Saxton iterative phase retrieval algorithm [87-95] and the Figure 4.7 showing the modified Gerchberg-Saxton algorithm (MGSA). We will consider the steps of Figure 4.7 in the next section.

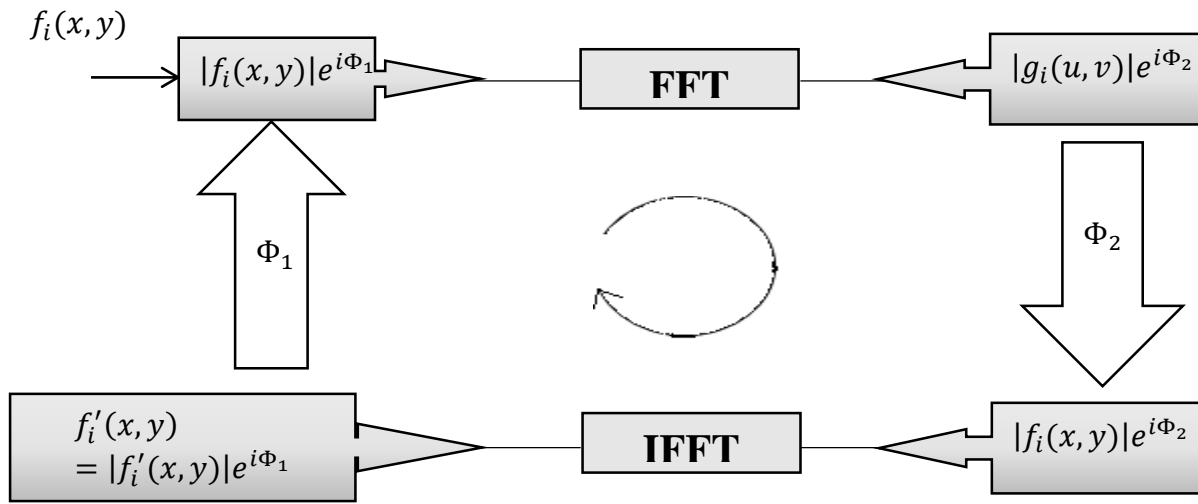


Figure 4.7: General calculation algorithm of a MGSA in the Fourier domain

We initially consider only the modulus of the field since the phase can be ignored in this step:

$$f_i(x, y) = \text{abs}(SEF) \quad (4.2)$$

This modulus forms the input to our error reduction iterative transform algorithm.

4.4 Error – Reduction Algorithm

First, we modified the Gerchberg Saxton algorithm (MGSA) to solve our specific problem. We use our reduction algorithm which is shown in Figure 4.7. The object which is the point source is a real and nonnegative function. We set up constraints in both the spatial domain field and the frequency domain field. At the i^{th} iteration, an estimate of the object $f_i(x, y)$ is obtained which is an estimate of the original object. We set up the iterative algorithm by marking the iteration number. The phase retrieval problem consists of estimating the phase of the complex-valued function from measurements of its modulus and additional *a priori* information.

The first successful reconstruction method for phase retrieval using the GS iterative algorithm was for a different problem, i.e. reconstructing signals from intensity information only. We consider the situation where we have only the intensity of our object (the point source). The magnitude function is going to be the constraint function of our iteration algorithm. We thus modified the GS algorithm to solve the current problem.

Firstly, we decided to reconstruct the binary amplitude FZP which is an array of zeros, the black areas, and ones which are the white areas. The reconstruction of the binary amplitude FZP is studied in detail in the next section.

4.5 The Iterative Method

There are many iterative methods, with a number of useful variations existing. We use the MGSA algorithm which was originally used to solve reconstruction problems in electron microscopy [96, 97]. The MGSA we use is a succession of Fourier transforms which is made between the hologram and the reconstruction spaces while the required constraints in each domain are imposed. The constraint in the object plane implies that the transmission function is real and positive. We modified the GS algorithm so it can be applied to the current problem.

We use the error-reduction approach to reconstruct the phase of the FZP. Each iteration of the algorithm we use consists of the following four steps as shown in Figure 4.7:

Step 1: Fourier transform (FFT) the first estimated modulus of the object:

$$\mathcal{F}[f_i(x, y)] = g_i(u, v). \text{ We are already introduced } f_i(x, y) \text{ in the Eq.4.2}$$

Step 2: apply the known constraint in the Fourier plane; replace the magnitude of the resulting computed Fourier transform $|g_i(u, v)|$ with the measured magnitude $|f_i(x, y)|$ to form a new estimate of the Fourier transform.

Step 3: Inverse Fourier transform (IFFT) the estimate of the Fourier transform.

Step 4: Replace the magnitude of the computed signal $|f'_i(x, y)|$ with the measured signal modulus $|f_i(x, y)|$ to form a new estimate of the signal.

We calculate the root mean square error (RMSE) to assess the quality of the resulting reconstructed image of the hologram. We need to calculate the RMSE in the Fourier (frequency) domain. The RMSE is the cumulative squared error between the iterated and original image. The formula for the RMSE is thus:

$$RMSE = \frac{1}{MN} \sum_{y=1}^M \sum_{x=1}^N [|g_i(u, v)| - |f_i(x, y)|]^2 \quad (4.3)$$

where $|f_i(x, y)|$ is the modulus of the original image, $|g_i(u, v)|$ is the modulus of the approximated version after the i^{th} iteration, and M, N are the dimensions of the images. A lower value for RMSE means less error and hence a more accurate reconstruction.

In Figure 4.6 it can be seen that the input is $f_i(x, y)$ and the output is $f'_i(x, y)$. The iteration process should stop when $|f_i(x, y)| \approx |f'_i(x, y)|$ i.e. with the measured modulus approximately equal to the computed modulus.

We calculate the RMSE equal to only 0.5759 for the case where the random phase is $random\ phase = \exp(-j\pi * random())$ but it is equal to 0.6389 when we apply the random phase ($random\ phase = \exp(-j\pi * random()/256)$). Clearly, the uniform distribution for the random phase is preferable.

4.6 Results of Applying the Iterative Reconstruction

Firstly, we try to reconstruct the binary FZP examples which are strictly transparent or opaque (1 or 0). Figure 4.7 shows our first binary FZP where $z_o = 0.5 \text{ mm}$ is the distance from the point source to the film.

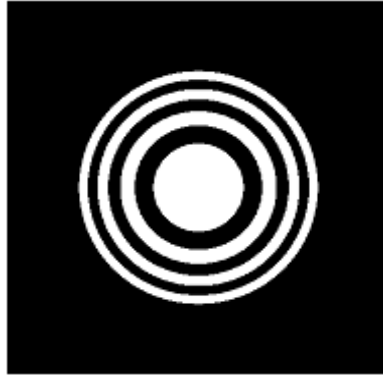


Figure 4.8: Binary FZP, $z = 0.5 \text{ mm}$

The binary FZP, as shown in the Figure 4.8, is a series of concentric ring-shaped zones of radii

$$r_n = r_1 \sqrt{n}, n = 1, 2, 3 \text{ which alternately absorb or transmit radiation.}$$

In the next step, we Fourier transform the diffraction pattern. This models the propagation through space where the light carries with it information on the amplitude and phase structure of the source. The amplitude and phase information can then be examined in the Fourier plane. We are only interested about the phase of the original object and Figure 4.9 illustrates the original phase after Fourier transformation.

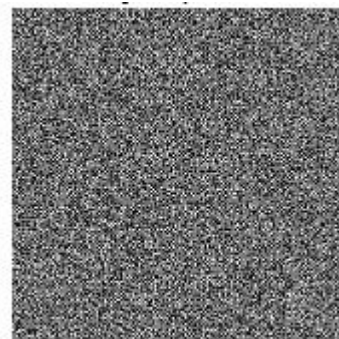


Figure 4.9: The original object Fourier plane phase

In the next step we add the random phase to our computed phase. Addition of random phase to the object wavefront is required in computer-generated holograms (CGHs) to widely diffuse the object light and to avoid its concentration on the CGH. Figure 4.10 shows an example of the random phase we employed which is a uniform distribution from 0 to 2π

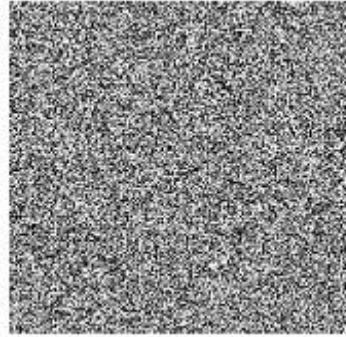


Figure 4.10: Example random phase function

This is now the addition of the two phases which is then Fourier transformed and results in the distribution shown in Figure 4.11. the intensity distribution is shown in Figure 4.12.

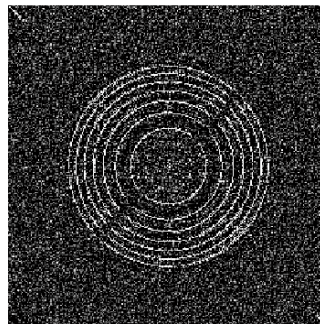


Figure 4.11: Phase distribution (represented as a grey-level) of the Fourier transform of the Fresnel pattern plus random phase distribution

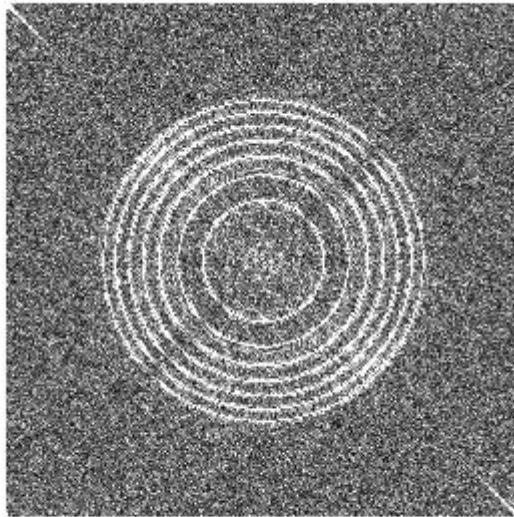


Figure 4.12: The intensity distribution of Figure 4.11

4.7 The Iterative Method

The GS iterative algorithm that we use is an example of a general class of iterative algorithm, and is described in terms of alternating projections onto convex sets.

We are using the iterative method to help us to solve our problem by reconstructing the original object from only the intensity information. The iterative technique uses a succession of Fourier transforms between the object and reconstruction spaces while the required constraints in each domain are imposed. This iterative process can converged to a stable solution, although slowly in our case.

The main principles of using the error reduction approach is to reconstruct the quadratic phase when only both moduli are known (i.e. the modulus of the complex valued image and the modulus of its Fourier transform) and the phase is unknown. This is the process for the phase hologram that we mentioned earlier for which we use MGSA (the modified GS algorithm) to reconstruct the phase by using the iterative process. For a reconstruction problem, only partial information is available and we have only the modulus of the combination.

Thus $f_i'(x, y)$ is the complex function in the object domain. A measure of the progress of the iterations, and a criterion by which the reconstruction error can be quantified, is defined already in Eq. 4.3. When the RMSE is near zero, then the object and its Fourier transform satisfy all the constraints, and a solution has been found.

We use MATLAB™ code to calculate the relation between the RMSE and the iteration number, Appendix D. Figures 4.13, 4.14, and 4.15 show the results for 10, 50, and 100 iterations, respectively.

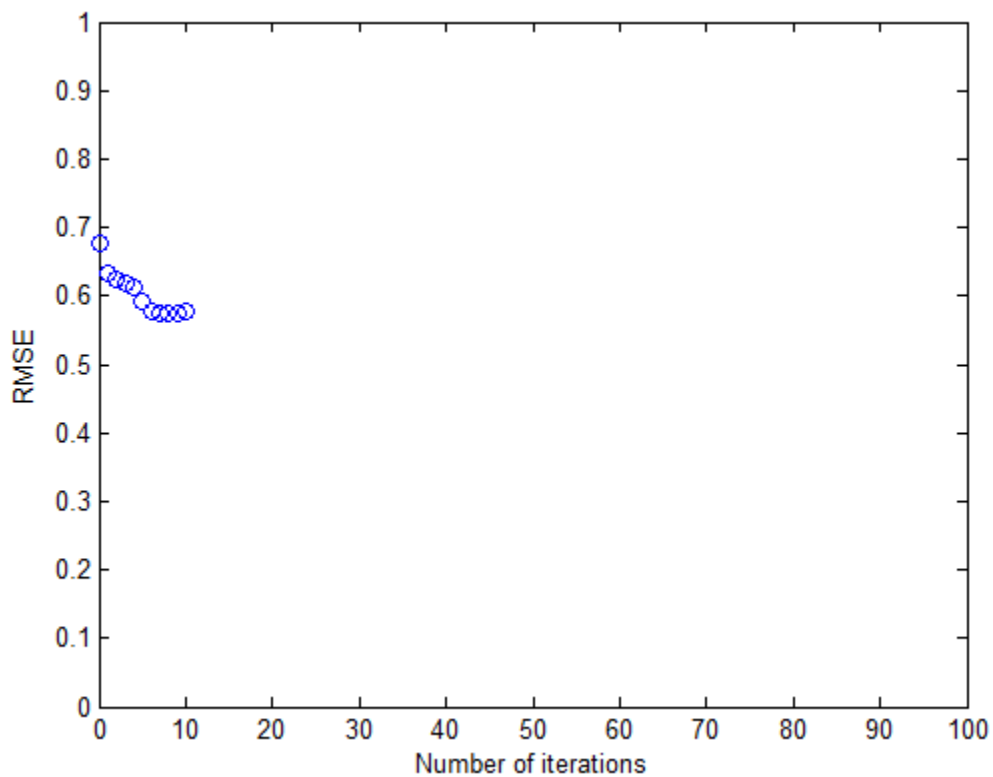


Figure 4.13: RMSE as a function of the number of iterations: 10 iterations

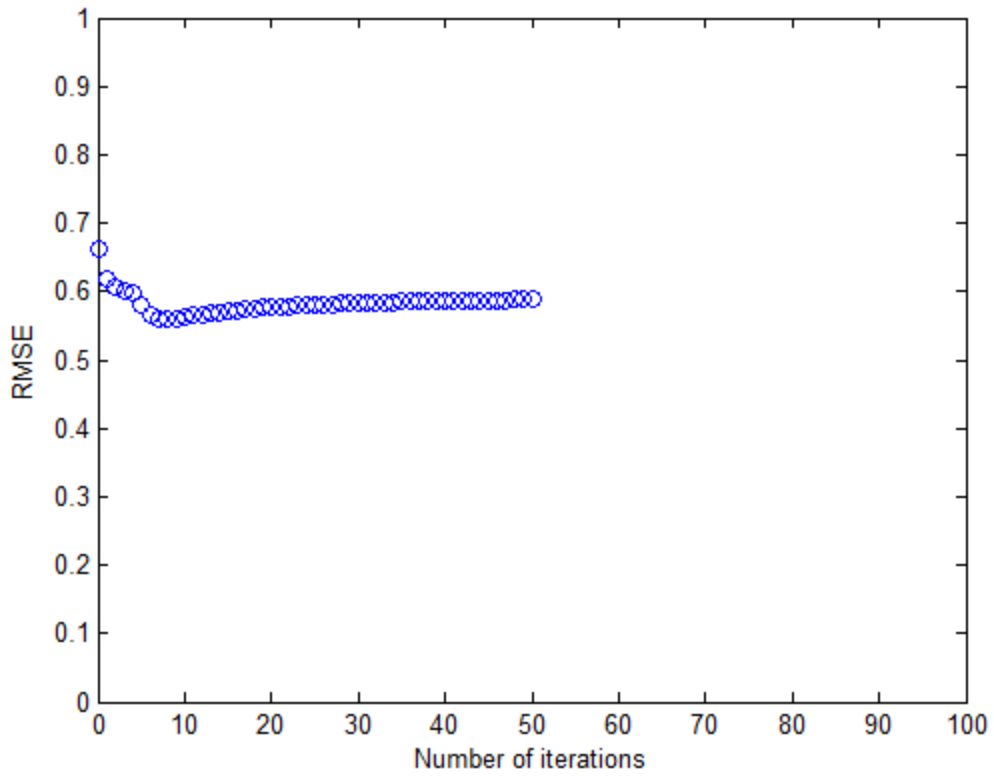


Figure 4.14: RMSE as a function of the number of iterations: 50 iterations

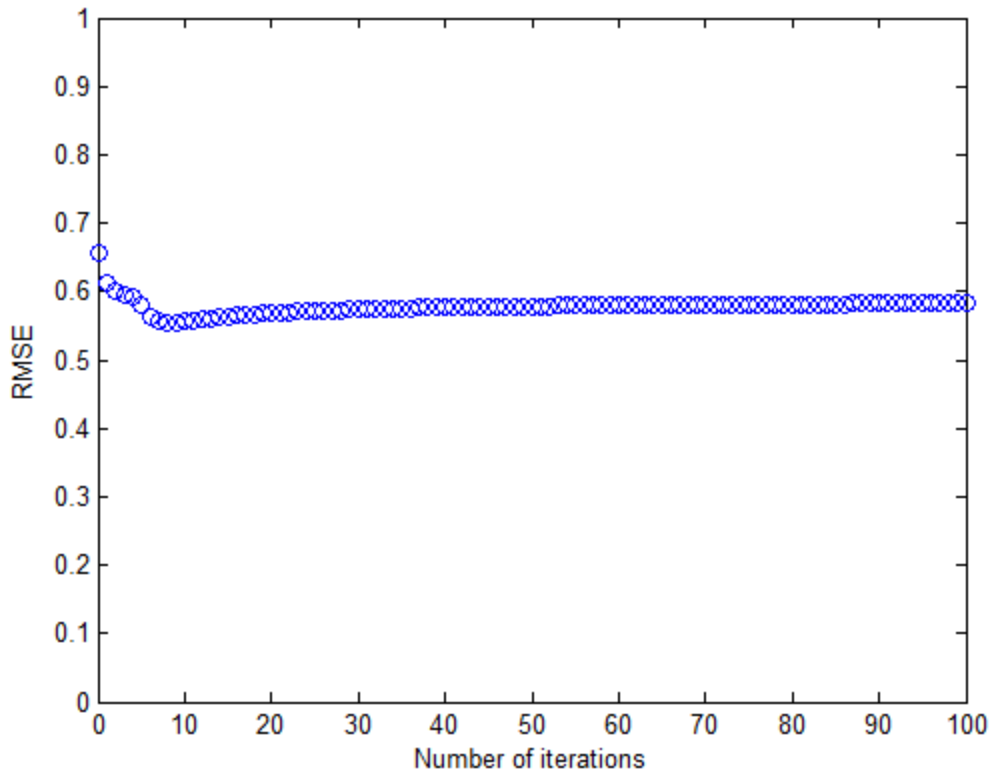


Figure 4.15: RMSE as a function of the number of iterations: 100 iterations

Figures 4.14 and 4.15 are clearly shown that the error is reduced very rapidly for the first few iterations but more slowly for later iterations.

The iterations thus make small changes by enforcing the intensity constraint. The phase will be the phase produced by the Fourier transform in the previous iteration step which is then the input of the next step in the iteration algorithm.

After the iteration has finished, we need to subtract the random phase from the phase combination. We have to subtract the random phase, which is not needed anymore, as we need to reconstruct the phase of the original object.

Figures 4.16 and 4.17 illustrate the resulting phase obtained. We run the program for a different number of iterations as shown below.

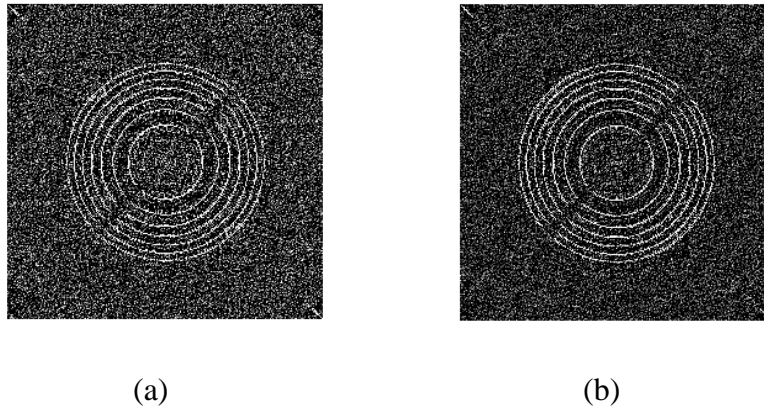


Figure 4.16: Phase produced after a number of iterations: (a) 3, (b) 10 iterations

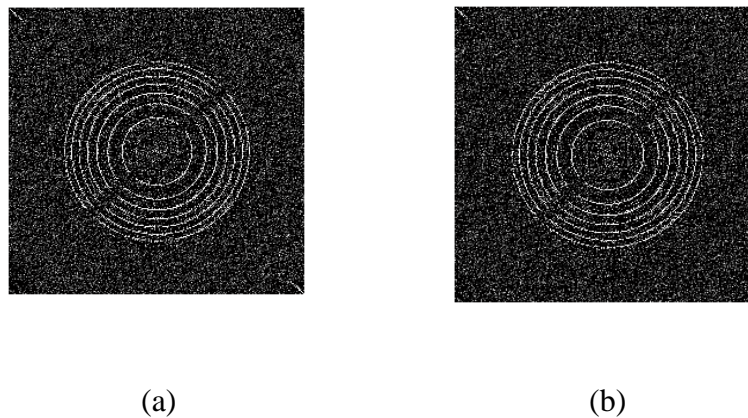


Figure 4.17: Phase produced after a number of iterations: (a) 50, (b) 100 iterations

As shown in Figures 4.16 and 4.17 we reconstruct the combination of the phases (the original phase and the random phase). In the next section we try to enhance these images by using averaging and median filters.

4.8 Image Enhancement

The main purpose of the image enhancement we conducted is to improve the visible appearance of an image for human perception or further computational analysis. One of the techniques used for image enhancement is filtering. In this project, to enhance the phase produced after the iterations, we use two filters (mean and median filters) to try and filter out the noise.

4.8.1 Mean Filter

We apply the mean filter [98] which is a simple and easy approach that smooth the reconstructed images. The purpose of using this filter is to reduce the amount of intensity variation between one pixel and the next and we thus use it in our project to reduce the noise in the reconstructed images.

The mean filter replaces each pixel value in the reconstructed image with the mean (average) value of its neighbours, including itself. We use a mean filter and Figure 4.18 the reconstructed phase after iteration completion and Figure 4.19 which show the resulting enhanced reconstructed images by using a 3×3 mean filter.

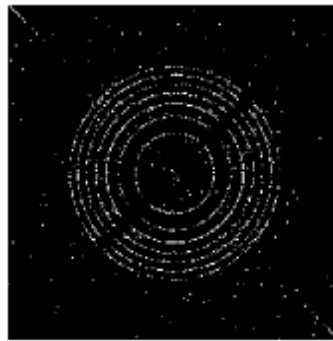
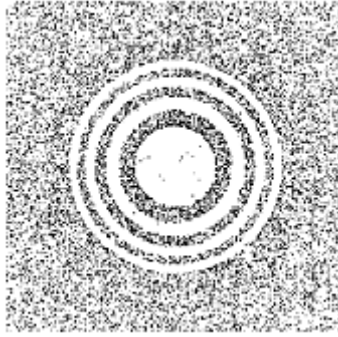


Figure 4.18: reconstructed phase



(b)

Figure 4.19: enhanced image by applying mean 3×3 filter

4.8.2 Median Filter

We use the median filter [99] to reduce the noise in the reconstructed images. This works to preserve the main details of the image. In this filter each pixel in the image is considered in turn and its nearby neighbours decide whether or not it is representative of its surroundings. The median filter thus replaces the pixel with the median of the surrounding pixel values. Figure 4.20 shows the phase produced after the iteration result is enhanced by using the median filter with size 256×256 .

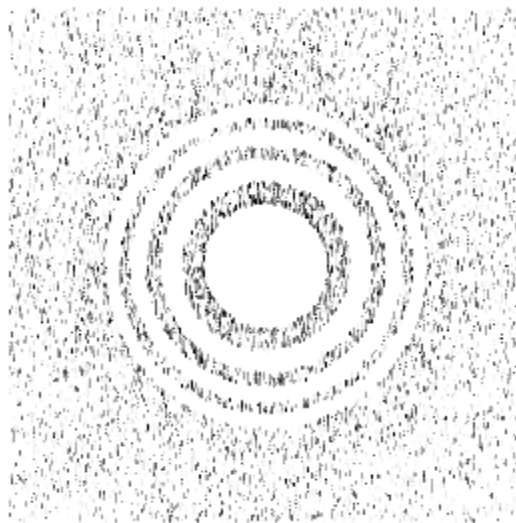


Figure 4.20: enhanced image by applying a median filter of size 256×256

4.9 Propagation of a Point Source

As we discussed earlier, holography is a technique that can be used to record the amplitude and the phase of a light wave and once we know how a single point is recorded, the recording of a complicated object can be regarded as the collection of displaced points. The transformation of a point object to a zone plate on the hologram corresponds to a recording or coding process.

In order to retrieve the point object from the hologram, we need a reconstruction process. We reconstruct our point source by illuminating the hologram with a reconstruction wave. In this work, we used a good learning about rapidly perform phase recovery and reconstruct the complex valued image of the point source. This process is very fast, requiring approximately 10 s in case of 100 iterations. We validate this approach by reconstructing the quadratic phase for different distances. These results are in general applicable to phase recovery problem. The iterative technique is shown that is a very effective technique in solving these problems. The results are attained in the iterative technique could not have been achieved by other method.

As outlined above, holography is a two-stage process. First a hologram is taken and stored digitally. Second, the role of reconstruction in holography is to obtain the 3-D structure of the object from the 2-D hologram on the screen, or, in technical terms, to reconstruct the wave front at the object. The outcome of this step is an image of the original object (the intensity of the wavefront at the object).

In the case of digital in-line holographic microscopy (DIHM) and (also for off-axis holography), we can numerically reconstruct the holograms. We use the numerical reconstruction of holograms in this project, which is based on reconstructing the samples of the object wavefront by using the discrete diffraction transforms. The process of sampling the object wavefront is accomplished by the hologram sampling device and a computer, in which the object wavefront samples are numerically reconstructed from the hologram. Briefly we can state that the reconstruction process is the stage where we compute the wave distribution over a surface as result of a diffraction process. The diffraction is a result of the interaction between the recorded hologram and the reconstruction wave.

4.10 Grey-Level Fresnel Zone Plate (FZP)

The FZP is the hologram of a point source object, leading, as already described above, to the concept that the hologram of an arbitrary 3-D object can be considered as a collection of FZPs.

We first consider the off-axis point source hologram which is the recording the point object at a distance z_o from the recording film. The pinhole aperture is then considered as located at: $(x - x_o, y - y_o)$. The object wave is a spherical wave and interacts with the reference wave which is a plane wave. The interference pattern is recorded on the film and the intensity distribution on the film, the off-axis hologram, can be described by the relation:

$$t(x, y) = A + B \sin \left\{ \frac{k_o}{2z_o} [(x - x_o)^2 + (y - y_o)^2] \right\} \quad (4.4)$$

where $t(x, y)$ is the intensity distribution that is recorded on the hologram, $A = a^2 + (\frac{k_o}{2\pi z_o})^2$, $B = \frac{k_o}{\pi z_o}$, and $k_o = 2\pi/\lambda_o$. Here a is the amplitude of the plane wave (the reference wave). For simplicity, Eq. 4.4 can be written as $t(x, y) = FZP(x - x_o, y - y_o; z_o)$ which represents the sinusoidal Fresnel zone plate (FZP), a hologram of a point source object, for the off-axis situation.

For an on-axis point source, $x_o = y_o = 0$, which is located at a distance z_o away from the film. The on-axis (in-line) hologram (FZP) is then described by the relation:

$$t(x, y) = A + B \sin \left\{ \frac{k_o}{2z_o} [x^2 + y^2] \right\} \quad (4.5)$$

$$t(x, y) = FZP(x, y; z_o) \quad (4.6)$$

Thus a point source located on-axis relative to the centre of the zone plate is specified by the location, x_o and y_o , of the point object. When the point source moves off-axis a sinusoidal spatial variation of the zone plate quadratic phase function is introduced. The first case we consider is an on-axis point source located at $x_o = y_o = 0$. More generally a hologram can be formed of the point source object, located a distance of z_o away from the film.

For the method we are developing, we take the phase of the original object and add a random phase. We then take the Fourier transform of this phase distribution. We decompose the result into the phase and modulus in the Fourier plane. We use the intensity as a constraint and through

application of the iterative algorithm estimate the modulus of the combination of the known random phase and the quadratic phase. The modulus of the phase combination, $f_i(x, y)$, is Fourier transformed, yielding:

$$g_i(u, v) = |g_i(u, v)| \exp[i\phi_2] \quad (4.7)$$

We flow the general flow chart to reconstruct the quadratic phase as shown in Figure 4.21

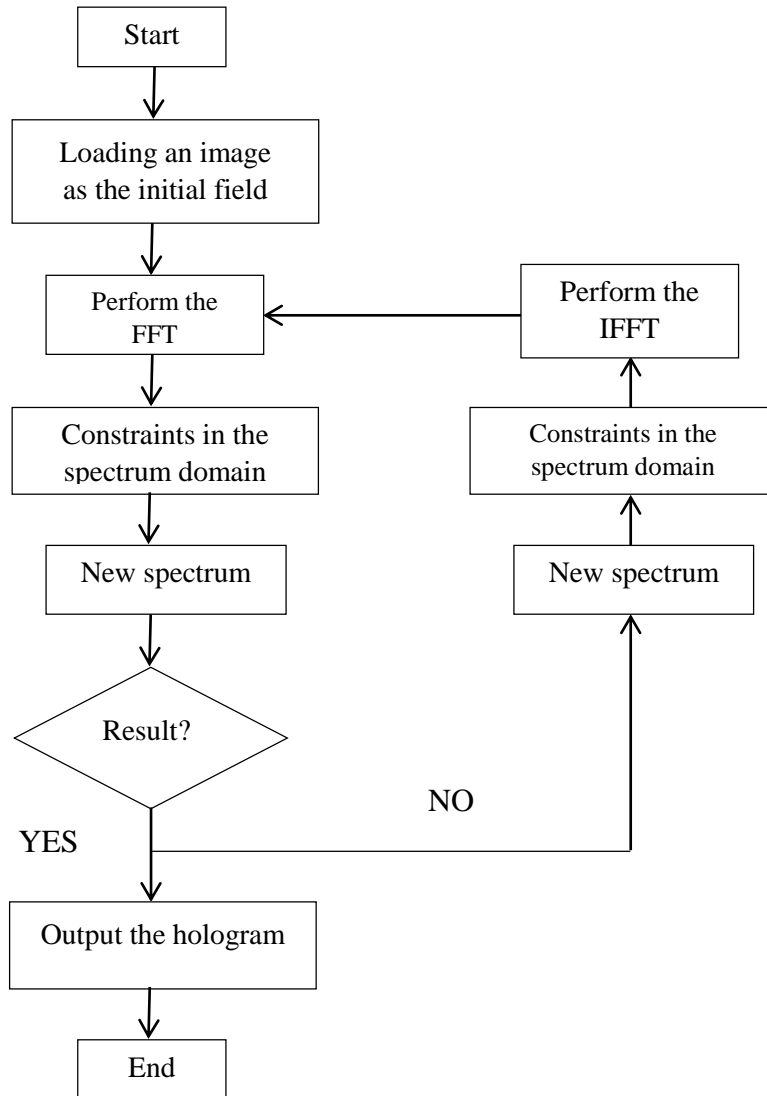


Figure 4.21: Flowchart of the general MGSA

We consider only the phase. We have to make sure that $|g_i(u, v)|$ satisfies the Fourier domain constraints. The new Fourier domain function is $g_i(u, v)$ which is formed from $|g_i(u, v)|$ by making the smallest possible changes in $|g_i(u, v)|$ that allow it to satisfy the constraints. For example, if the Fourier domain constraint is such that the Fourier transform has a modulus equal to $|f_i(x, y)|$, then:

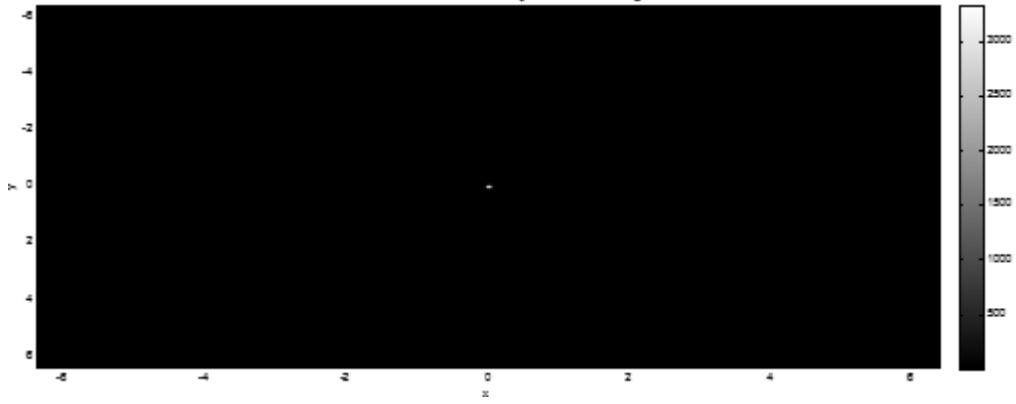
$$g_i(u, v) = |f_i(x, y)| \exp[i\Phi_2] \quad (4.8)$$

That is, the given (or measured) modulus $|f_i(x, y)|$ is substituted for the modulus of $|g_i(u, v)|$ and the phase of $g_i(u, v)$ is left unchanged. The resulting $|f_i(x, y)|$ which satisfies the Fourier domain constraints is inverse Fourier transformed yielding the object domain function, $f'_i(x, y)$. Then the iteration is completed by forming a new function $f_i(x, y) = |f_i(x, y)| \exp[i\Phi_1]$ by making $f_i(x, y)$ satisfy the object domain constraints. The iterations continue until a Fourier transform pair is found that satisfies all the constraints in both domains.

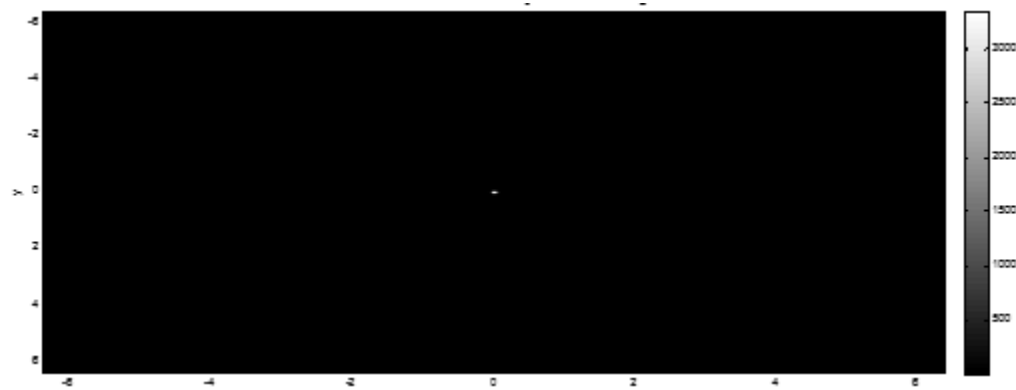
After all the iterations have finished, the reconstruction yields a phase that contains both phases (original object phase and the added random phase). We subtract the (known) random phase and we retain the original phase due to the field in the plane of the FZP originating from the point source.

The next stage is to propagate the phase by a distance z_o away from the hologram to determine the location of the point source in the object plane.

We choose z_o as 0.05, 0.1 mm. The final stage is to calculate and display the reconstructed image of the original object i.e. the point source. This is calculated by Fourier transforming the field distribution at the plane of the FZP. The calculated intensity distribution, i.e. an estimate of the point source at z_o distance away from the hologram, for a wide range of distances, is shown in Figures 4.22 and Figure 4.23, as grey-level plots, in isometric form in Figures 4.24, 4.25, 4.26, and 4.27 and in cross-section in Figures 4.28, 4.29, 4.30, 4.31, and 4.32 which is in the object plane.

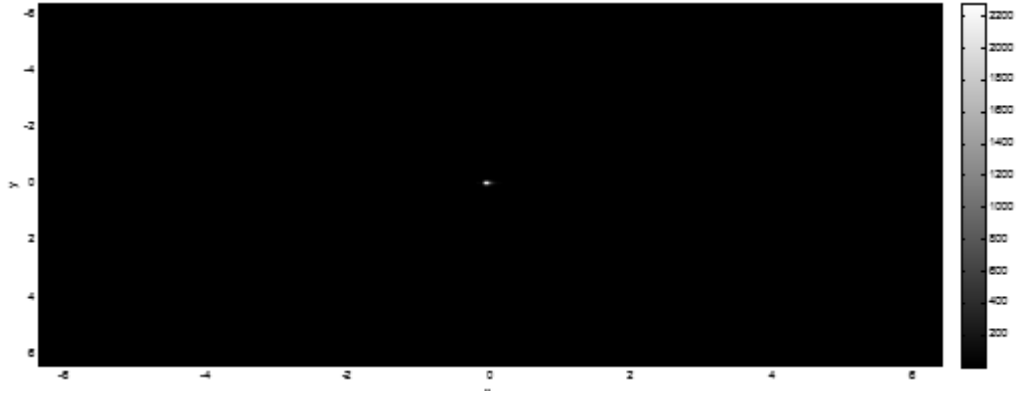


(a)

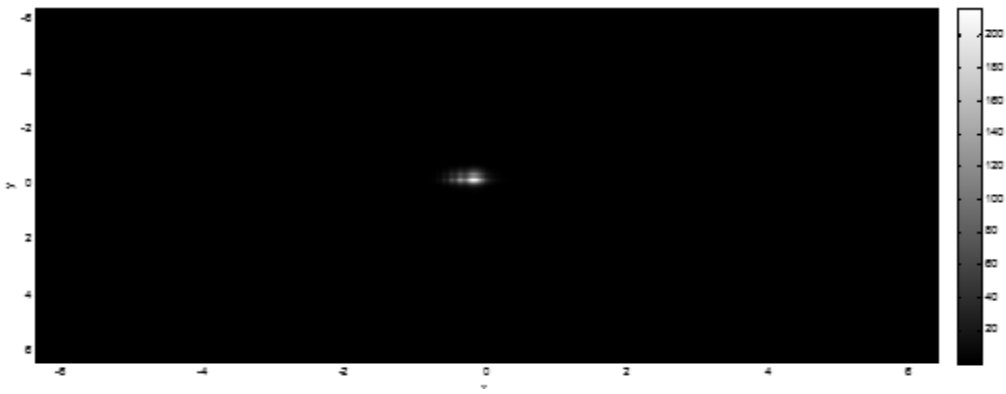


(b)

Figure 4.22: Reconstructed point sources for different distances: (a) 0.05mm, (b) 0.1 mm



(a)



(b)

Figure 4.23: Reconstructed point source intensity for different distances: (a) 20mm, (b) 100 mm.

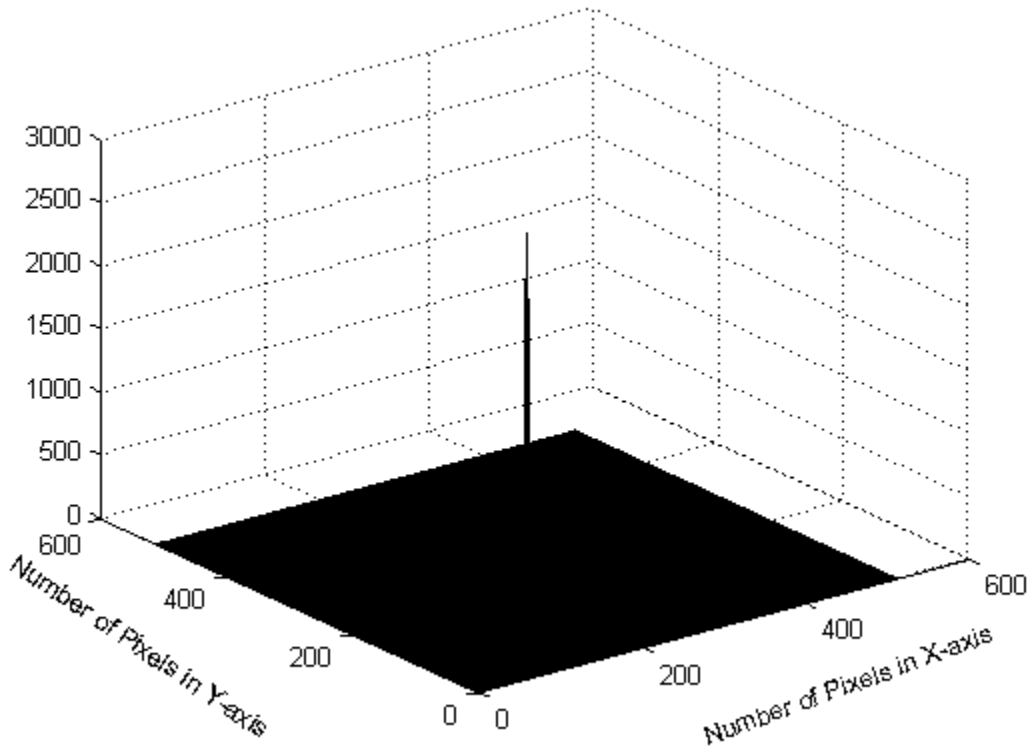


Figure 4.24: Reconstructed point source intensity for distance 0.05mm

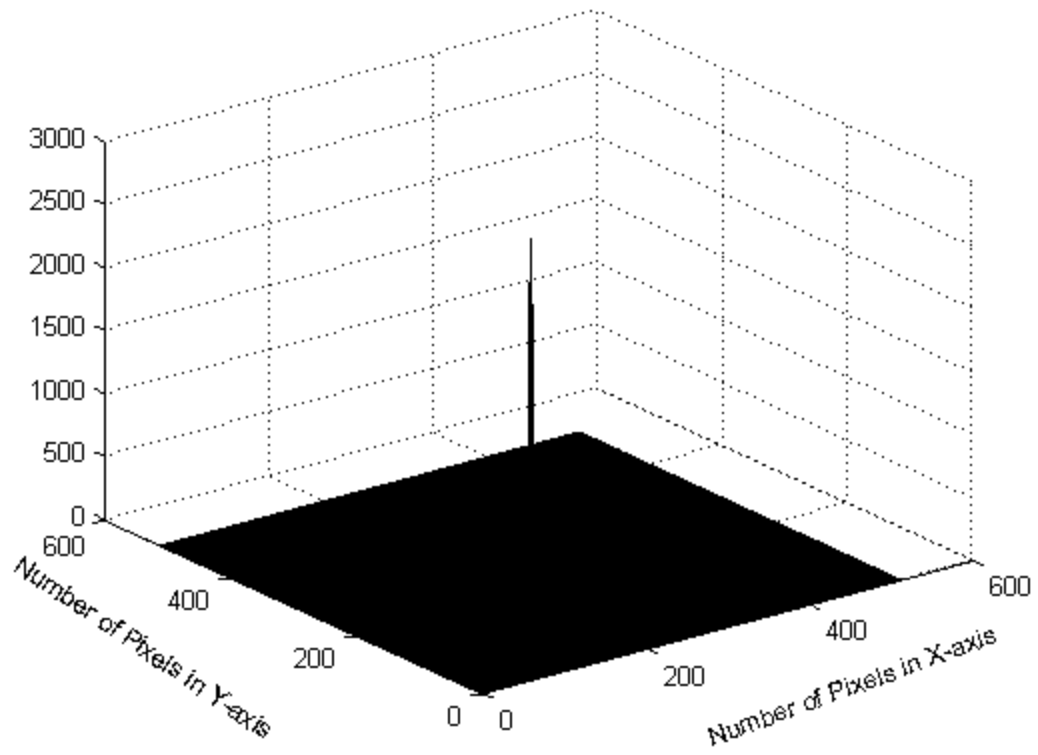
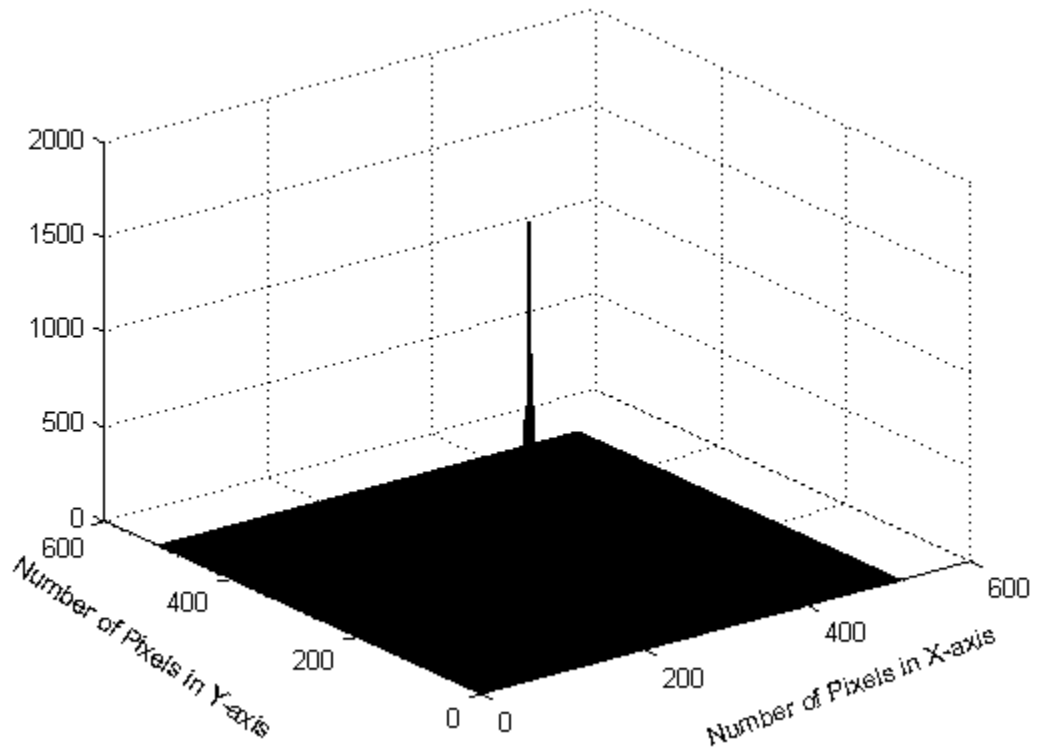
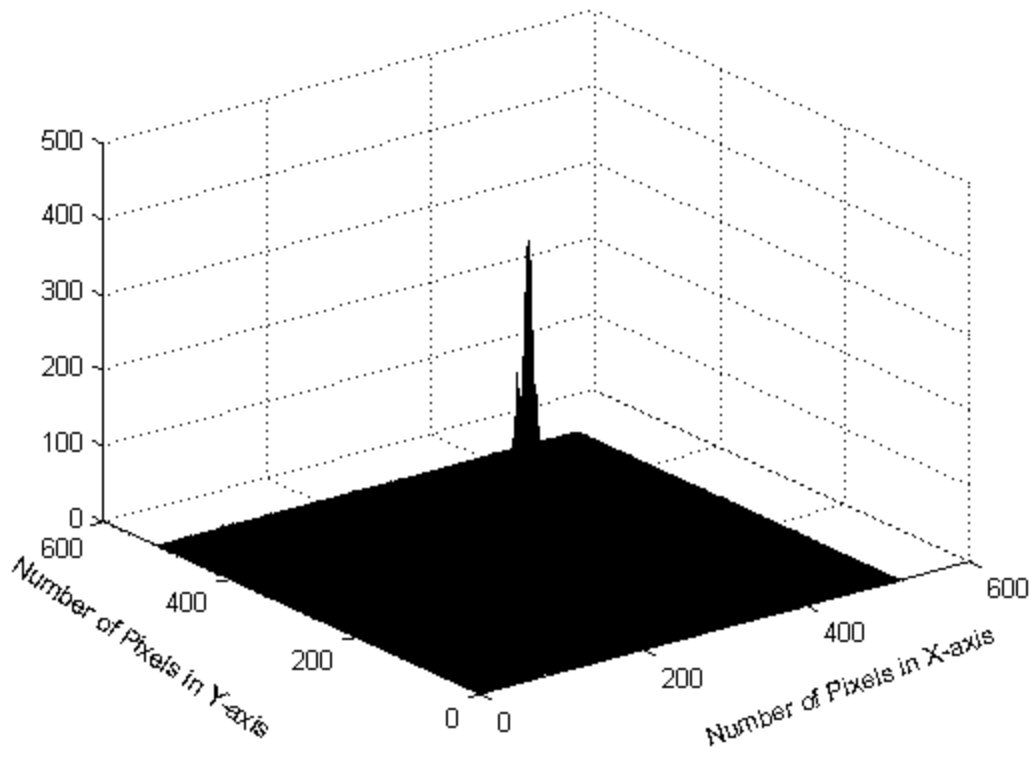


Figure 4.25: Reconstructed point source intensity for different distance: 0.1 mm



**Figure 4.26: Reconstructed point source intensity for different distance:
20mm**



(d)

**Figure 4.27: Reconstructed point source intensity for different distance:
100mm**

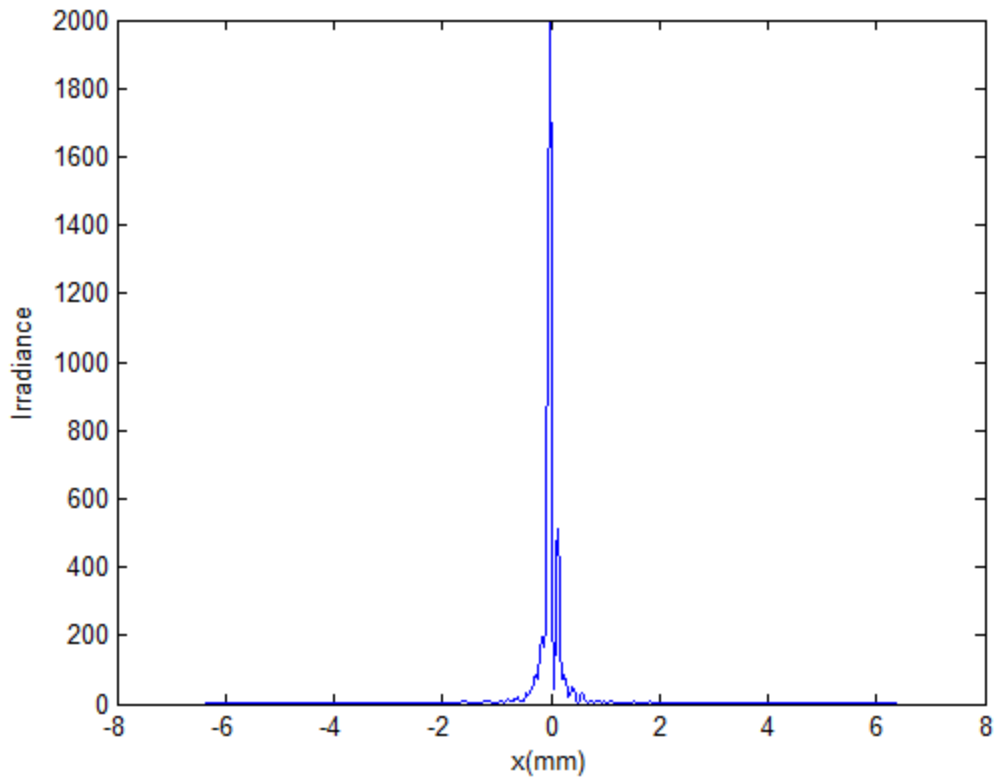


**Figure 4.28: Reconstructed point source intensity for different distance:
0.05mm**

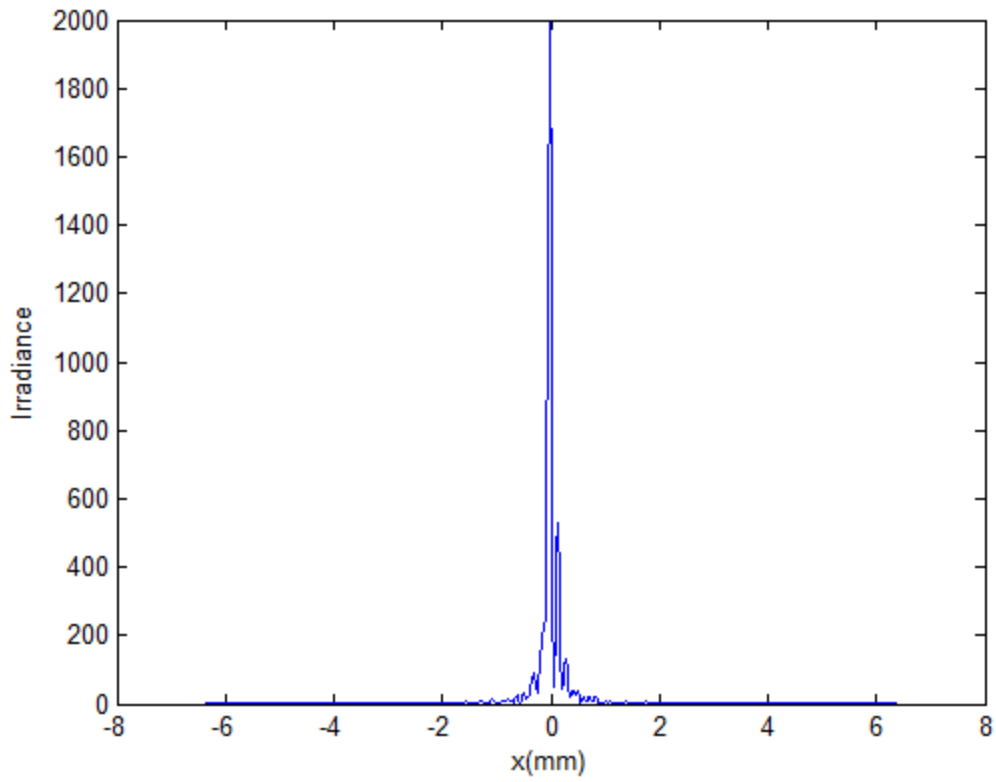


**Figure 4.29: Reconstructed point source intensity for different distance:
0.1mm**

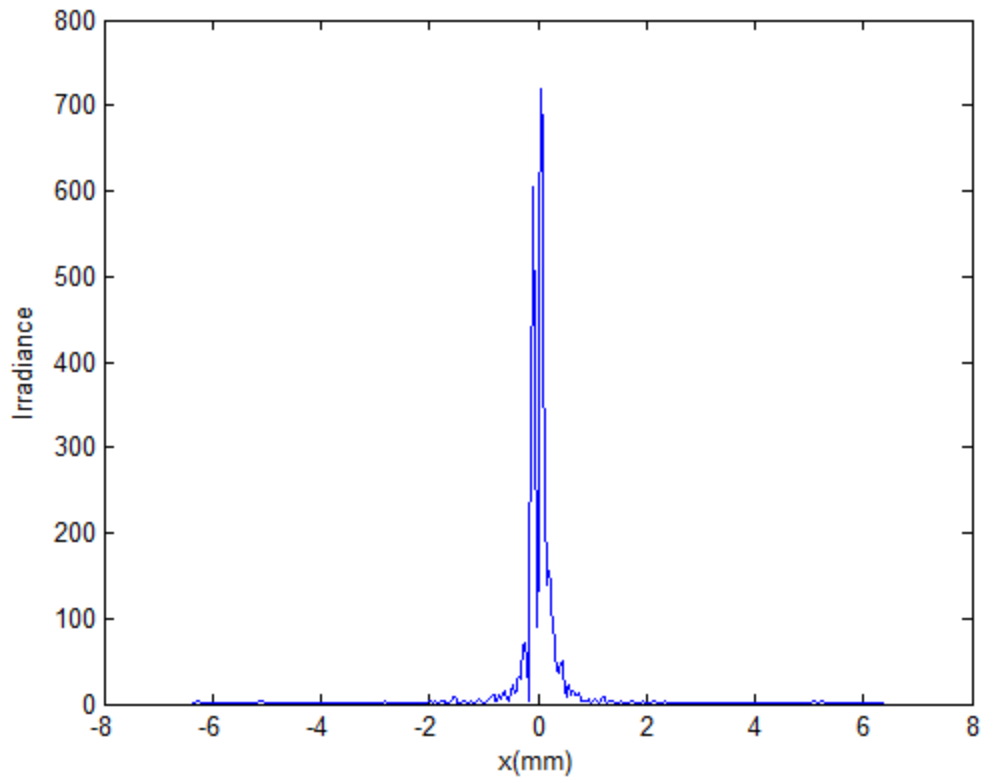


**Figure 4.30: Reconstructed point source intensity for different distance:
20mm**

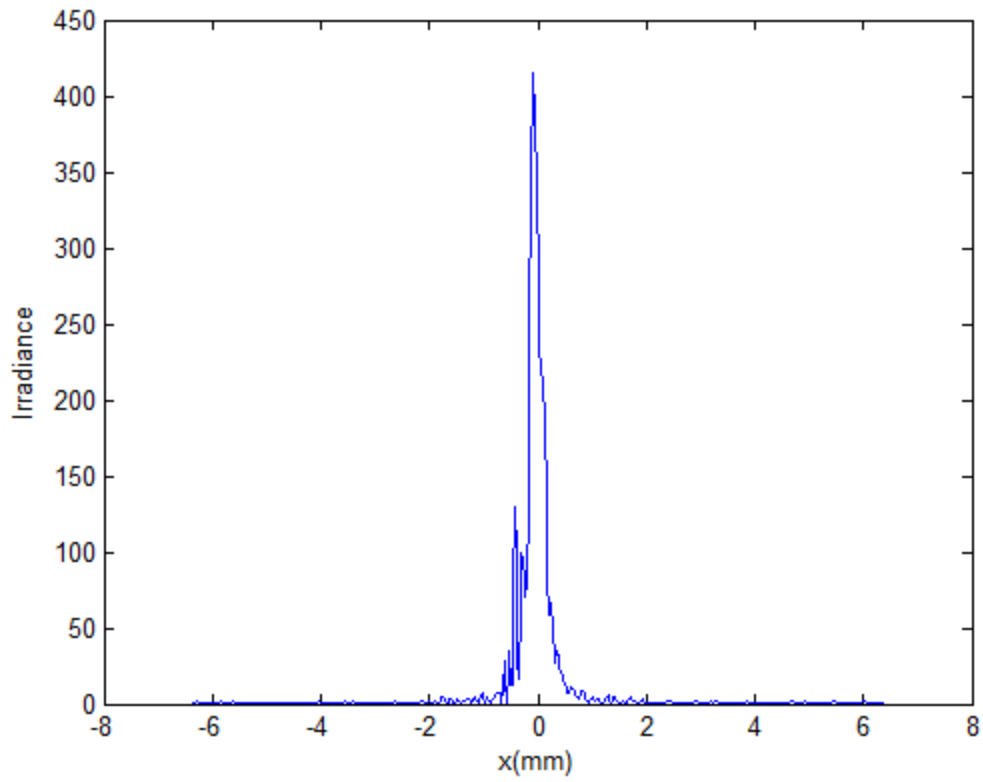


**Figure 4.31: Reconstructed point source intensity for different distance:
100mm**

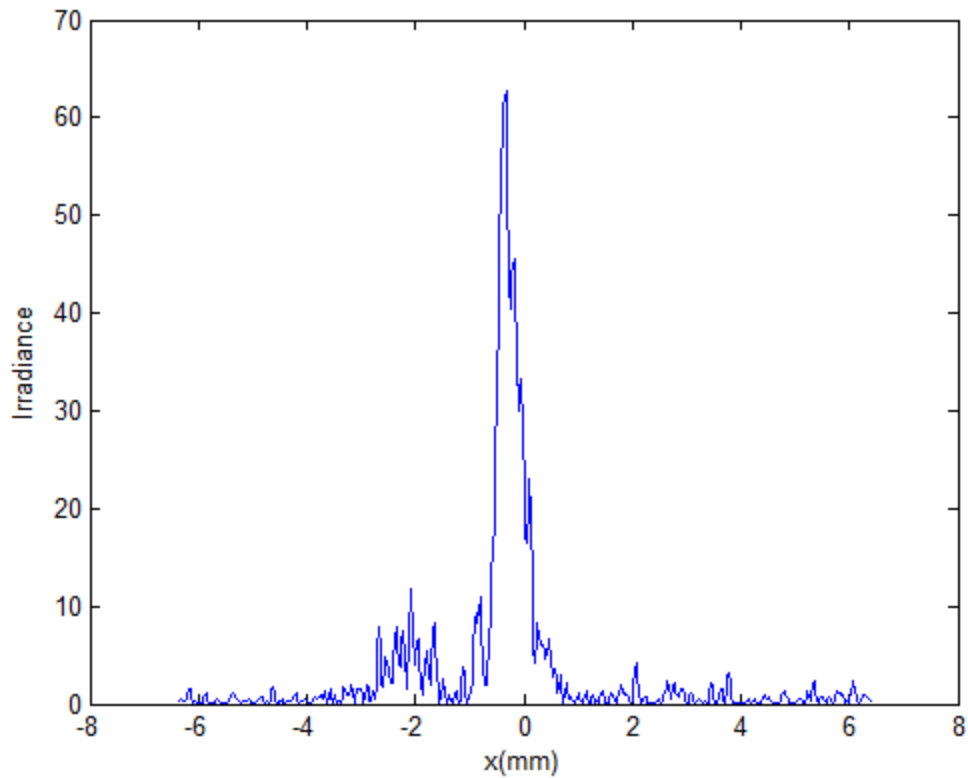


**Figure 4.32: Reconstructed point source intensity for different distance:
5000mm**

As can be seen from Figure 4.32, at the very large distance of 5000 mm the reconstruction fails as this is too large a distance. There will be very little phase variation over the plane of the FZP for a location of the point source this far from the FZP, resulting in a very inaccurate estimate of the point source. As the distance between the reconstructed image and the hologram is close (i.e. 0.05mm, and 0.1mm), the hologram can be regarded as an image hologram and we can thus see the reconstructed image.

4.11 Conclusion

In this chapter, we have presented an iterative method for reconstructing the quadratic phase from the modulus of the Fourier transform. The process starts with making a FZP which represents the hologram of a point source (the original object). We take the Fourier transform and keep only the phase and add a random phase with uniform distribution. The Fourier transform decomposes the combination and we take only the modulus to be the input of the modified Fourier transform algorithm. We successfully run the modified Fourier transform algorithm (MGSA) which is an iterative algorithm transforming backward and forward for a certain number of iterations.

The iterations were controlled by the root mean square error (RMSE) and we are able to track graphically the change in RMSE with the iteration number. The graphs show that the error reduces very rapidly for the first few iterations but more slowly for the later iterations. When the RMSE is zero, then the object and its Fourier transform satisfy all the constraints and a full solution has been reached.

The known random phase is then subtracted from the phase produced as a result of the MGSA. We thus reconstruct the unknown quadratic phase which we are able to show it in more than one example. We demonstrate that the random phase used affects the quality of the reconstructed image. To validate our code, we back propagate the quadratic phase to reconstruct the point source giving rise to it at the plane of the hologram. We present the effect of the propagation distance on the quality of the reconstructed point source image with several examples.

5 CHAPTER 5

5.1 Multiple-Point Source Locations

Introduction

The hologram one of the best optical elements [100] when high resolution and large object field area are both required as in holographic microscopy. The quality of the digital hologram depends on the finite wavelength and the aperture. To compute a hologram of a 3D point source object, we set up many holograms whose image is a single point. In this project the 3D object is represented by two point sources and the holograms corresponding to each point are computed and superimposed to construct a whole hologram of 3D point sources.

In the last decade, three dimensional optical imaging has become a very important tool in many fields, including material science and biology. Constructing 3D images using optical microscopy requires a scan of the field of view mechanically and for a thin sample. These techniques have a limitation which is that the time scale of changes in the sample should be slower than the acquisition time. Also, the cost of the confocal microscope can reach hundreds of thousands of dollars.

This chapter describes a digital holographic microscopy (DHM) (point source objects) [101-102] method that could be used to overcome the limitations of the current optical microscopy techniques.

In the next section, we describe the 3D reconstruction image for the case when there is a coherent plane wave illuminating off-axis point sources or point scattering particles, and these points can represent any object that scatters light in the microscope sample.

As we have already seen, the 3D scene can be represented by a number of point sources, and we use an algorithm which divides the 3D object into multiple point sources. The light field that is emitted by each point source is collected to form the whole light field of the 3D object. We use the MGSA algorithm, the same algorithm we used in chapter four, to reconstruct two point sources. The algorithm we use can compute a phase only hologram with high precision and this means this algorithm can alleviate the problems of computing speed and can directly record the light field details of the whole 3D object.

5.2 Digital Holographic Microscopy for 3D Imaging

In this case we place a screen in front of the particle, and this will produce an interference pattern between the original plane wave (unscattered wave) and the scattered wave. This pattern of interference is represented by concentric circular fringes with different intensity. The number and the diameter of fringes depend on the distance between the screen and the point source (the particle), hence the interference pattern can tell us about the location of the origin of the particle in 3D.

In this project, the DHM is done digitally. The hologram is a set of point sources and this is mathematically equivalent to the Fourier convolution of the FZP. For the reconstruction we use a modified iterative Fourier transform. Thus, the DHM can enable us to obtain a 3D object from only a single 2D image and this technique is thus potentially better than the other 3D acquisition techniques. The main drawback is associated with the unwanted twin image which obscures the reconstructed image.

5.3 Resolution and Depth of Field in Digital In-Line Holographic Microscopy

The resolution of the digital in-line holographic microscopy (DIHM) method depends on many factors which include: (1) pinhole size, which controls the illumination cone; and (2) the wavelength used in recording. We study the pinhole size in detail and conduct an analytical analysis coupled with numerical simulations of holograms and their reconstructed images. The results of this analysis are then used to enhance the reconstructed images.

5.4 Pinhole Size

The pinhole acts as a point source for a coherent spherical wave, and its size is very important in the diffraction phenomena. A large pinhole has two effects: (1) it reduces the spatial coherence; and (2) it narrows the zero-order emission cone which is used to create the holographic interference pattern of the emitted light. We use a circular aperture of radius (a), then most of the energy passing through the aperture is diffracted through an angle (θ) which is equal to (λ/a) , where λ is the light wavelength employed, from its original propagation direction.

We notice that when the light beams emitted from a point source pass through the circular apertures as we have used in this project, they do not produce bright dots as images, but rather a diffuse circular disc surrounded by much fainter concentric circular rings.

To show the effect of the pinhole size on the reconstructed images of the hologram, we run the MATLAB™ code we have developed with different sizes of the pinhole. Figure 5.1 and Figure 5.2 showing the FZPs for different resolved point sources. It is noticed that the FZP constructed with the smallest pinhole is the largest in diameter.

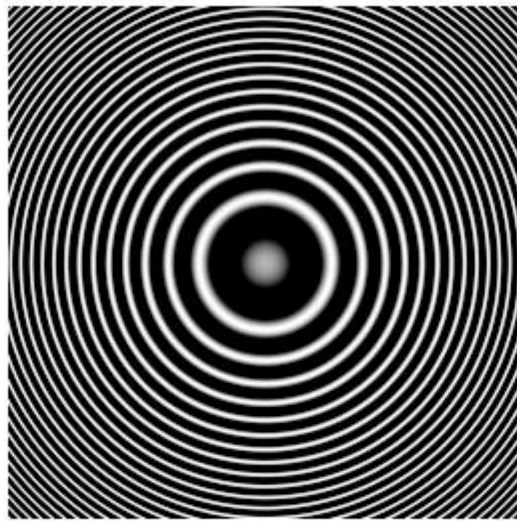


Figure 5.1: FZP for different pinhole size: for $d=180\text{nm}$

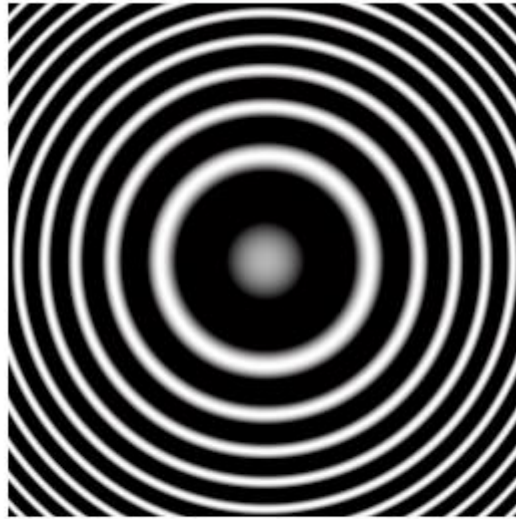


Figure 5.2: FZP for different pinhole size for 220nm

5.5 Distance between the Point Source and the Hologram

We study the effect of the distance between the original object (the point source) and the hologram to construct the FZP. We validate this process by taking different distances and using the MATLAB™ code we developed to construct the FZP hologram. The FZP is constructed for different distances, the distance between the point source and the hologram, and the fringe frequency which changes with the distance. Figures 5.3, 5.4, and 5.5 are showing the FZP for different distances.

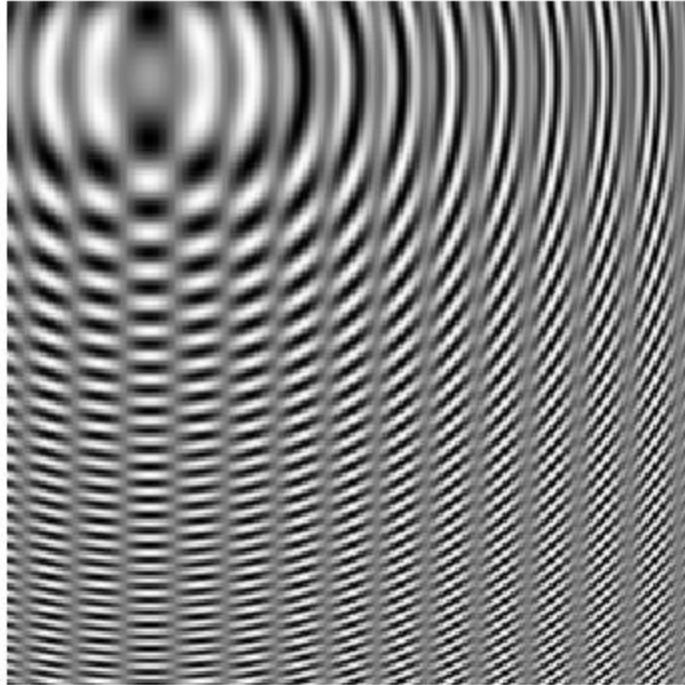


Figure 5.3: Off axis Fresnel zone plate (a hologram of two point sources, two point sources located side by side and separated by a distance z): for $z=3\text{mm}$,

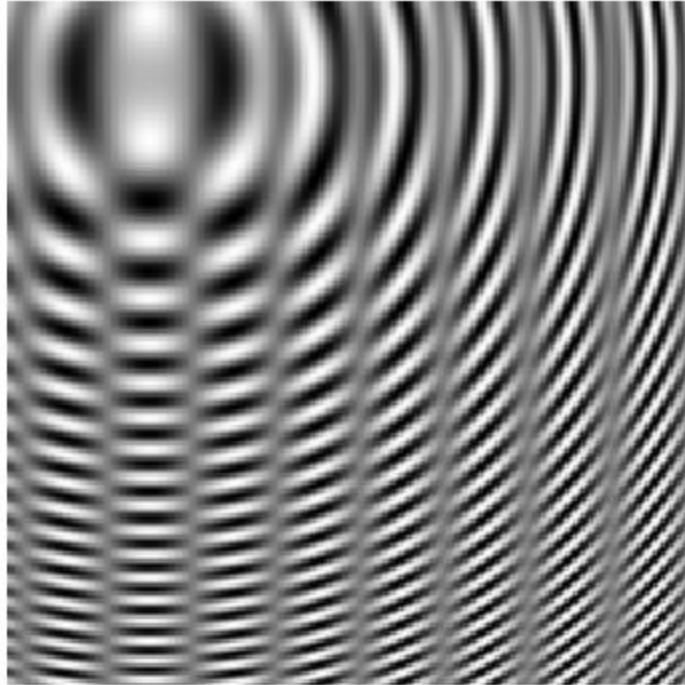
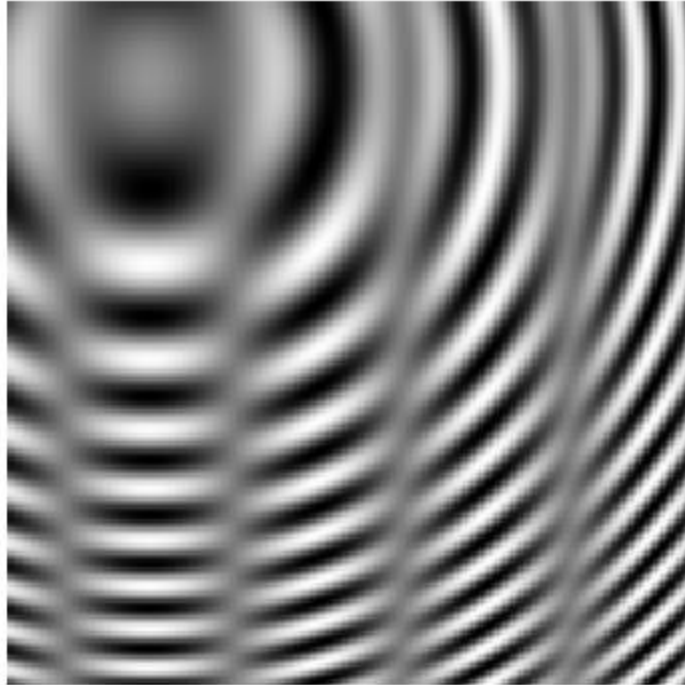


Figure 5.4: Off axis Fresnel zone plate (a hologram of two point sources, two point sources located side by side and separated by a distance z): (a) for $z=5\text{mm}$,



(c)

Figure 5.5: Off axis Fresnel zone plate (a hologram of two point sources, two point sources located side by side and separated by a distance z): for $z = 10m$

Also, we show the FZP in the case of the on-axis hologram. Figures 5.6, 5.7, and 5.8 show the on-axis hologram for different distances (two point sources located at the same coordinates), we construct this hologram to validate our code and seems working fine as the result only one FZP for two point sources are located at the same coordinates.

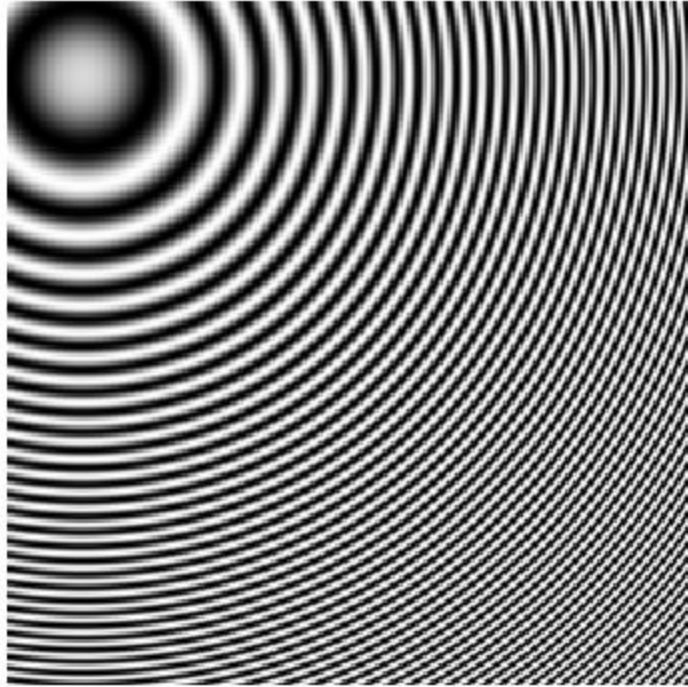


Figure 5.6: On-axis Fresnel zone plate (a hologram of two point sources are located at same coordinates): for $z=3\text{mm}$,

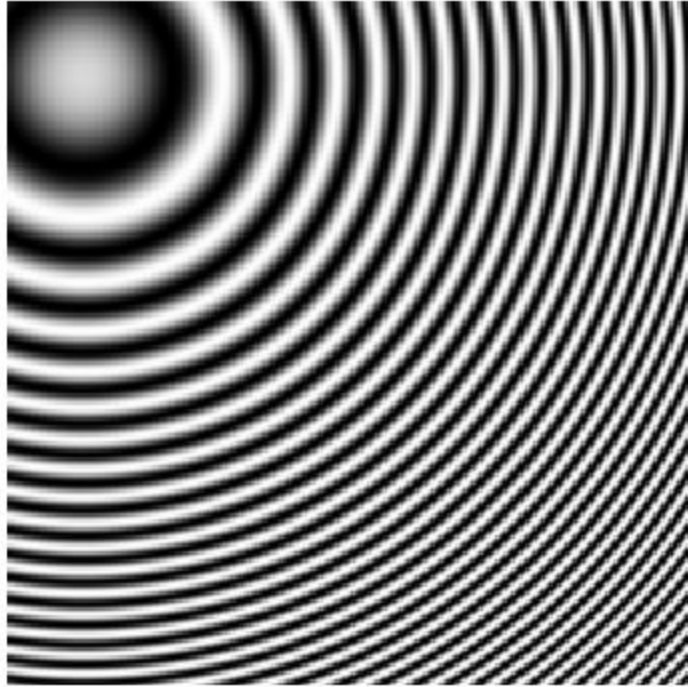


Figure 5.7: On-axis Fresnel zone plate (a hologram of two point sources are located at same coordinates): for $z=5\text{mm}$,

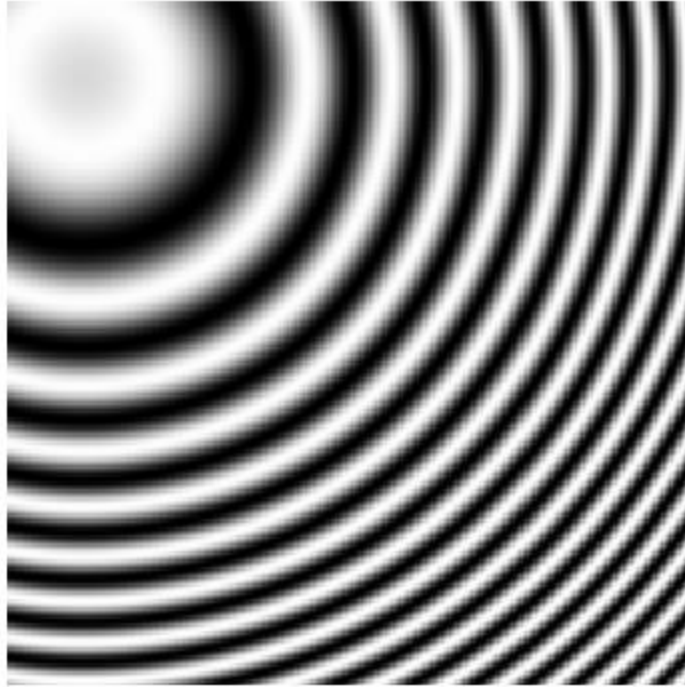


Figure 5.8: On-axis Fresnel zone plate (a hologram of two point sources are located at same coordinates): for $z = 10mm$

5.6 Hologram as a Collection of Fresnel Zone Plates

Any object can be considered as a collection of points, therefore recording a point object represents the basic principle of the holographic method. We can examine the holographic recording stage of a point source object and show the equations that represent the point source object.

Firstly, we consider a point source object at a distance z_o away from the holographic plate. Figure 5.9 shows the recording and reconstruction stages of a point source object. The pinhole aperture is represented by a delta function $\delta(x, y)$. The point source object is given by:

$$\varphi_o(x, y; z_o) = \exp(-jk_o z_o) \frac{jk_o}{2\pi z_o} \exp\left(\frac{-jk_o}{2z_o} (x^2 + y^2)\right) \quad (5.1)$$

Eq. 5.1 represents the object wave, the wave scattered from the pinhole, which is a paraxial spherical wave. The total recorded intensity distribution on the hologram is then given by:

$$t(x, y) = A + B \sin \left[\frac{k_0}{2z_0} (x^2 + y^2) \right] \quad (5.2)$$

where A and B are constants related to the wave number and z_0 is the point source object distance from the hologram. The Eq. 5.2 represents the hologram of the point source object and is called the FZP. In case of two point source objects at locations given by: $\varphi(x, y) + \varphi(x - x_1, y - y_1)$ and both of them (the objects) are located at z_0 distance away from the hologram, the recorded hologram is represented by the equation:

$$\tau(x, y) = c + \frac{ab_0k_0}{\pi z_0} \sin \left[\frac{k_0}{2z_0} (x^2 + y^2) \right] + \frac{ab_1k_0}{\pi z_0} \sin \left\{ \frac{k_0}{2z_0} [(x - x_1)^2 + (y - y_1)^2] \right\} \quad (5.3)$$

where c is a constant and the second and third terms represent the FZPs which we can recognise are the two FZPs associated to each point source.

Figure 5.9 illustrates the holographic recording and reconstruction of a 3 point object. From Figure 5.9, the virtual image appears at the correct 3D location of the original object. The real image is a mirror image of the original object with the axis of reflection on the plane of the hologram.

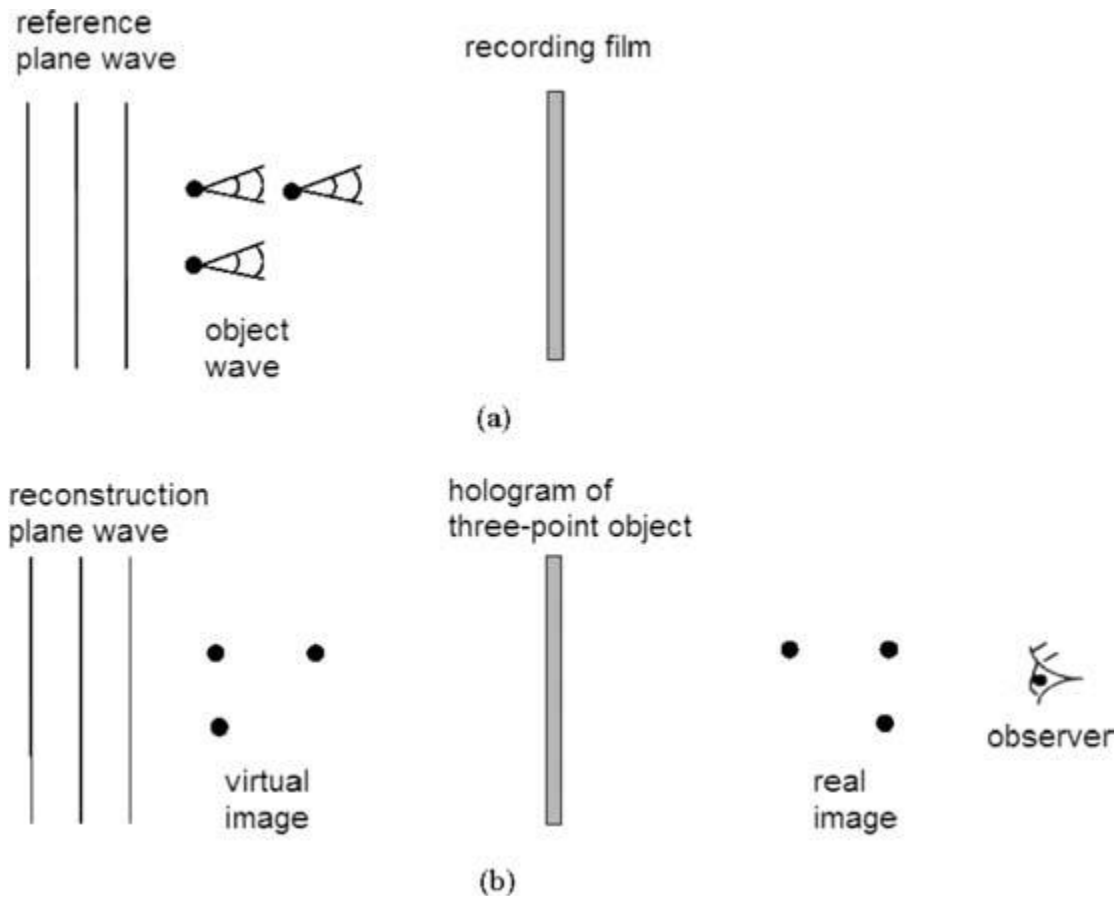


Figure 5.9: Holographic recording and reconstruction of a three-point object

5.7 Two-Source Interference

In the two dimensional case and if we have a stationary source that generates a wave at constant frequency, the pattern of the wave will be represented by a set of concentric circles. If we assume the two point objects are close together, than the spherical waves will arrive and intersect on the hologram at small angles. Interference pattern consists of two areas: the white (bright) and the black (dark) areas. The bright areas are the regions of the constructive interference. The constructive interference is made by coincidence of the crest from both point sources as well as the troughs. These will cause the wave to go up and down with twice the amplitude of each wave alone. The dark areas represent the destructive interference and this occurs when the crest of one wave encounters the trough of the other wave, producing a cancellation of wave amplitude at that point.

5.8 Reconstruction of Two Point Source Objects

We start by creating two grey-level FZPs plates which represent two point source objects. The zone plate pattern as shown in Figure 5.10 consists of alternating opaque and transparent rings, the point source of light illuminating a large Fresnel zone plate.

Rogers [103] was the first scientist who noticed the similarity between the FZP and the hologram of a point source, the hologram being considered as a zone plate with a complex pattern. Mertz and Young in 1961 developed the first zone plate hologram [104].

If we consider the light source to consist of many point sources, then the pattern that is recorded on the photographic plate represents the linear superposition of the wavefronts from each of these sources. Therefore this photographic plate acts as a hologram. To reconstruct this zone plate hologram, we proceed in the same way as a Gabor hologram which is by illumination of the hologram with a coherent light. The advantage of this technique over the other methods is that the hologram is independent of the coherence length of the illumination source.

To fully understand the Mertz and Young technique, we consider a point source of radiation which is used to illuminate a large Fresnel zone plate. To simulate the hologram of a point source, we only need to record the binary pattern of the zone plate on a photographic plate or transparency.

5.9 Thesis Project

We create two sinusoidal FZPs as our point source objects. We use the MATLAB™ code developed to make both FZPs and for different distances, Appendix E. Figure 5.10 shows the superposition of both FZPs.

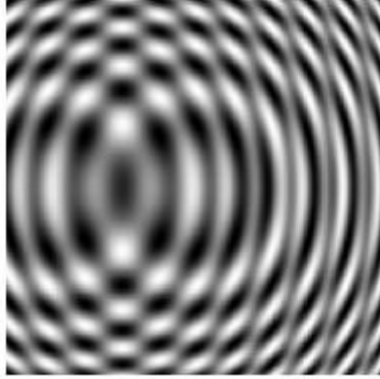


Figure 5.10: Zone plate with two point sources

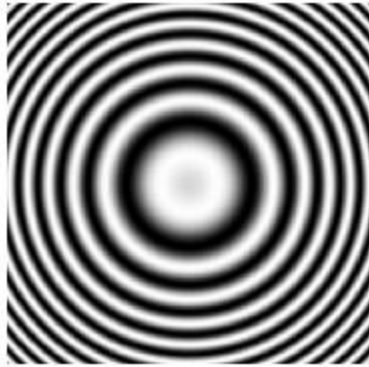
In Figure 5.10 the interference of one light wave with another is clearly shown. The wave propagates outward from the point sources, which creates a series of concentric circles about the source. In Figure 5.10, we can easily notice the crests and troughs from the two sources interfering with each other at a regular rate and making nodes and antinodes.

Since sources located at different distances from the zone plate will cast different size shadows and the images will be reconstructed at different distances from the hologram, thus giving rise to a 3D image. The magnitude and frequency of the FZP compared to the magnitudes of the Fresnel functions from the individual points will depend upon the separation of the points, as well as the frequency of light used, and the distance of the transparency from the hologram.

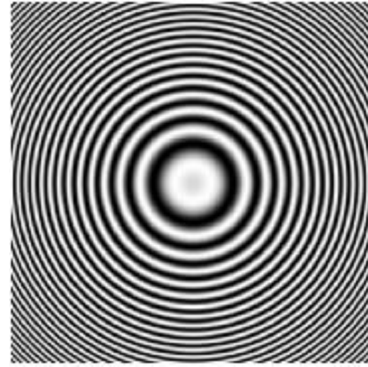
5.10 In-Line Digital Hologram Microscopy

The point source digital in-line holography with numerical reconstruction has been developed into a new microscopy, specifically for microfluidic and biological applications [105].

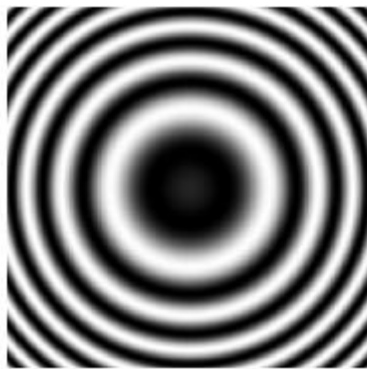
The in-line hologram is a spherical wave with a wavelength λ which emanates from a point source. The digital in-line hologram with numerical reconstruction has been developed into a new tool, especially for biological applications. Figure 5.11 shows the dependence of the FZP characteristic as a function of the depth parameter z_o for ($z_o = 2mm, 5mm, 8mm, and z = 10mm$). As the point source becomes further away from the recording film, the recorded FZP has a lower local fringe frequency.



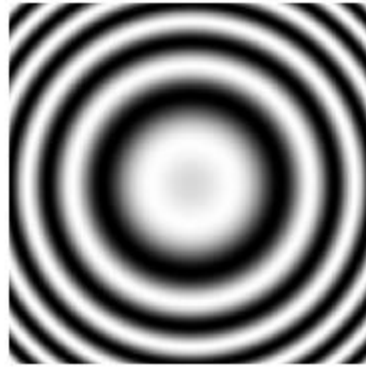
(a)



(b)



(c)



(d)

Figure 5.11: On-axis Fresnel zone plate as a function of depth, z_o : a) $z_o = 2mm$, b) $z_o = 5mm$, c) $z_o = 8mm$, and d) $z_o = 10mm$

In the last twenty years, the digital in-line hologram (DIH) has been preferred for use in the biological applications. The advantages of using DIH are listed below:

- I. The in-line hologram is a form of microscopy that does not need any lenses.
- II. Maximum information: where a single hologram can contain all the details about the original 3D object.
- III. The reconstructed images can have a maximum resolution which is similar to the single point source object which we covered in Chapter 4.

Firstly, we use the MATLABTM code developed to create the in-line two point sources for different separation distances between them and the hologram. Figure 5.11 illustrates the in-line FZPs.

5.11 Off-Axis Hologram

Digital off-axis hologram microscopy (DOHM) is a technique which can provide quantitative information about samples in three dimensions. DOHM can be used for the analyses after processing the reconstructed image of living cells in their growth medium without any type of additional marker which can affect the values of many physiological parameters.

The DOHM has many biological applications. Such as analysis of blood cells, yeast cells, neurons and cancer cells. The DOHM is considered as an optoelectronic technique and can be used to make real-time measurements of the phase and amplitude information at the level of single living cell, and the ability to gain 3D morphological dimensions (length, width, and height).

In DOHM, using a single hologram, does not need any lenses in the recording process. The DOHM can become more effective when modern sensors such as CCD detectors became available for use in the industry. The off-axis configuration allows one to obtain separately the +1, 0, and -1 orders of the reconstructed angular spectrum whereas in in-line hologram microscopy, all these are overlapped. In this case, we can remove the twin image and the reconstructed image is thus more accurate. Figure 5.12 illustrating the off-axis Fresnel zone plate as a function of depth.

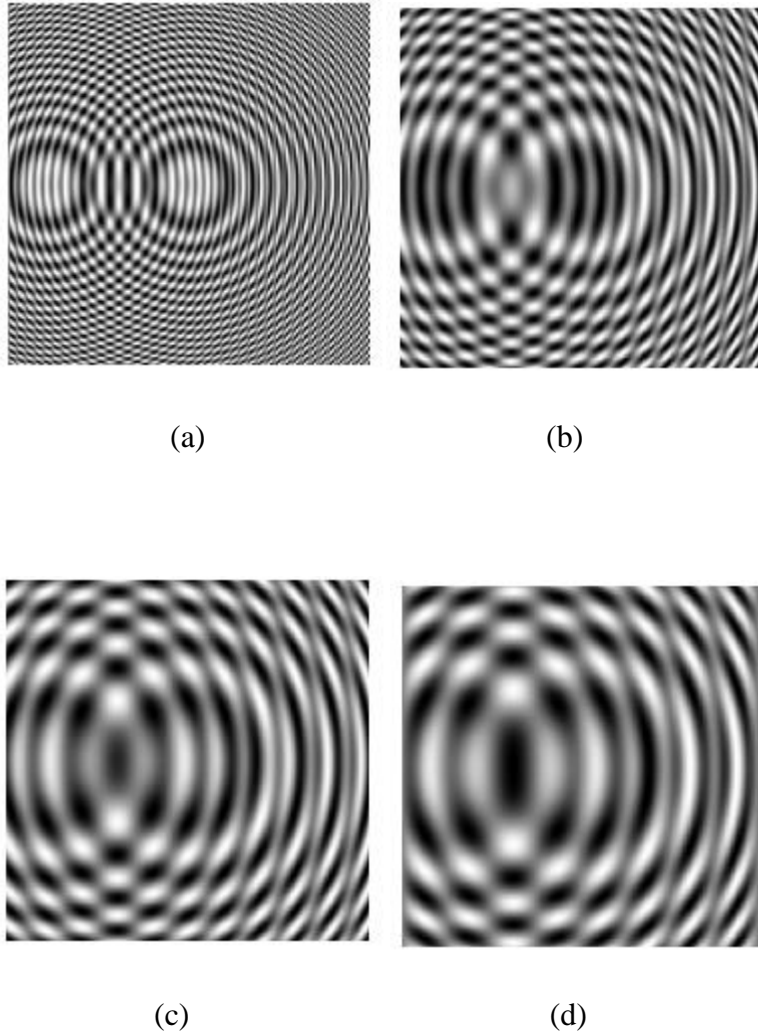


Figure 5.12: Off-axis Fresnel zone plate as a function of depth, z_o : a) $z_o = 2mm$, b) $z_o = 5mm$, c) $z_o = 8mm$, and d) $z_o = 10mm$

We created the two point source object for two different cases which are the in-line and off-axis hologram. The next step required is to take the Fourier transform of the recorded diffraction pattern of the hologram which will allow the phase and intensity of the image to be separately recorded. This represent the recording stage of the CGH. The output will be in the frequency domain and should be sampled in a rate which is enough to represent the original image.

We take samples in 2D and place in an array of size $M=256$, and $N=256$. We are dealing with large images and so we use the FFT for the calculation in two dimensions. We create the phase and intensity images as a product of the complex FFT but we are only interested in the phase image, i.e.:

$$phase = angle(I(x,y)) \quad (5.4)$$

where $I(x,y)$ is our multi-FZP and we are taking only the phase of their images. We should include a random phase mask with the original object phase in order to broaden its spectrum. If the random phase mask is not employed, most of the energy will concentrate in the zeroth-order beam and the effective dynamic range of the recorded hologram will be reduced.

The first random phase we use is $random\ phase = \exp(-j\pi * random())$ and the reconstructed intensity variance is shown in the Figure 5.13. When we use a different random phase (the second one), which is $random\ phase = \exp(-j\pi * random()/256)$, the reconstructed image intensity is different as shown in Figure 5.14. Also, we use three more random phases are listed in Table 4.1 but we only showing the results of using the first two with corresponding results shown in Figures 5.13 and 5.14.

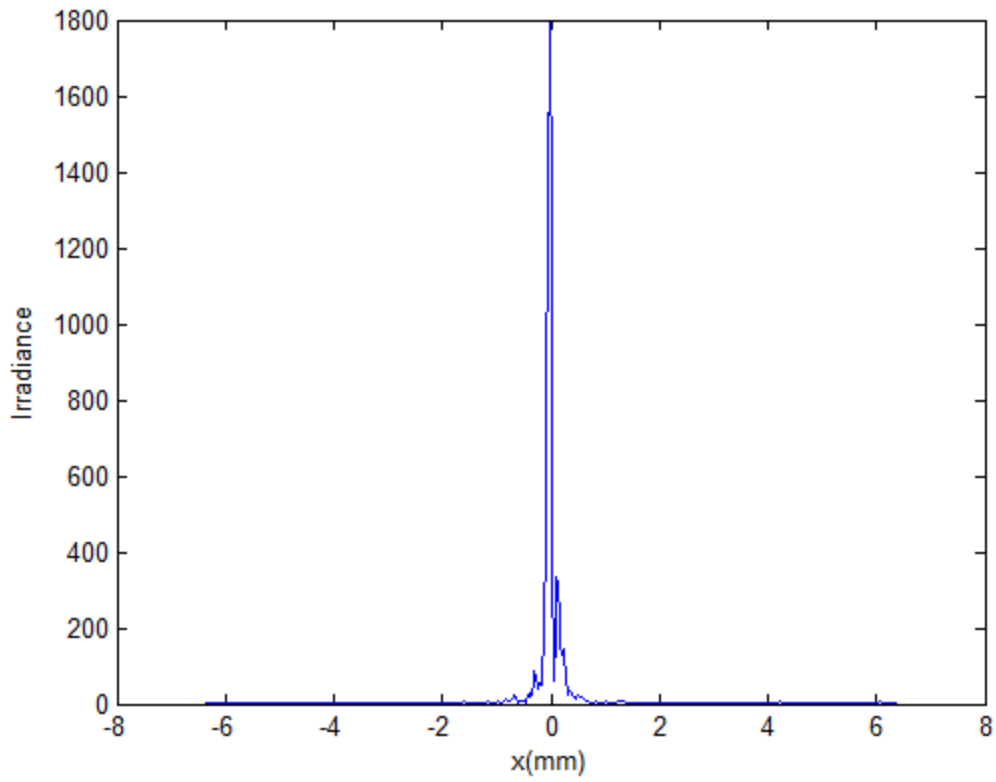
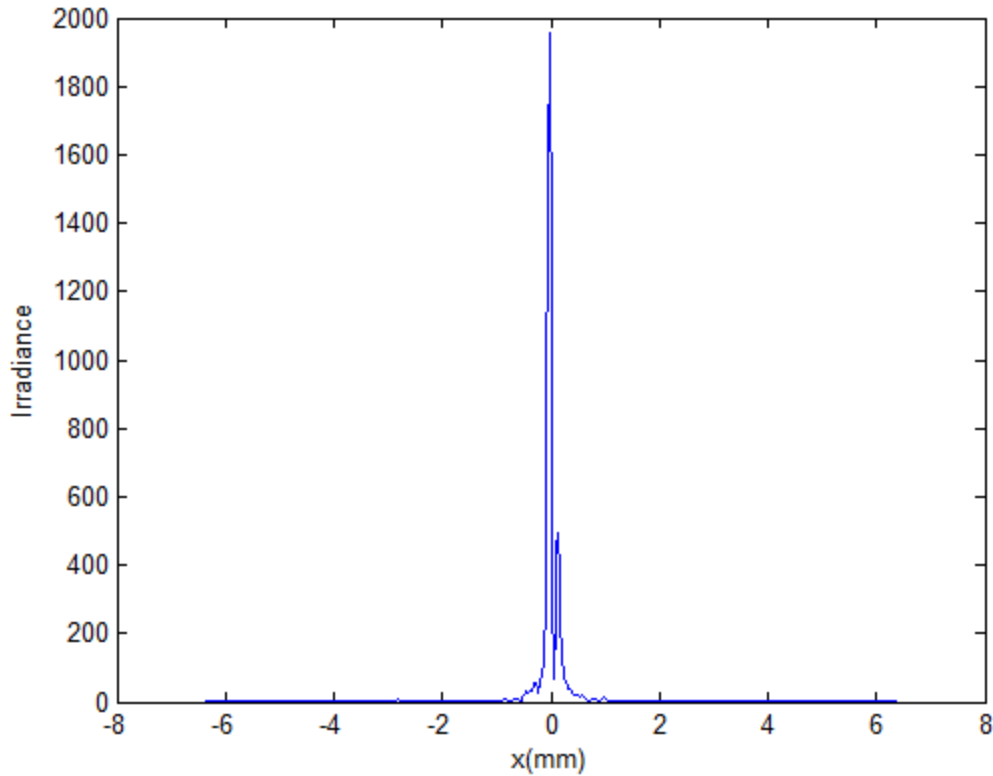


Figure 5.13: Intensity at z_0 for the random phase: $\text{phase}=\exp(-j\pi*\text{random}())$



(b)

Figure 5.14: Intensity at z_o for the random phase: $random\ phase = \exp(-j\pi * random()/256)$

During our simulation work, the random phase we use in the beginning of the procedure is an important factor in the quality of the reconstructed images.

We apply the Fourier transform for the combination of the two phases, ($phase + random\ phase$). The Fourier transform is used to study the geometric characteristics of the original object (i.e. the spatial domain image). The Fourier transform produces a complex number valued image which can be displayed with two images, the magnitude and phase. We describe here our reconstruction method that works for our point source object. We take the FFT to the phase combination as shown in Eq. 5.5:

$$SEF = \mathcal{F}(phase + random\ phase) \quad (5.5)$$

We are considering only the intensity and the phase can be ignored in this step, thus:

$$f_i(x, y) = abs(SEF) \quad (5.6)$$

This modulus only is input of our error reduction iterative transform algorithm. In this work the point sources are real and nonnegative functions. We thus set our constraints in both domains (spatial and frequency fields) according to these constraints.

5.12 Modified Error-Reduction Algorithm

We use a similar algorithm to that described in Chapter 4 which is the MGSA. The algorithm starts with only the modulus of the phase combination and each i^{th} iteration, which is a forward and backward Fourier transform process, starts with this modulus, $f_i(x, y)$, and we choose 100 as the total number of the iterations. Our aim is to reconstruct the phase of the complex object from only the modulus. In each iteration we have a fixed procedure which is explained in the next section

First, the complex distribution of the holographic plane is obtained by calculating the FFT of the input modulus and this produces the complex distribution $g_i(u, v)$. Then an amplitude constraint is applied on the holographic plane; namely, the amplitude factor is forced to unit value, and the phase factor remains unchanged and thus the new complex distribution can be given by $|f_i(x, y)|e^{i\Phi_2}$. Second, the complex distribution of the imaging plane is obtained by calculating the inverse FFT (IFFT) of the updated complex distribution of the holographic plane. This step produces a new complex distribution $f'_i(x, y)$. We apply the constraints again and this time apply in the image plane in which the amplitude is replaced by the measured signal modulus. These steps are repeated until we have reached a limit in the number of iterations or the iteration is repeated until the phases Φ_1 and Φ_2 converge. Here Φ_1 is the phase as the result of applying the IFFT in the first iteration as explained in the Figure 4.7. The phase produced by this process is considered as an overall phase only.

5.13 Simulation Results

We subtract the known random phase and keep only the original phase which has come from FZP's field and represents the hologram of the original point sources. The next step is to propagate the phase resulted from the calculation to produce the point sources as the original objects. We validate the MATLABTM code by taking different values for the propagation distance z_o . The last stage of this project is to reconstruct the original point sources. To illustrate this, we show two point sources for different geometries: off-axis, and propagated at different distances away from the hologram by $-z_o$. Figures 5.15, 5.16, 5.17, 5.18, and 5.19 showing the two point sources at the

off-axis location and propagated at $-z_o = 0.05mm, 5mm, 10mm, 50mm$ and $150mm$. We take different distances to validate that our code is working well. Figures 5.15, 5.16, 5.17, 5.18, and 5.19 clearly shows the twin reconstructed images of the original point sources. Note that the virtual image appears at the correct 3D location as the original object, while the real image (the twin image) is the mirror-image of the original object, with the axis of reflection on the plane of the hologram. We use 100 iterations which takes only 9.3s each run on a Pentium processor (Intel Pentium-N3710). However, the original object cannot be fully reconstructed even when we try to run the code for many more than 100 iterations due to the approximations inherent in the calculation. Figures 5.15, 5.16, 5.17, 5.18, and 5.19 show the actual reconstructed point source in 3D but Figures 5.35, 5.36, 5.37, and 5.38 illustrate the intensity of the reconstructed point source in 3D.

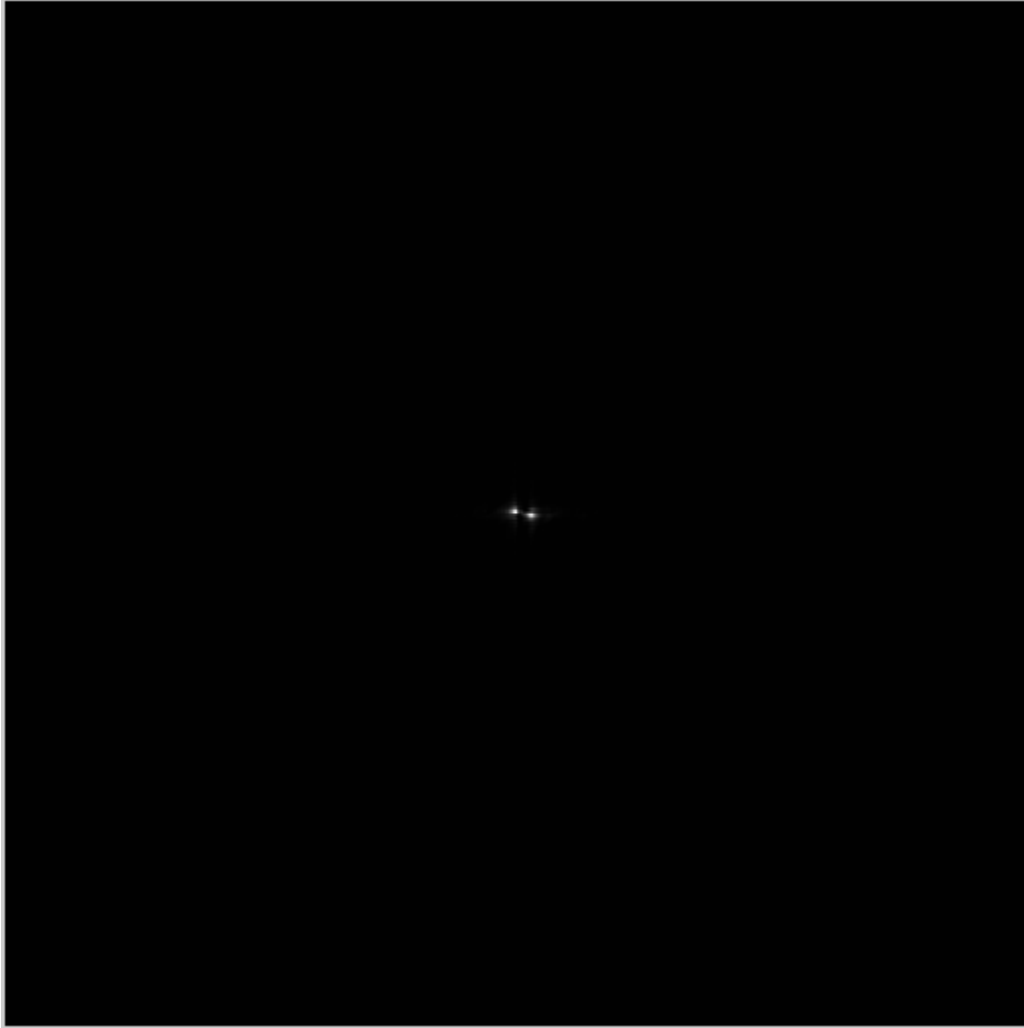


Figure 5.15: Reconstructed original point sources for different propagation distance: for $-z_0=0.05\text{mm}$

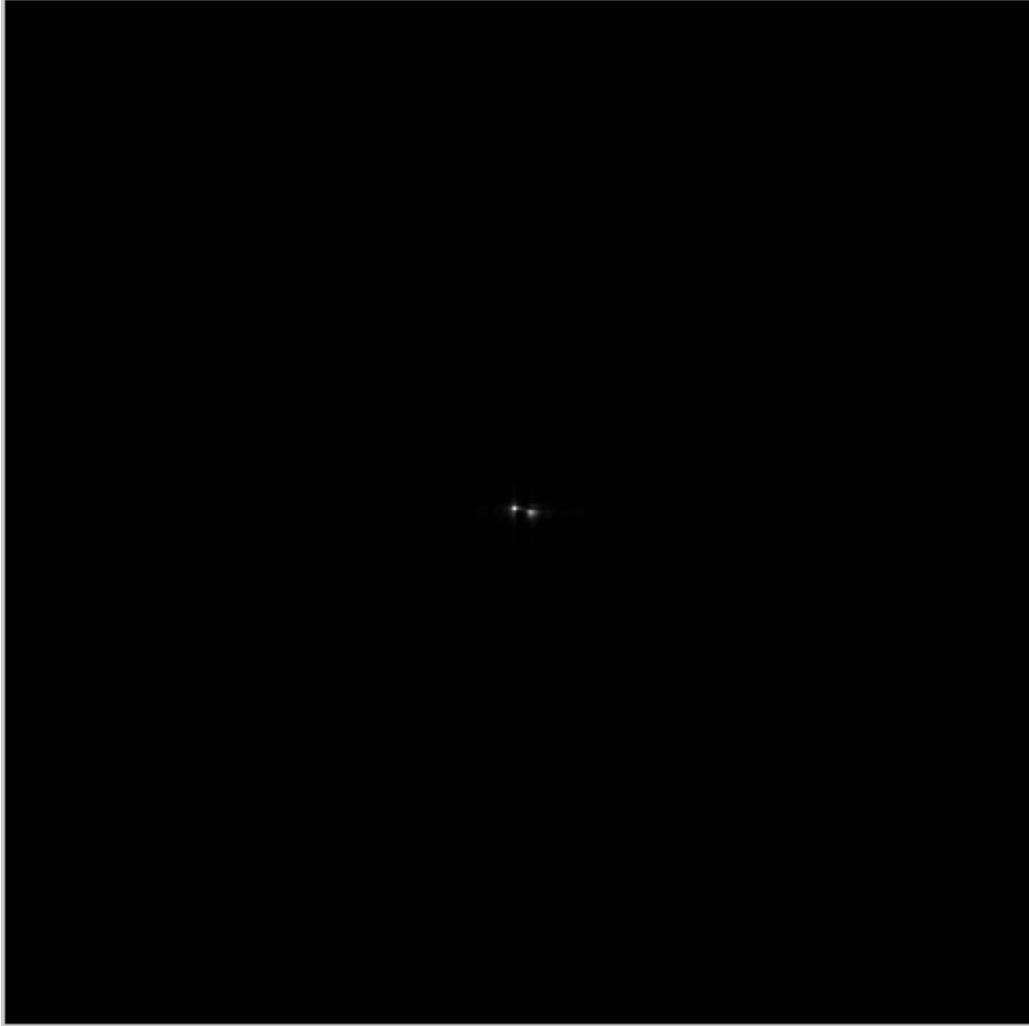


Figure 5.16: Reconstructed original point sources for different propagation distance: for $-z_0=5\text{mm}$

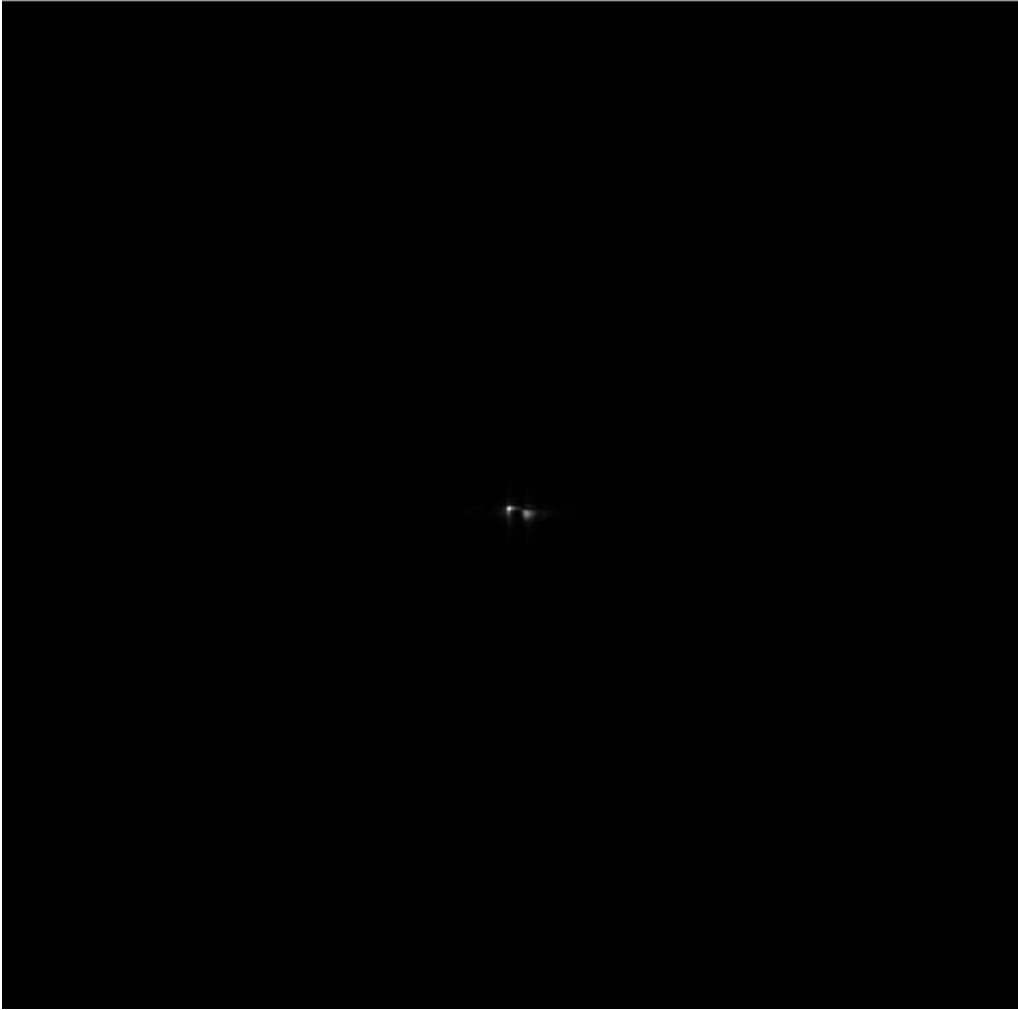


Figure 5.17: Reconstructed original point sources for different propagation distance: for $-z_0=10\text{mm}$

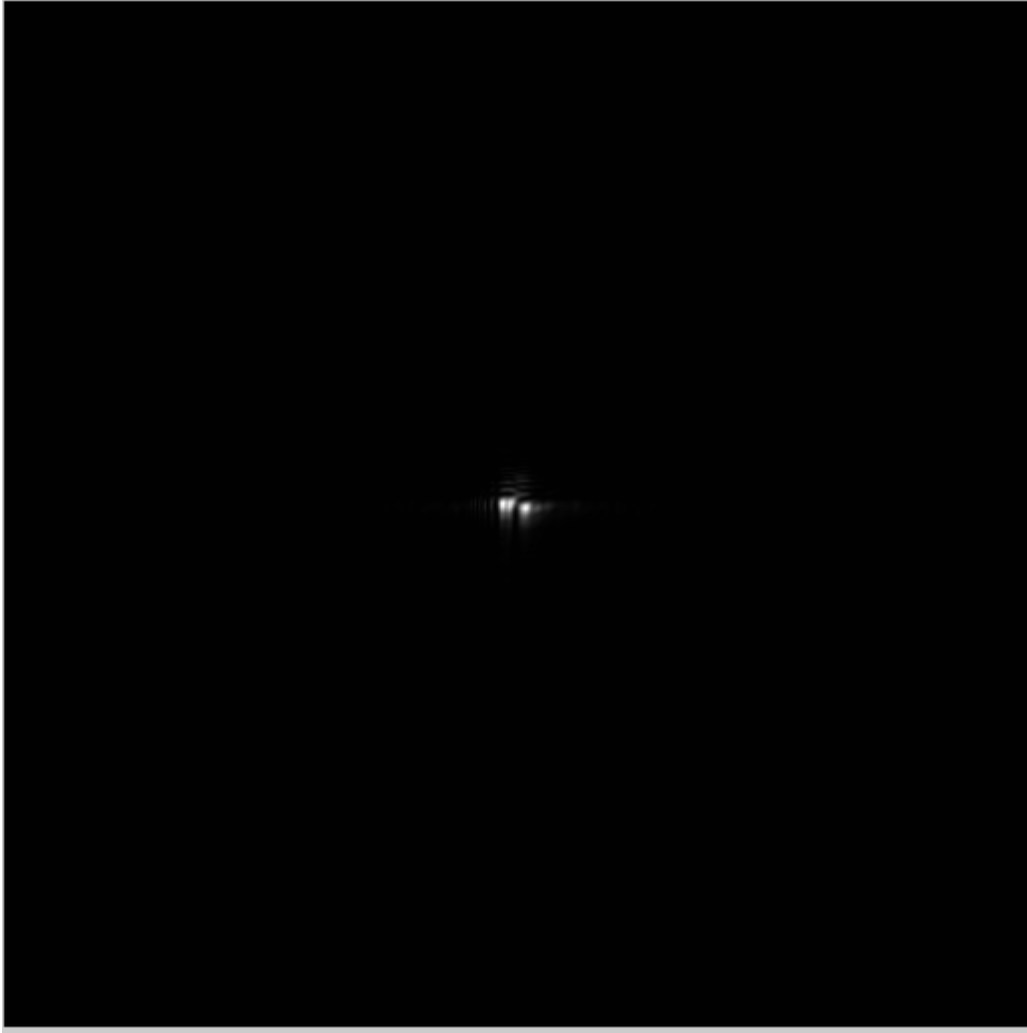


Figure 5.18: Reconstructed original point sources for different propagation distance: for $-z_0=50\text{mm}$

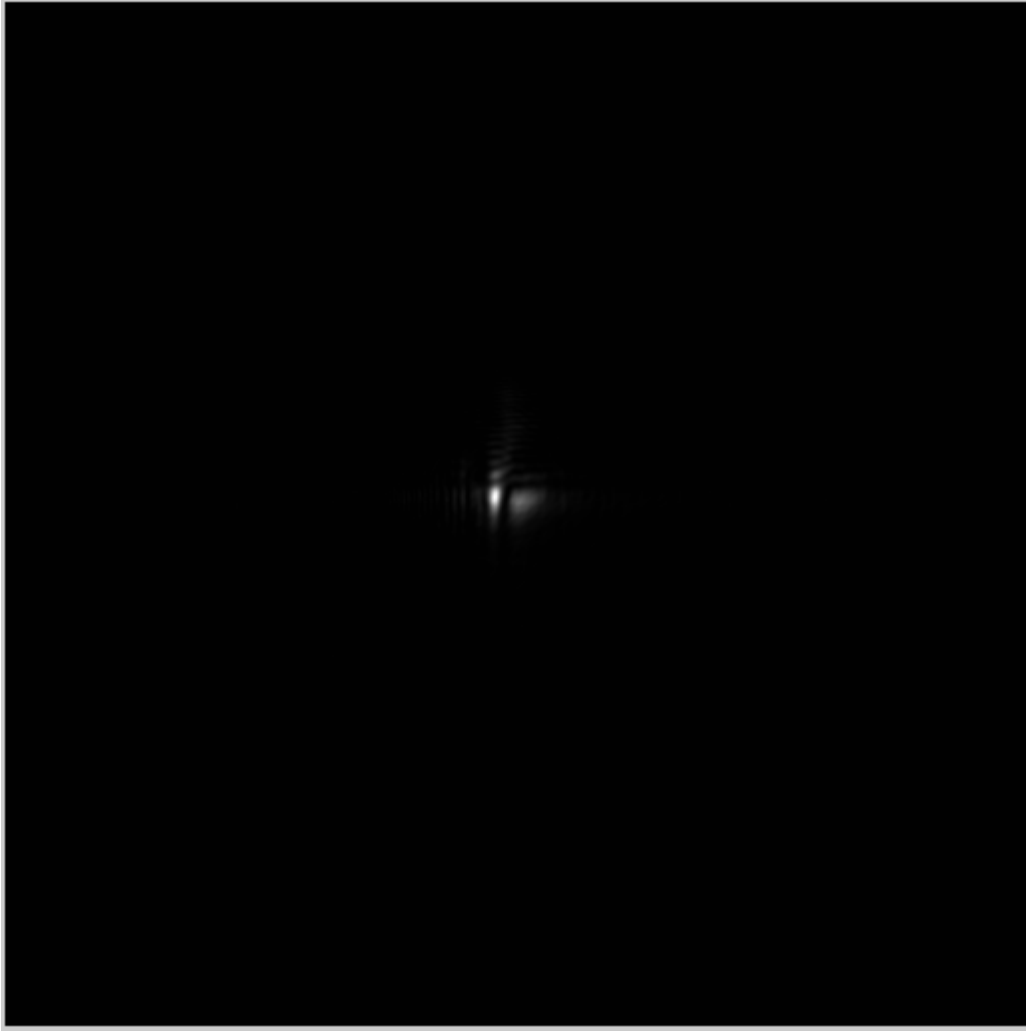


Figure 5.19: Reconstructed original point sources for different propagation distance: for $-z_o = 150mm$

To validate our MATLABTM code we ran the code for different cases such as the in-line hologram, and further holograms due to different propagation distances and different pinhole sizes. Below, we show the intensity diagram for each reconstructed point source according to the propagation distance.

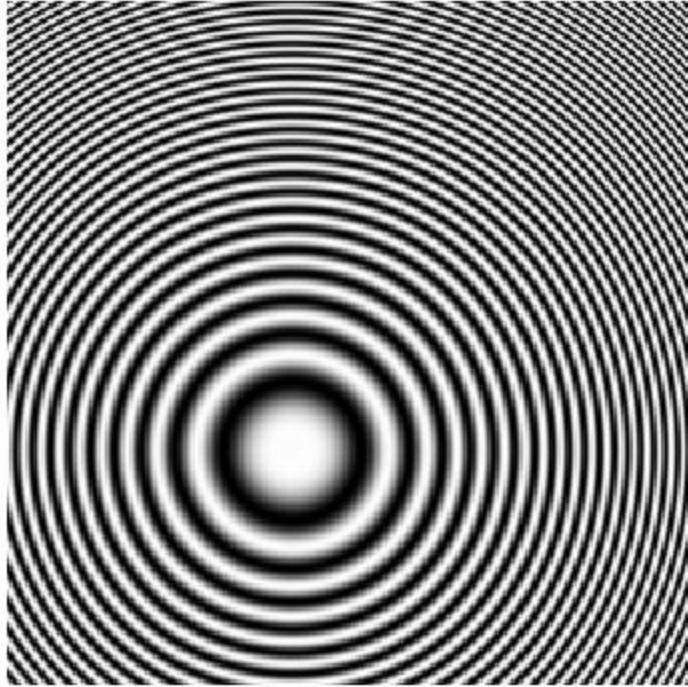
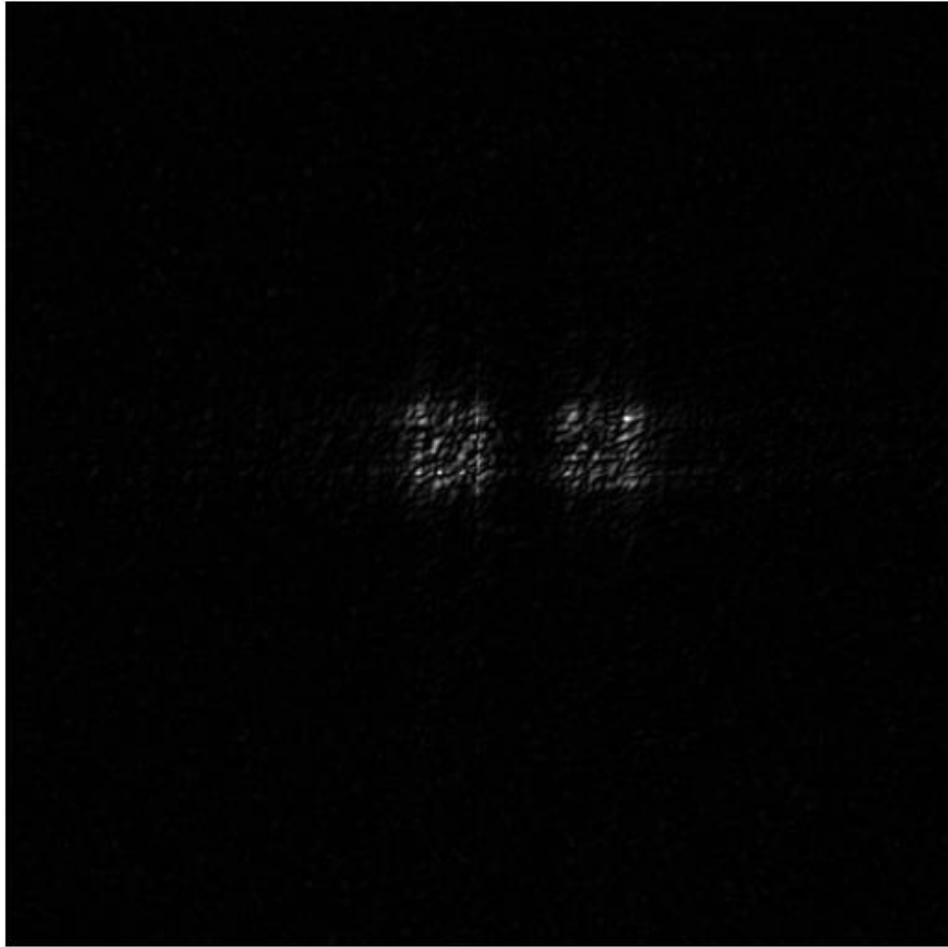
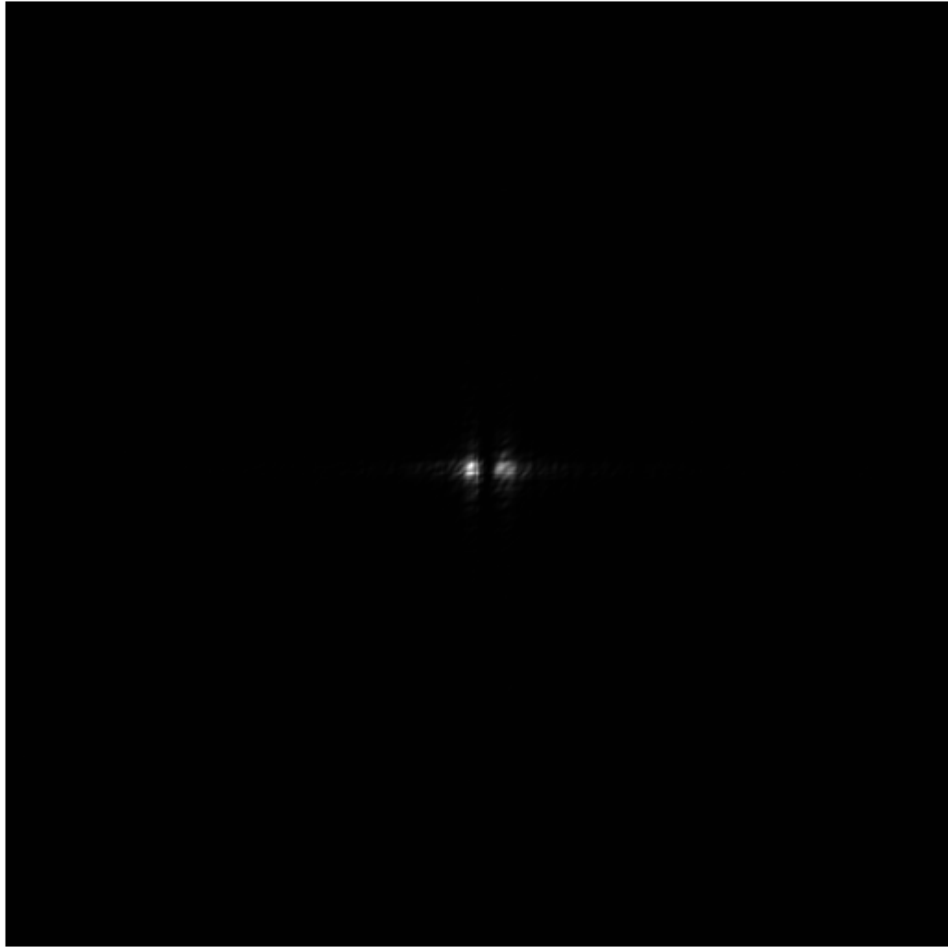


Figure 5.20: In- line FZPs for a 2mm propagation distance (distance between the point sources and the hologram)



**Figure 5.21: Reconstructed point sources for different propagation distance:
 $z=50\text{mm}$**



**Figure 5.22: Reconstructed point sources for different propagation distance:
 $z=75\text{mm}$**

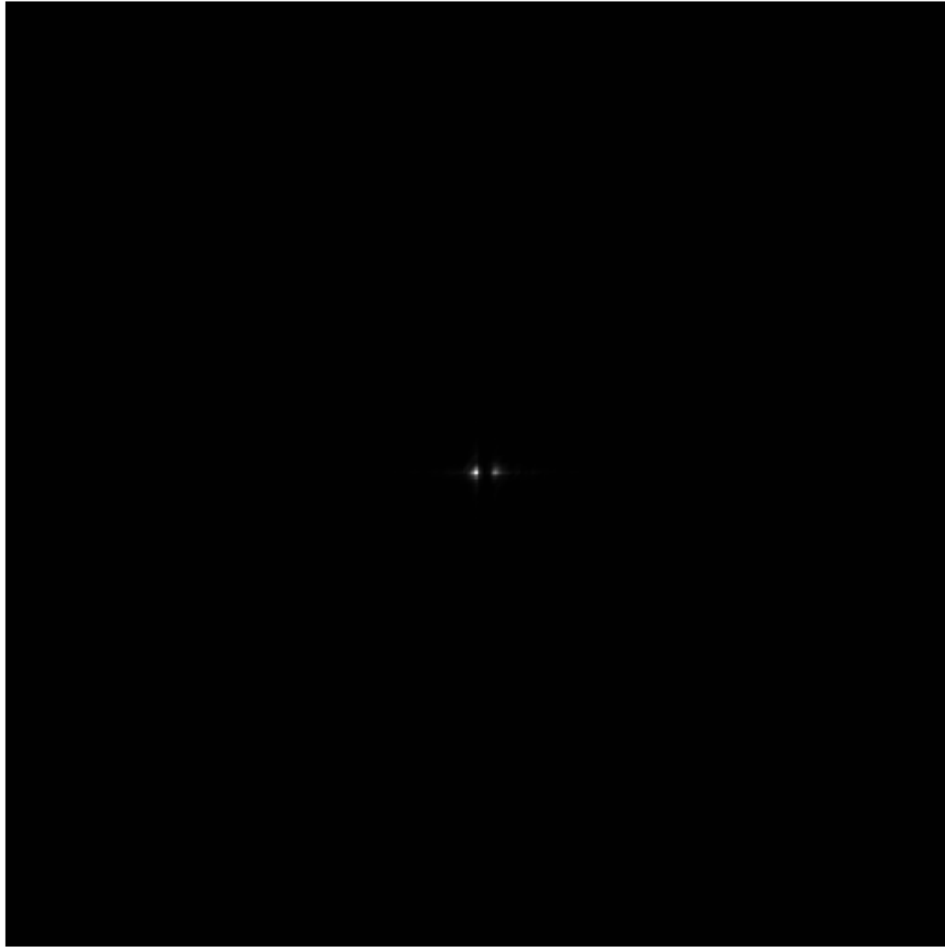


**Figure 5.23: Reconstructed point sources for different propagation distance:
 $z=100\text{mm}$**

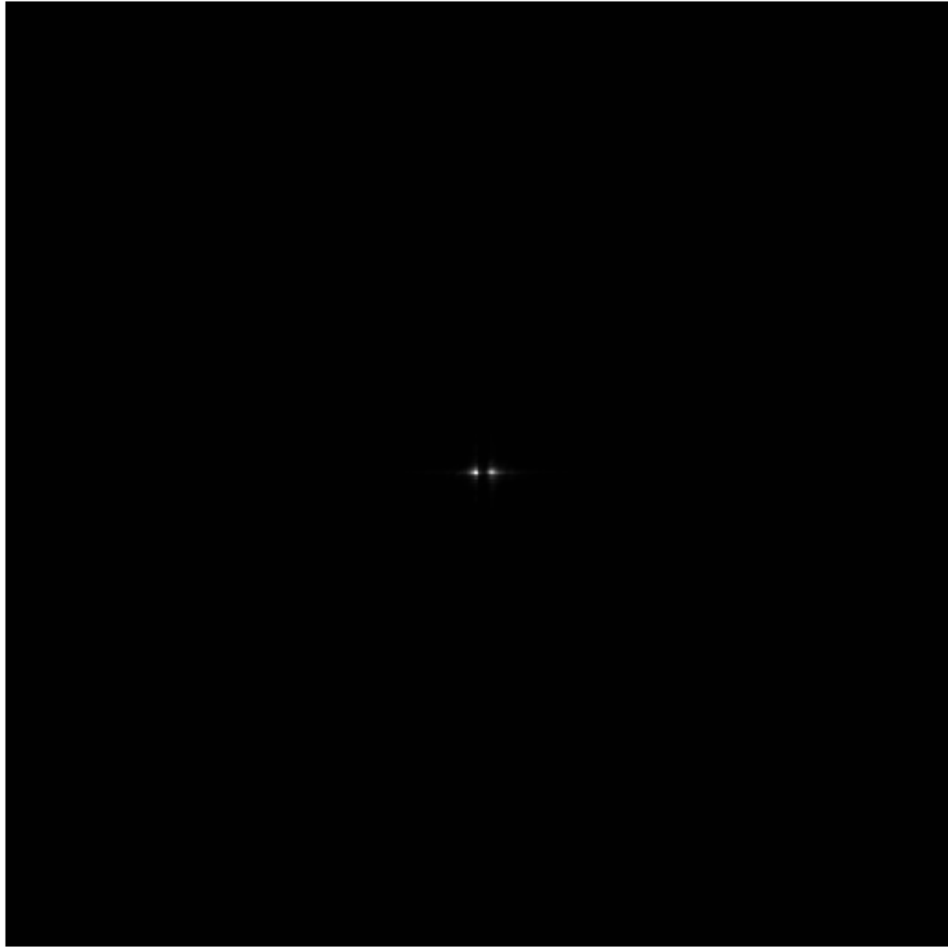


**Figure 5.24: Reconstructed point sources for different propagation distance:
 $z=110\text{mm}$**

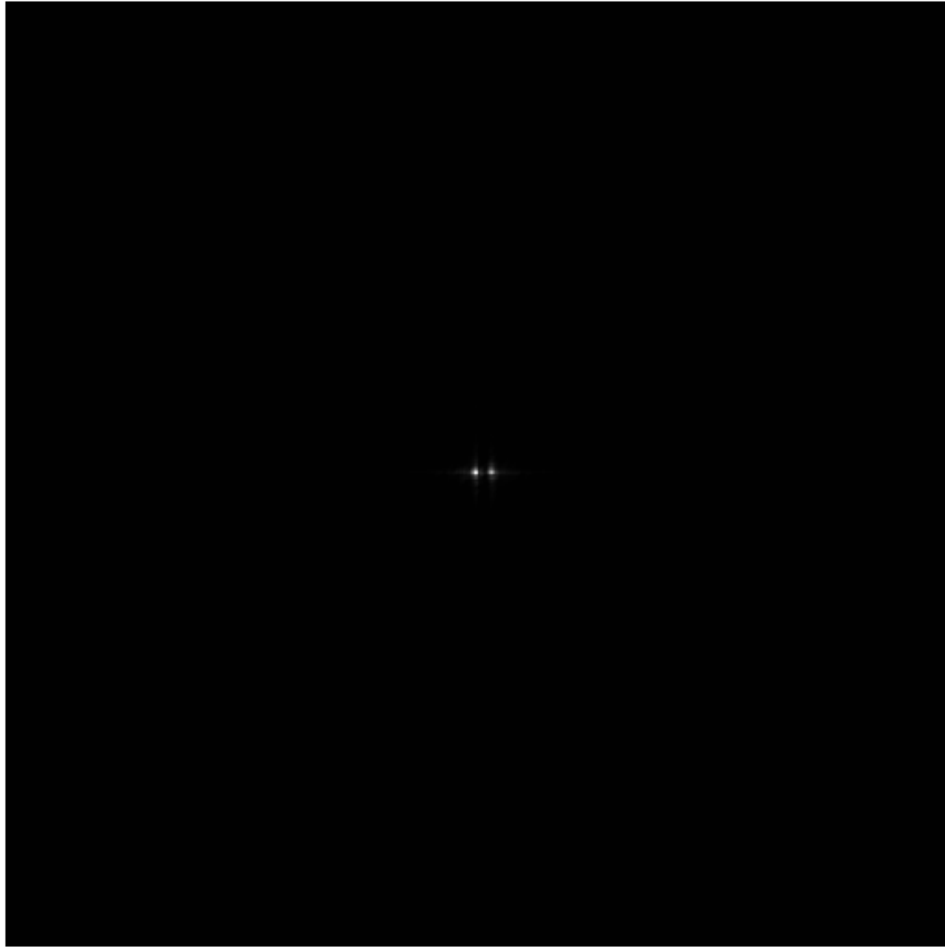


**Figure 5.25: Reconstructed point sources for different propagation distances:
 $z = 150\text{mm}$**

To achieve the validity condition, the correct calculation of the reconstructed image from the achieved pattern may be performed if the propagation distance is longer than the critical distance. Reconstruction the point source (original object) fails in the Figure 5.21 as the distance is less than the critical propagation distance.

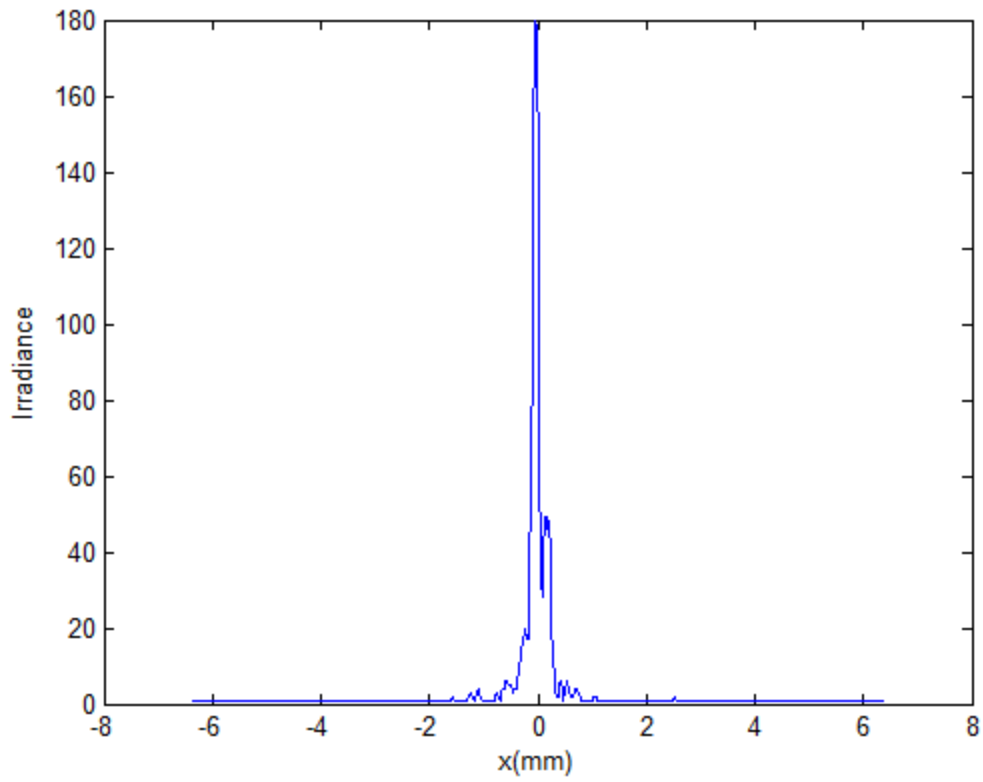


Figure 5.26: Reconstructed point sources intensity for different propagation distances (distance between the point sources and the FZPs): (a) $z=50\text{mm}$

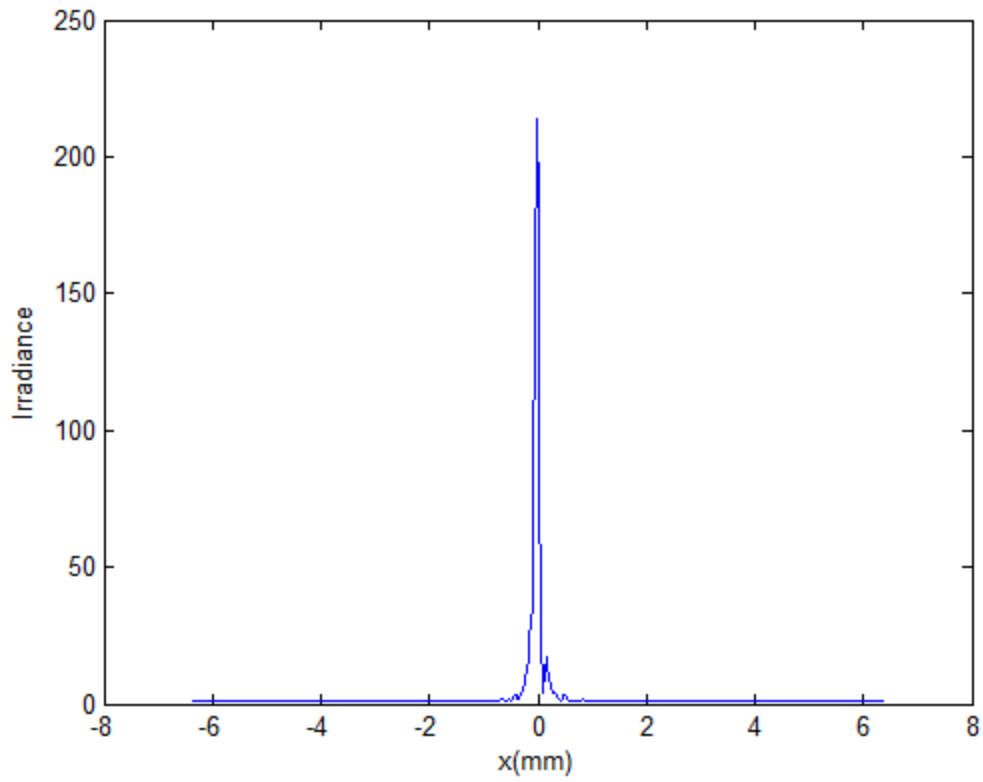


Figure 5.27: Reconstructed point sources intensity for different propagation distances (distance between the point sources and the FZPs): $z=75\text{mm}$

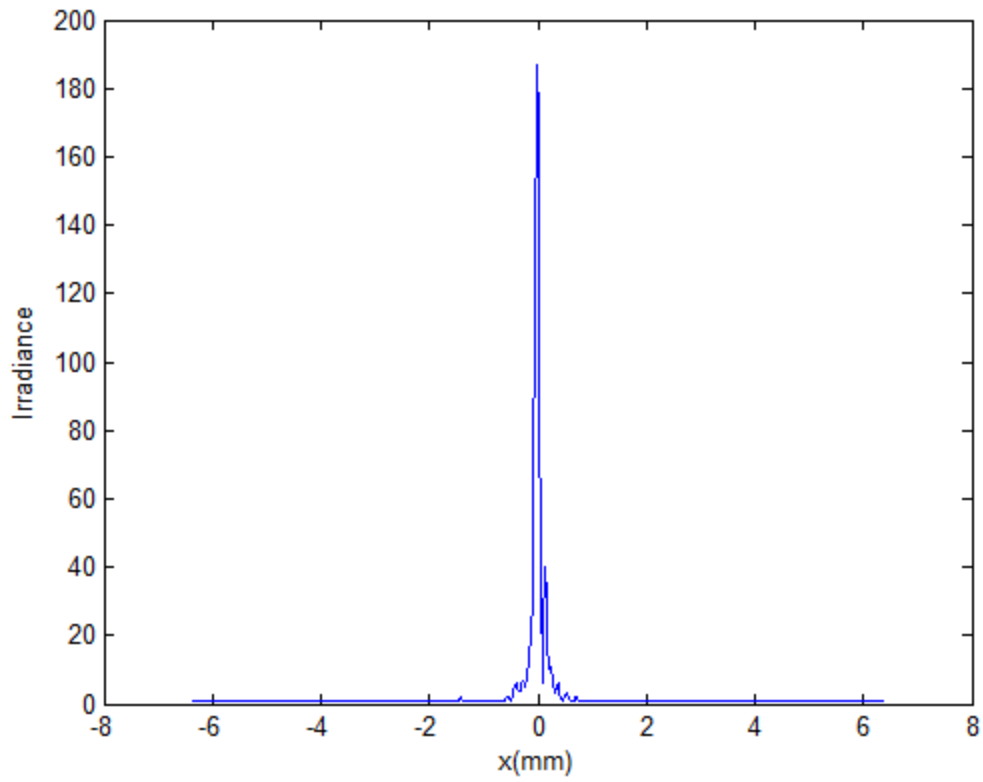


Figure 5.28: Reconstructed point sources intensity for different propagation distances (distance between the point sources and the FZPs): $z=100\text{mm}$

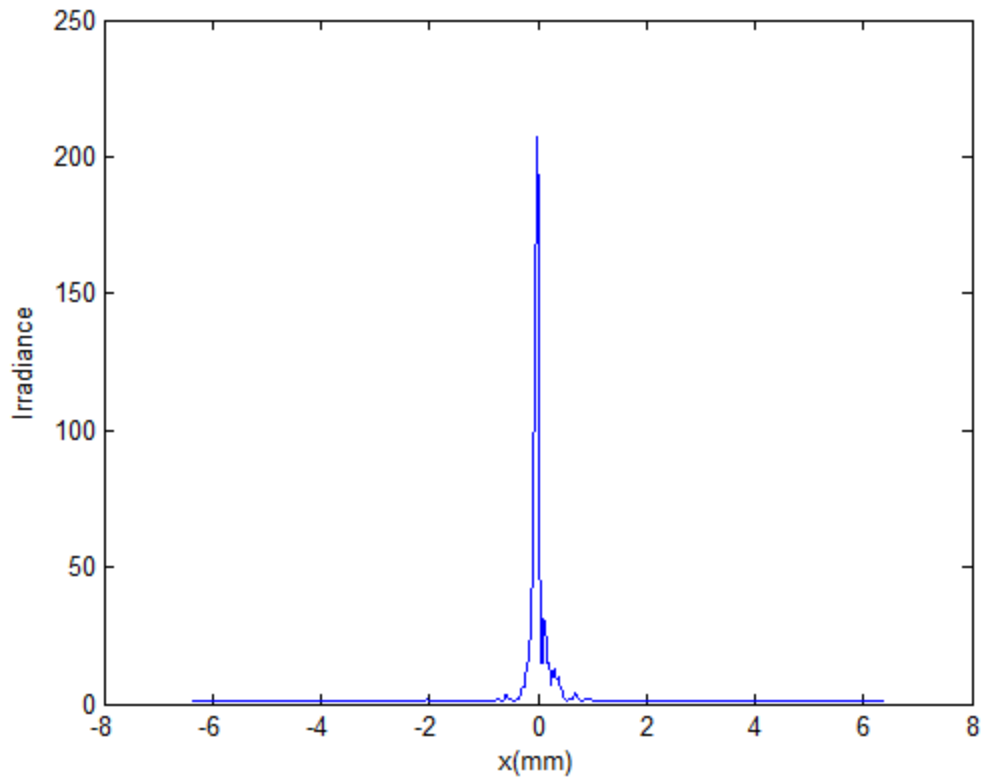


Figure 5.29: Reconstructed point sources intensity for different propagation distances (distance between the point sources and the FZPs): $z=110\text{mm}$

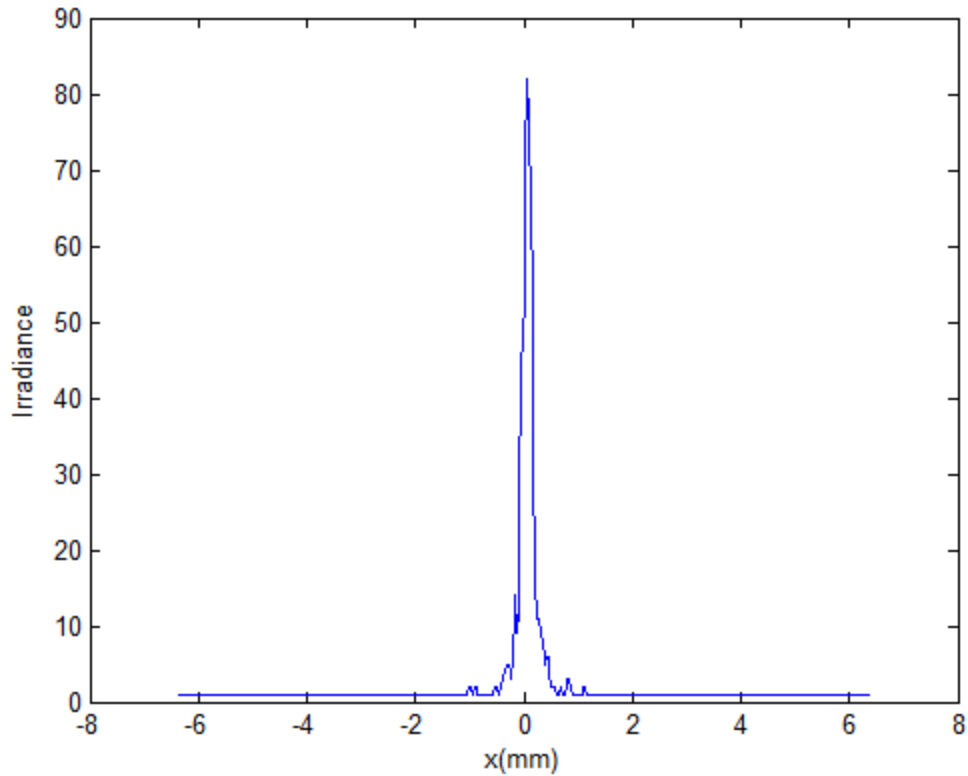


Figure 5.30: Reconstructed point sources intensity for different propagation distances (distance between the point sources and the FZPs): $z = 150\text{mm}$

We validate our simulation results against the propagation distance between the hologram and the screen and we find that the reconstructed point sources change accordingly. Figures 5.26, 5.27, 5.28, 5.29, and 5.30 showing the results for different propagation distances between the FZPs and the screen.

We use the MATLABTM to reconstruct the original point sources and the Figures 5.31, 5.32, 5.33, and 5.34 showing the point sources in the object domain.

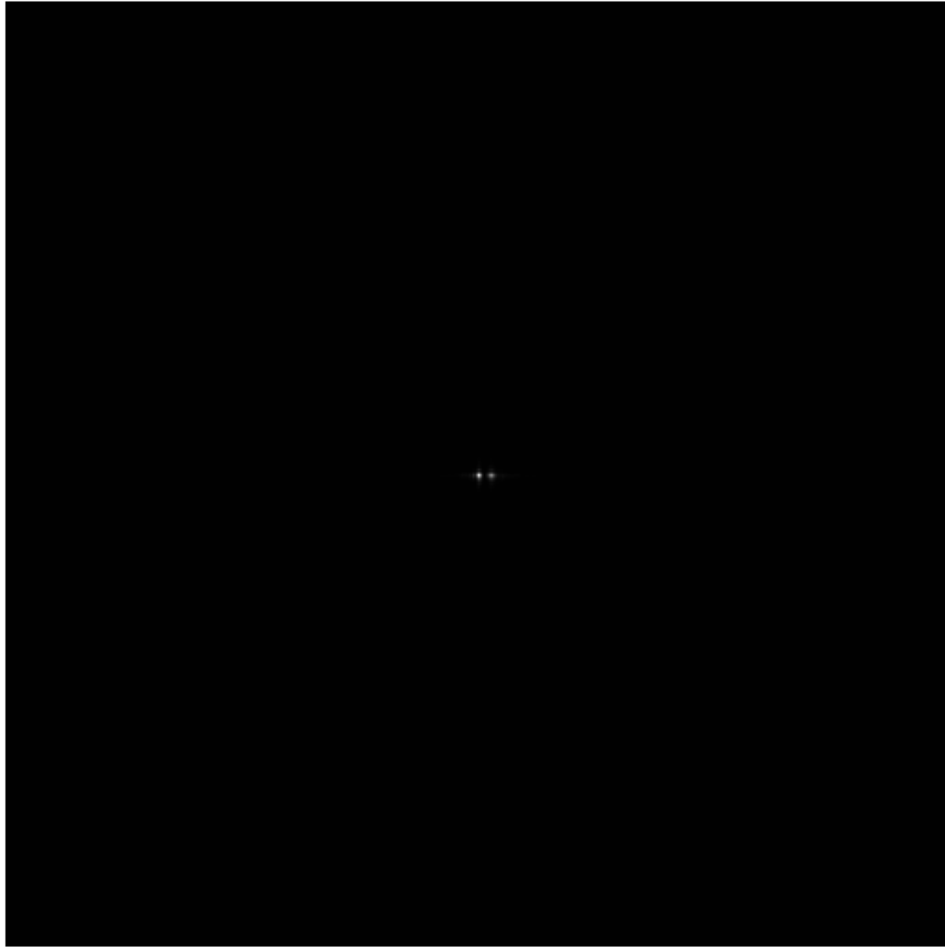


Figure 5.31: Reconstructed point sources intensity for different propagation distances (distance between the hologram and the screen): $-z=0.05\text{mm}$

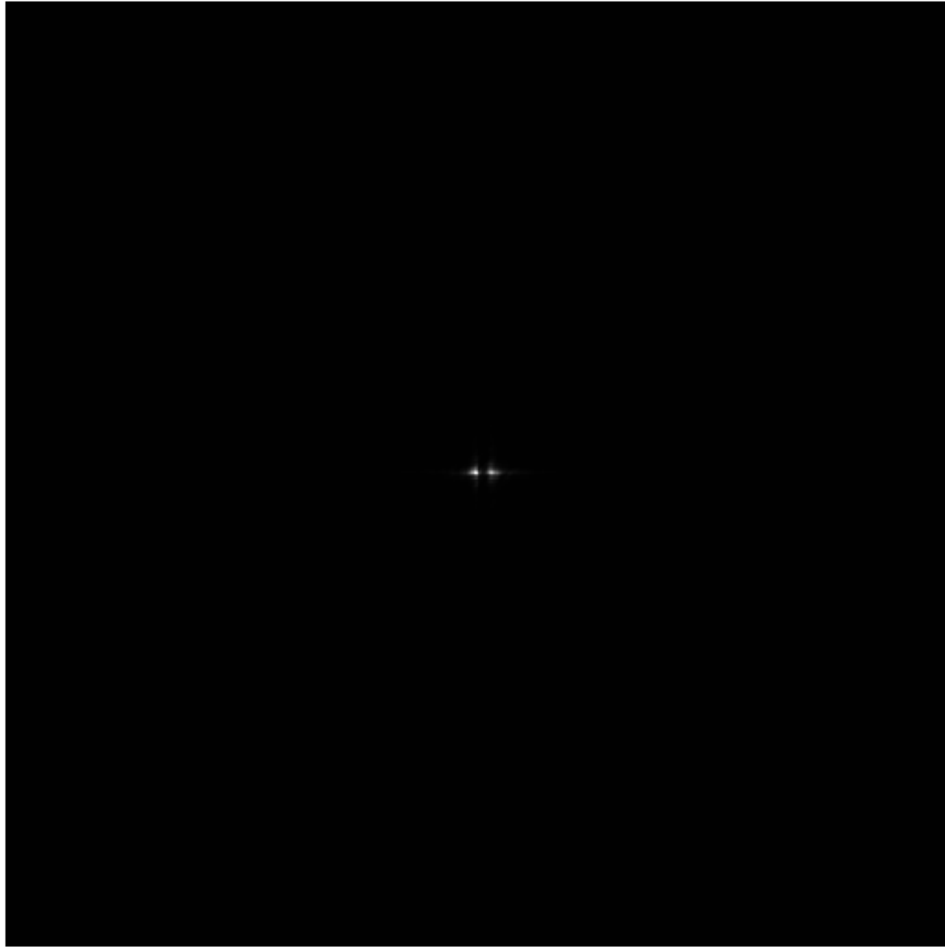


Figure 5.32: Reconstructed point sources intensity for different propagation distances (distance between the hologram and the screen): $-z=5\text{mm}$

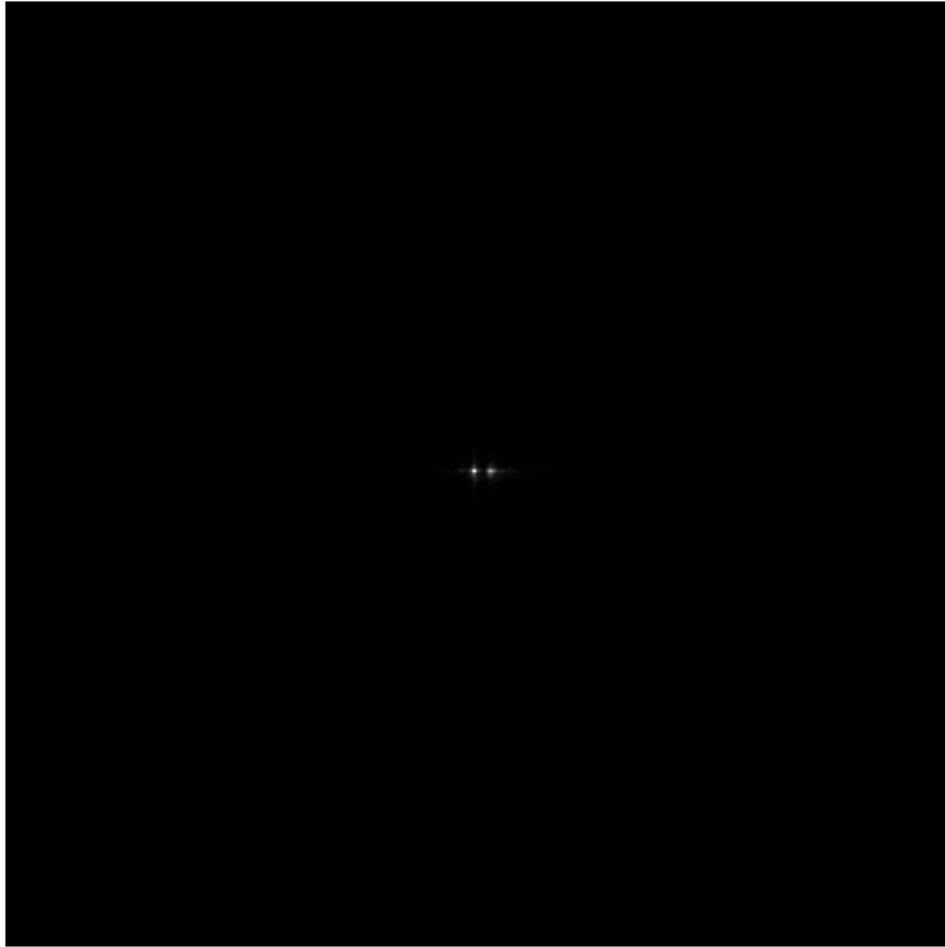


Figure 5.33: Reconstructed point sources intensity for different propagation distances (distance between the hologram and the screen): $-z=50\text{mm}$

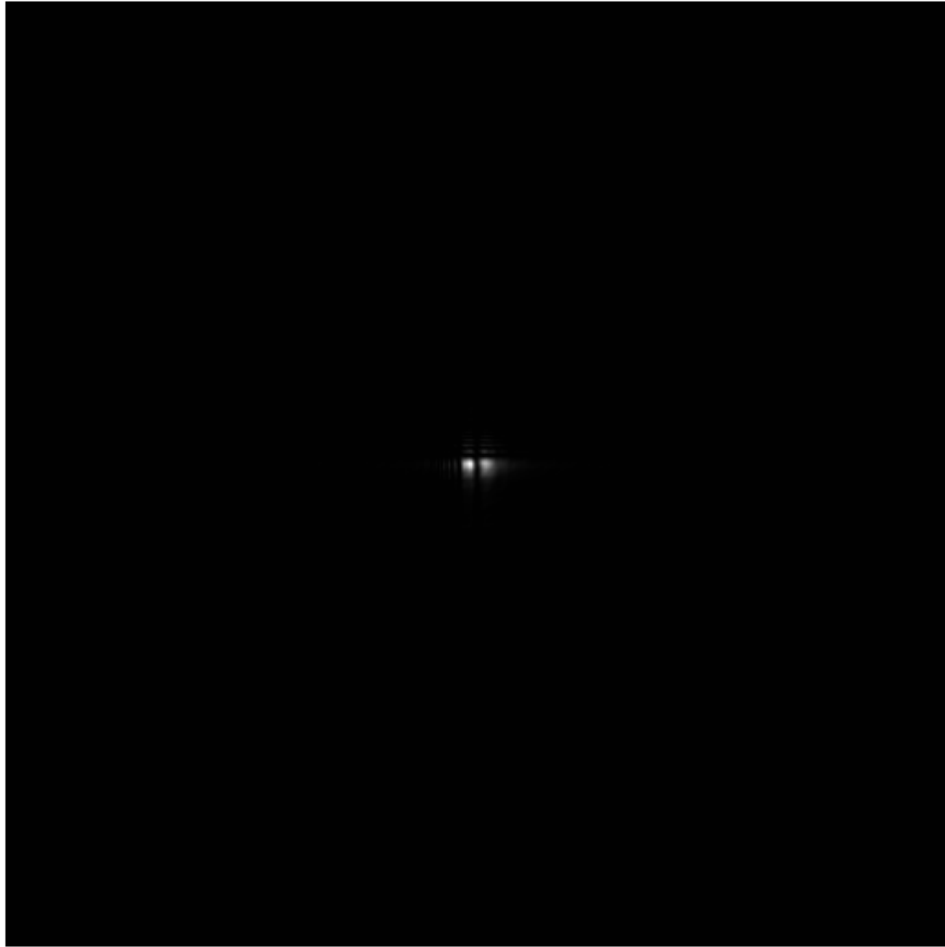


Figure 5.34: Reconstructed point sources intensity for different propagation distances (distance between the hologram and the screen): $-z = 100mm$

We validate our simulations by taking different distances between the FZPs. Figures 5.35, 5.36, 5.37, and 5.38 illustrate the reconstructed intensity points for $x = 1mm, 5mm, 50mm,$ and $150mm$ where x is the distance between the centres of the FZPs.

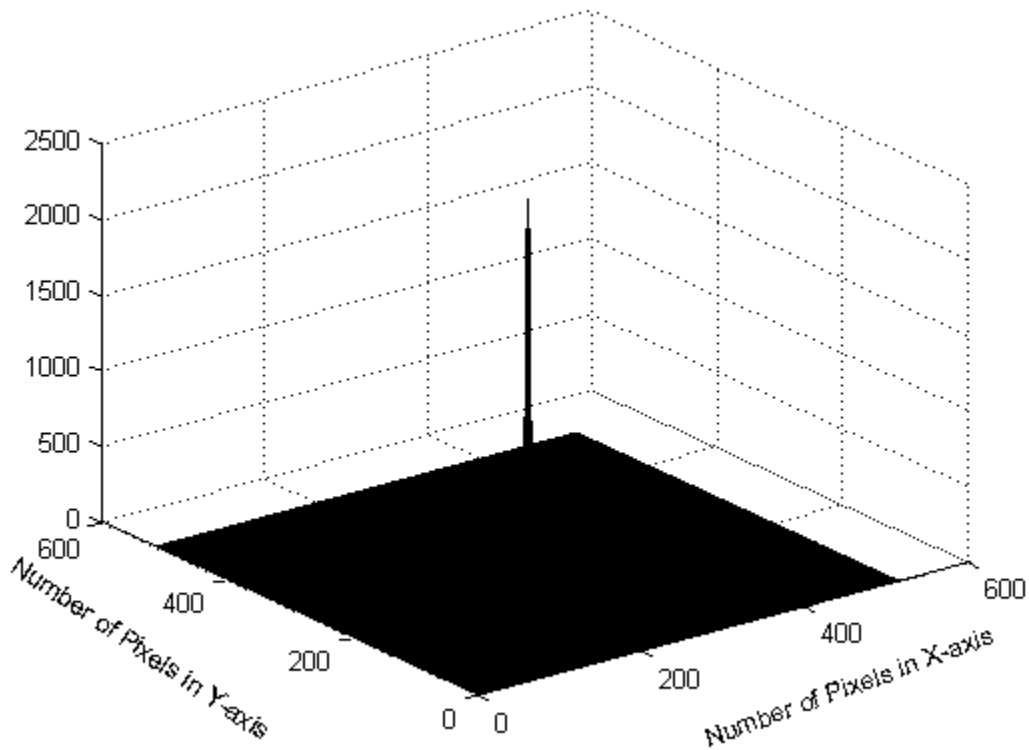


Figure 5.35: Isometric views of the reconstructed two point sources intensity for different distances between the FZP centres: $x=1mm$

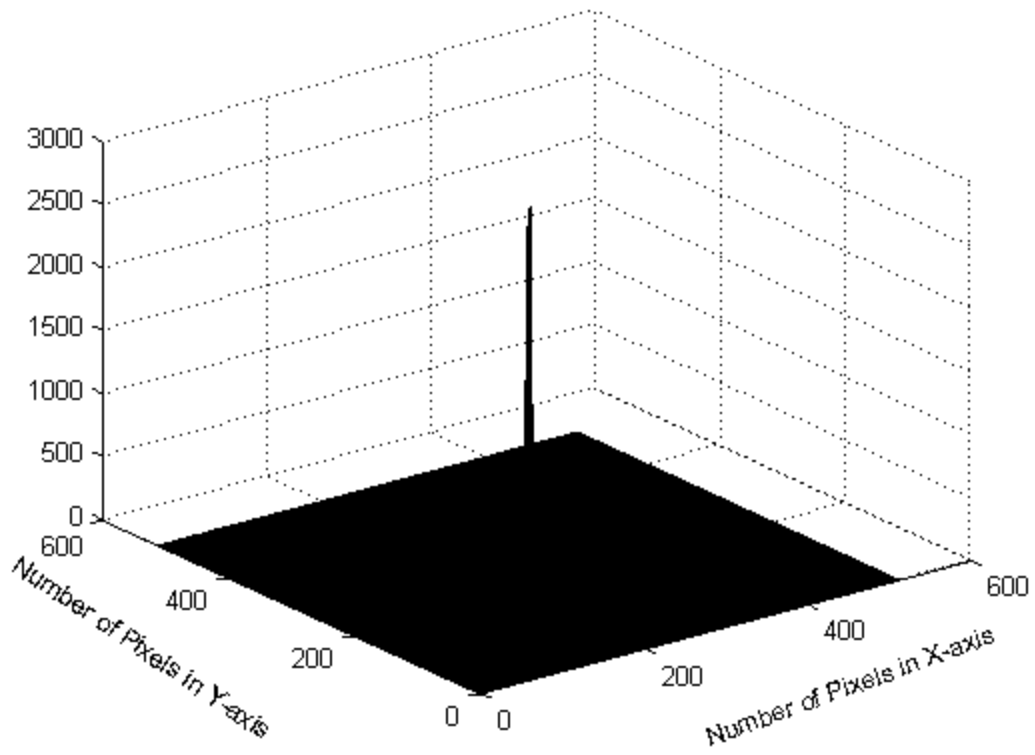


Figure 5.36: Isometric views of the reconstructed two point sources intensity for different distances between the FZP centres: $x=5\text{mm}$

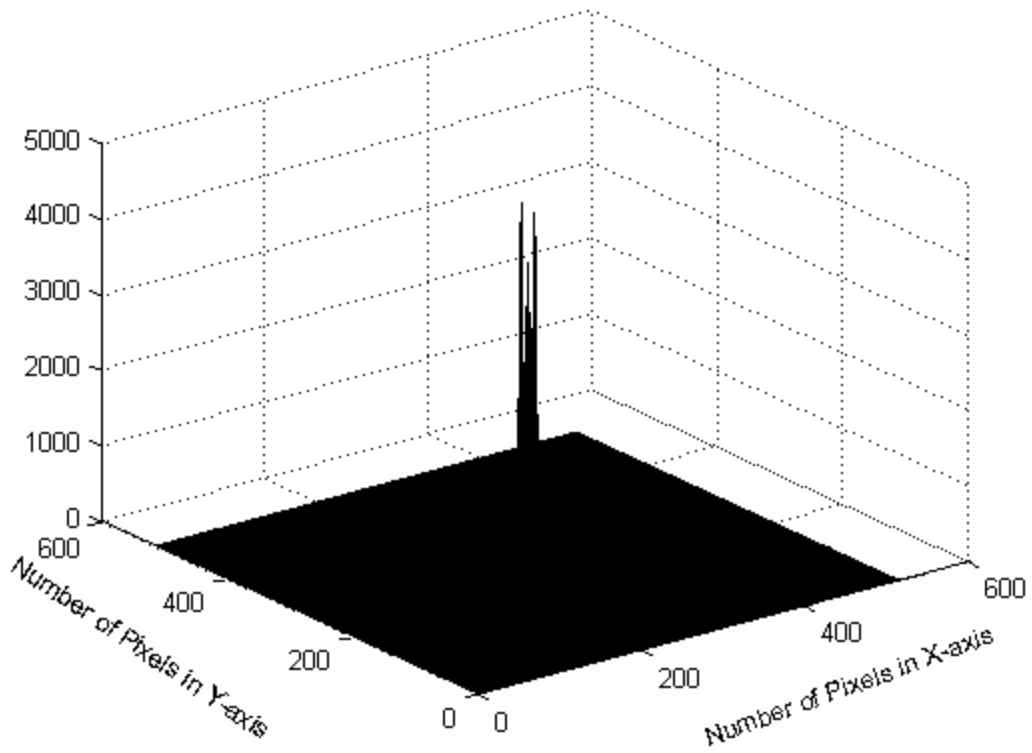
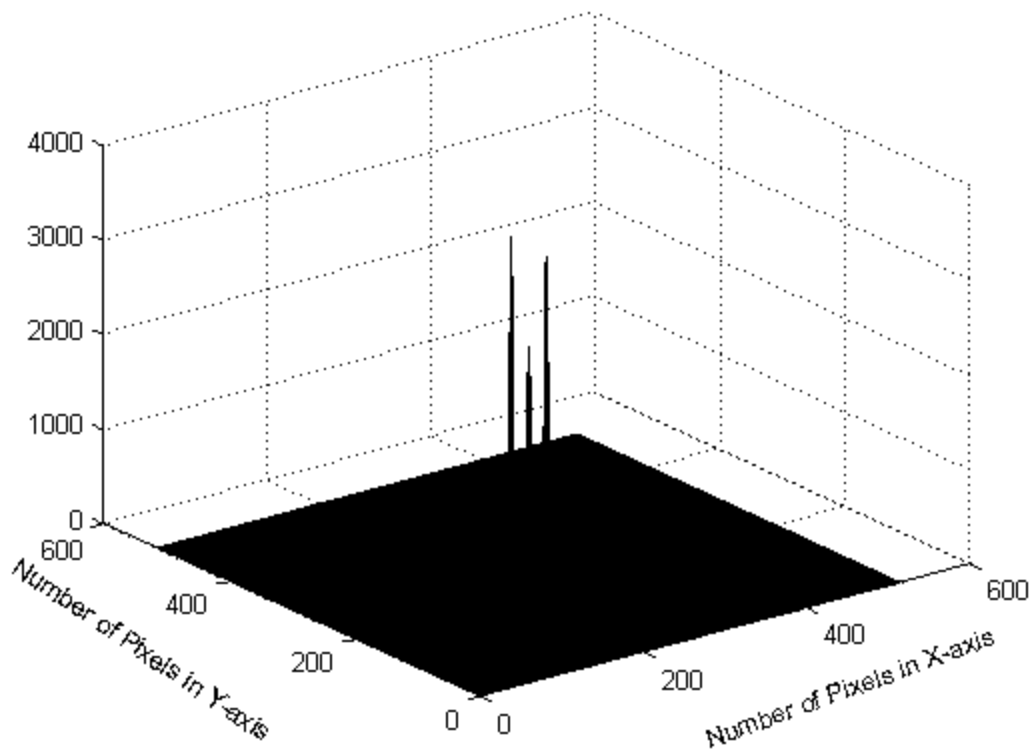


Figure 5.37: Isometric views of the reconstructed two point sources intensity for different distances between the FZP centres: $x=50\text{mm}$



(d)

Figure 5.38: Isometric views of the reconstructed two point sources intensity for different distances between the FZP centres: $x = 150mm$

5.14 Conclusion

In this chapter, we consider two point objects which each emit spherical waves. Both spherical waves interfere on the recording medium to produce a hologram. This recording stage yields real and an imaginary images that reconstruct only real images, where the hologram is illuminated with a reconstruction wave that is spherical wave, originating from a point source. We have to constrain that the wavelength used in the reconstruction stage is the same as the wavelength that is used to construct the hologram. We calculate the total complex field away from the hologram plane and this will produce two reconstructed point sources.

Holographic imaging produces a reliable and quick technique to store complete 3D information of a scene in a 2D format.

The type of the hologram we consider in this chapter is the iterative digital Fresnel hologram. In this means a hologram of a single point has the form of a FZP. The axial position of the point source is encoded by the Fresnel number of the FZP, that is the ring density in the FZP. Thus the Fresnel holographic system can be represented by a set of rings which project the FZP onto the image plane for each of the original object points. Encoding the depth of the points is created by the density of the rings; denser rings when the point object is closer to the hologram plane while less dense rings for point sources farther away from the plane of the hologram. This encoding technique indicates that the 3D information of the original object is recorded into the hologram.

In the reconstruction stage, each plane in the image space which is reconstructed from the Fresnel hologram will in focus at different axial distances. The technique of creating Fresnel holograms vary from each other in the way that the FZP and the 3D object are spatially correlated. This correlation should be done in such a way that the FZP is sensitive to the axial locations of the object point. Without this, these locations cannot be encoded into the hologram. This means that the points that are further away from the system will project on to the FZP with fewer cycles per radial length than nearby points. This is then the condition for creating the 3D reconstructed holographic image.

In summary, an object is assumed to be composed of self-illuminated points which each will create an individual FZP. To create a hologram for the 3D object we take the summation of the FZP corresponding to each individual object point. This is the technique of generating the Fresnel hologram, where the object is considered as a set of 3D object points of different intensity and axial distance from the plane of the hologram.

We have presented an overview on the topic of the phase retrieval problem. We have presented some interesting perspectives with three different approaches: digital holography, iterative phase retrieval and multiple measurement methods. The phase retrieval methods, mentioned in this chapter, are commonly used in different three dimensional applications. Space telescopes, such as the James Webb space telescope [106], use the multiple measurement iterative approach. Electron microscopy uses the multiple measurement method as well. Iterative phase retrieval algorithms are also used for planning diffractive optical elements (DOE) used as phase only filters for beam shaping [107]. Digital holography microscopes (DHM) also use different interferometer based setups [108].

In this chapter we presented a new reconstruction method using two intensities measured in the Fourier plane. One is the magnitude of the sought after signal's Fourier transform, and the other is the intensity resulting from the superimposition of the original image and an approximately known reference beam. While the method was originally developed for the phase retrieval problem, it can be useful in digital holography, because it poses less stringent requirements on the reference beam. The method is designed specifically to allow severe errors in the reference beam without compromising the quality of reconstruction. Numerical simulations justify our approach, exhibiting a good reconstruction quality for a wide range of depths from the hologram.

We have also presented the constraints in CGH design and shown that it is possible to record any required phase using CGH techniques. The IFTA is the technique we used in this project which is a technique that optimises CGH phase only Fourier holograms. Our work has shown that using IFTA improves the reconstructed holographic image and use this to show that the use of the computational method in digital holography is preferable over conventional holography in terms of dealing with spurious noise, fringes, optical system aberrations, etc. We have described how the IFTA algorithm involves forward and backward iteration between two planes. The phase retrieval technique, namely, the recovery of a function given the magnitude of its Fourier transform, is employed in many fields of science and engineering, including electron microscopy, astronomy, and optical imaging. However,, we showed that the IFTA procedure is time consuming and iteration may not fully coverage the original point sources.

6 CHAPTER 6

6.1 Conclusion and Future Work

Conclusion

Chapter 2 gives an overview of the techniques employed in optical holography. In this chapter we noted that optical holography consists of the acquisition of images from diffracted optical field measurements. Our review dated back to the initial holographic imaging which was proposed by Gabor for electron microscopy. Also, we noted that optical holograms were recorded on high resolution photographic plates, originally with an in-line configuration. The advantage of using the in-line technique is that the setup of the recording the hologram and reconstruction of the object are very simple. However, the hologram reconstructions were disrupted with a twin image and zero order contributions, which overlapped with the signal image. Thus the in-line hologram cannot be used in many applications as the amplitude variation should be very small. The in-line problem was resolved in 1962 by Leith and Upatnieks who proposed to introduce an off-axis reference beam to separate, in the spatial frequency domain, the real image from the twin image and zero order diffraction terms. The off-axis hologram is based on separating the reference beam from the object beam and thus separate the real image from the twin image. There should be a few degrees between the reference and object wave and only one acquisition required to reconstruct the information of the original object.

In chapter 3, we presented digital holography and we discussed the detour phase hologram which is the oldest holographic technique for encoding the complex wavefront. To construct the detour phase hologram we should divide the area of the hologram into an array of unit cells. In each cell we make an aperture and control the phase by shifting the centre of the aperture. In this technique most of the energy is concentrated in the zeroth-order and it therefore yields a blurred reconstructed image. We can improve the quality of the image by applying a random phase mask to the original object to widen the object spectrum. We show the benefit of using a random phase mask on the original object by illustrating clear reconstructed images and comparing these with holographic images that are reconstructed without a random phase mask.

We present the kinoform which is another technique of generating a computer hologram. The main difference between the kinoform and the detour phase hologram is that the kinoform has a high

light efficiency. Also, in using the kinoform method, there is not any conjugate wavefront in the reconstructed stage which is unlike the wavefront reconstructed using the detour phase hologram.

As for the detour phase hologram, in the kinoform hologram we are also able to use a random phase mask with the original object to diffuse the object light which is necessary to record the whole object dynamic range on the kinoform. In the case of not using the random phase mask, we show that the reconstructed image is blurred with most of the energy concentrating in the zeroth-order.

Also, we conclude that the intensity efficiency increases by adding a random phase mask with the main object, the clarity of the reconstructed image increasing by using a random phase mask, and the intensity of the central bright spot reducing to zero.

Also, in this chapter, we present the Gerchberg-Saxton (GS) algorithm which is normally used to solve the problem of phase retrieval of a field at two different planes, when at those planes only the field moduli are known and given that the fields are related by a Fourier transform. We include a block diagram of the GS algorithm. In Chapter 3 the steps can be summarised by the following steps.

At the beginning there is a field with an amplitude which is given by the square root of the expected intensity and the phase is constant. We propagate the field from the image plane to the object plane, neglect the amplitude information and keep only the phase information. In the next step the amplitude and phase of the illumination field are added to the phase information to obtain the resulting object field we then propagate the field to the image plane and the resulting reconstructed image is compared with the expected one. We use the root mean square error to control the iteration processes. We take a different number of iterations and we notice that increasing the iteration number produces a better image quality.

In Chapter 4 we reconstruct a phase quadratic function from intensity only. First, we present the light point source, from which emanating radiation originates at the same point in space. The point source emanates a diverging spherical wave toward the recording medium. The intensity distribution is recorded as the hologram which is the Fresnel Zone Plate (FZP) and represents the hologram of the point source object. Also, we represent the local fringe frequency that increases linearly with the spatial coordinates, with higher local spatial frequency when the point source

object is further away from the centre of the FZP. We take the FFT to the FZP plane and the Fourier transform decomposes the image into frequency domain phase and magnitude terms. We are only interested in the phase and add a random phase to it and then take the FFT of the combination.

The amplitude is the only information we need as the input of the modified iterative Fourier transform. We have proposed this iterative FT algorithm to reconstruct the quadratic phase. The algorithm is based on error reduction iterative method to solve the phase retrieval problem.

The algorithm consists of four simple steps which start with the Fourier transform of an estimate of the original object which is the point source in this project. We then replace the modulus of the resulting computed Fourier transform with the measured Fourier modulus to form an estimate of the Fourier transform. We then take the inverse Fourier transform and in the last step replace the modulus of the resulting computed image with the measured object modulus to form a new estimate of the object.

To monitor the quality of the resulting reconstructed image of the hologram, we apply the root mean square error (RMSE) between the target and evaluated images. We used a different number of iterations to validate our algorithm. We find that the error-reduction algorithm decreases the error rapidly for the first few iterations but much more slowly for later iterations. We then subtract the known random phase and the quadratic phase is then the phase recovered by the algorithm.

We reconstruct the original point source when we propagate the quadratic phase for a distance away from the hologram. We validate this process by taking different propagation distances and we show the results of this in the final part of Chapter 4.

In Chapter 5 present multiple point sources as the original objects, which create multiple FZPs. In the first example, we use only the diffraction pattern of two point sources. We proposed a new fast algorithm for producing Computer Generated Holograms of 3D objects using the superposition of FZPs. We been able to show how the distance between the FZPs create a different pattern and reconstruct a different quadratic phase after the iterations have finished. Also, we discussed off-axis holography and using this how we are able to separate the twin image and the zero order beam from the desired image and produce very clear reconstructed images of the point sources.

6.2 Future work

The hologram created in this work is a phase only hologram as this allows us to reconstruct the quadratic phase of the FZP. We find that the quadratic phase is critical to reconstructing a high-quality image. Therefore, in the future, a Spatial Light Modulator (SLM) which is capable of displaying the phase image with high fidelity could be employed. The phase hologram has theoretically a 100% diffraction efficiency and no conjugate image, as we have seen in Chapters 4 and 5 although, in practice, the pixellation of the device will cause diffraction into multiple orders. In future, we are planning to use such an SLM for experimentally reconstructing the point source object and assessing its quality.

In an experimental set-up, the light from a coherent point source (or multiple mutually coherent point sources) propagates to a plane in which we place an SLM displaying a known but random phase mask. The coherent field is scattered by this mask and Fourier transformed by a lens to an output plane. A detector in this plane records the two dimensional intensity pattern. This distribution is then used as the starting point for the iterative recovery algorithm described in the thesis. Upon convergence, the known random phase distribution is removed and the remaining quadratic phase distribution (for a single point source) is numerically back propagated to determine the point source location and thus satisfy the objective of the procedure developed in this thesis.

List of Published Papers

M. Al-Shamery, R.C.D Young, C.R. Chatwin, “Kinoform Optimisation Using Gerchberg-Saxton Iterative Algorithm,” ICDHTDI 2015: 17th International Conference on Digital Holography and Three-Dimensional imaging (WASET), Dubai, UAE, November 24-25th, 2015.

REFERENCES

- [1] R. Kelner, J. Rosen and G. Brooker, “Enhanced resolution in Fourier incoherent single channel holography (FISCH) with reduced optical path difference,” *Opt. Express* 21(17), 20131–20144 (2013).
- [2] J. Swoger, M. Martinez-Corral, J. Huisken, and E. Stelzer, “Optical scanning holography as a technique for highresolution three-dimensional biological microscopy,” *J. Opt. Soc. Am. A* 19, 1910–1918 (2002).
- [3] W. Xu, M. H. Jericho, I. A. Meinertzhagen, and H. J. Kreuzer, “Digital in-line holography of microspheres,” *Appl. Opt.* 41, 5367–5375 (2002).
- [4] M. H. Jericho and H. J. Kreuzer, “Point source digital in-line holographic microscopy,” in *Coherent Light Microscopy*, Vol. 46 of Springer Series in Surface Sciences, P. Ferraro, A. Wax, and Z. Zalevsky, eds. (Springer-Verlag, 2011), pp. 3–30.
- [5] S. K. Jericho, J. Garcia-Sucerquia, W. Xu, M. H. Jericho, and H. J. Kreuzer, “Submersible digital in-line holographic microscope,” *Rev. Sci. Instrum.* 77, 043706 (2006).
- [6] Barrett, H. H., and F. A. Horrigan. “Fresnel zone plate imaging of gamma rays; theory.” *Applied optics* 12.11 (1973), 2686-2702.

- [7] Sun, Ping, & Xie, Jing-hui. "Method for reduction of background artifacts of images in scanning holography with a Fresnel-zone-plate coded aperture.(Author Abstract)," *Applied Optics*,43(21) (2004), 4214-4218.
- [8] T. D. Beynon, & A. G. Pink. "Neutron holography using Fresnel zone plate encoding," *Nature*, 283(5749), (1980), 749-751.
- [9] J. D. Stack and M. R. Feldman, "Recursive mean-squarederror algorithm for iterative discrete on-axis encoded holograms," *Appl. Opt.* 31, 4839-4846 (1992).
- [10] Jericho, M., Kreuzer, H., Kanka, M., & Riesenber, R. "Quantitative phase and refractive index measurements with point-source digital in-line holographic microscopy," *Applied Optics*, 51(10), (2012), 1503-15.
- [11] M.H. Jericho and H.J. Kreuzer, in 'Coherent Light Microscopy, Chapter 1 Point Source Digital In-Line Holographic Microscopy', (Springer, NY, 2011), pp. 3–30.
- [12] S. Schedin, G. Pedrini, H.J. Tiziani, "Pulsed digital holography for deformation measurements on biological tissues," *Appl. Opt.* 39, (2000), 2853-2857.
- [13] M.K. Kim, "Tomographic three-dimensional imaging of a biological specimen using wavelength-scanning digital interference holography," *Opt. Express*, 7, 305-310 (2000).
- [14] F. Charrière, N. Pavillon, T. Colomb, C. Depeursinge, T.J. Heger, E.A.D. Mitchell, P. Marquet, B. Rappaz, "Living specimen tomography by digital holographic microscopy: morphometry of testate amoeba," *Opt. Express* 14, (2006): 7005-7013.

- [15] W. Xu, M. H. Jericho, I. A. Meinertzhagen, H. J. Kreuzer, "*Digital in-line holography for biological applications*," *PNAS* 98, (2001):11301-11305.
- [16] Kemper, Bjorn, & Von Bally, Gert. "*Digital holographic microscopy for live cell applications and technical inspection.*"(Author abstract)(Report). *Applied Optics*, 47(4), (2008), A52-A61.
- [17] M. Simonutti, M. Paques, J. A. Sahel, M. Gross, B. Samson, C. Magnain, and M. Atlan, "*Holographic laser Doppler ophthalmoscopy*," *Opt. Lett.* 35, 1941-1943 (2010).
- [18] Fienup, James R. "*Reconstruction of an object from the modulus of its Fourier transform.*" *Optics letters* 3.1 (1978): 27-29.
- [19] Fienup, James R. "*Phase retrieval algorithms: a comparison.*" *Applied optics* 21.15 (1982): 2758-2769.
- [20] Gerchberg, R.W. and Saxton W. O., A. "*A practical algorithm for the determination of phase from image and diffraction plane pictures*". *Optik* 35, (1972):237-46.
- [21] Saxton, W., & Cowley. "*Computer Techniques for Image Processing in Electron Microscopy*," *Physics Today*, 32(3), (1979): 74-76.
- [22] Fienup, J. R. "*Iterative method applied to image reconstruction and to computer-generated holograms.*" *Optical Engineering* 19.3 (1980): 193297.

- [23] Liu, B. and N. C. Gallagher, “*Convergence of a Spectrum Shaping Algorithm,*” *Appl. Opt.* 13, (1974) 2470-71.
- [24] P. M. Hirsch, J. J. A. Jordan, and L. B. Lesem, “*Method of making an object-dependent diffuser,*” *U. S. patent* 3,619, 022 (1971).
- [25] Fineup, J. R., “*Reduction of Quantization Noise in Kinoforms and Computer-Generated Holograms,*” *J. Opt. Soc. Am.* 64, 1395 (1974) (Abstract).
- [26] Fineup, J. R., “*Improved Synthesis and Computational Methods for Computer-Generated Holograms,*” *Ph.D. thesis, Stanford University,* May 1975 (University Microfilms No. 75-25523), Chapter 5.
- [27] Fienup, J. “*Reconstruction of a complex-valued object from the modulus of its Fourier transform using a support constraint,*” *Journal of the Optical Society of America A*, 4(1), (1987): 118-123.
- [28] F. Wyrowski, “*Diffraction optical elements: iterative calculation of quantized blazed phase structure,*” *J. Opt. Soc. Am. A* 7, (1990): 961–969.
- [29] J. R. Fienup, “*Phase-retrieval algorithms: a comparison,*” *Appl. Opt.* 21, (1982): 2758–2769.
- [30] J. R. Fienup, “*Phase-retrieval algorithms for a complicated optical system,*” *Appl. Opt.* 32, (1993):1737–1746.

- [31] S. Buhling and F. Wyrowski, “Improved transmission design algorithms by utilizing variable-strength projections,” *J. Mod. Opt.* 49, (2002): 1871–1892.
- [32] V. V. Kotlyar, P. G. Seraphimovich, and V. A. Soifer, “An iterative algorithm for designing diffractive optical elements with regularization,” *Opt. Lasers Eng.* 29, (1998): 261–268.
- [33] H. Kim and B. Lee, “Iterative Fourier transform algorithm with adaptive regularization parameter distribution for the optimal design of diffractive optical elements,” *Jpn. J. Appl. Phys., Part 1* 43, (2004): L702–L705.
- [34] D. Gabor, “A new microscopic principle,” *Nature*, 161, (1948): 777.
- [35] J. W. Goodman, *Introduction to Fourier Optics*. (McGraw-Hill, New York, 1988).
- [36] Collier, R., Burckhardt, C., & Lin, L. (1971). *Optical Holography*. Academic P.
- [37] Hariharan, P. (1996). *Optical Holography: Principles, Techniques, and Applications*.
- [38] Gao, J., Lyon, J., Szeto, D., & Chen, J. “In vivo imaging and quantitative analysis of zebrafish embryos by digital holographic microscopy,” *Biomedical Optics Express*, 3(10), (2012): 2623-2635.
- [39] E. N. Leith and J. Upatnieks, “Reconstructed wavefronts and communication theory,” *J. Opt. Soc. Am.* 52, 1123–1130 (1962).

[40] ECN, p. ECN “*Holography Approach Improves Heads Up Displays For Planes And Cars,*” (2018, March 12).

[41] Breilkopf, David. “*Holograms Have a Back Problem. (use of holograms on payment cards).*” *American Banker*, 171(51), 1. (2006).

[42] Mityureva, A., & Smirnov, V. “*X-ray holography with an atomic scatterer.*”, *Ultramicroscopy*, 167, 1-4. (2016).

[43] Gauthier, D., Ge, X., Boutu, W., & Carre, B. (2010). “*Single-shot Femtosecond X-Ray Holography Using Extended References.*” *Physical Review Letters*, 105(9), 2010.

[44] A. W. Lohmann and D. P. Paris, “*Binary Fraunhofer holograms, generated by computer,*” *Appl. Opt.* 6, (1967): 1739–1749.

[45] Reichelt, S., Häussler, R., Fütterer, G., Leister, N., Kato, H., Usukura, N., & Kanbayashi, Y. “*Full-range, complex spatial light modulator for real-time holography,*” *Optics Letters*, 37(11), (2012): 1955-7.

[46] W. H. Lee, “*Sampled Fourier transform holograms generated by computer,*” *Appl. Opt.* 9, (1970): 639–643.

[47] B. R. Brown, and A. W. Lohmann, “*Complex spatial filtering with binary masks,*” *Applied Optics* 5, 967-969 (1966).

[48] C. B. Burkhardt, “*A simplification of Lee’s method of generating holograms by computer,*” *Appl. Opt.* 9, (1970): 1949.

- [49] L. B. Lesem, P. M. Hirsch, and J. A. Jordan, “*The kinoform: a new wavefront reconstruction device,*” *IBM Journal of Research and Development* 13, (1969): 150–155.
- [50] Harm, W., Jesacher, A., Thalhammer, G., Bernet, S., & Ritsch-Marte, M. “*How to use a phase-only spatial light modulator as a color display,*” *Optics Letters*, 40(4), (2015): 581-4.
- [51] Hilario, P., Villangca, M., & Tapang, G. “*Independent light fields generated using a phase-only spatial light modulator,*” *Optics Letters*, 39(7), (2014): 2036-9.
- [52] N. C. Gallagher, and B. Liu, “*Method for computing kinoforms that reduces image reconstruction error,*” *Applied Optics* 12, (1973): 2328–2335.
- [53] Takaki, Y., & Taira, K. “*Speckle regularization and miniaturization of computer-generated holographic stereograms,*” *Optics Express*, 24(6), (2016): 6328-40.
- [54] Fienup, J. “*Lensless coherent imaging by phase retrieval with an illumination pattern constraint,*” *Optics Express*, 14(2), (2006): 498-508.
- [55] J. R. Fienup, “Phase retrieval algorithms: a personal tour [Invited],” *Applied Optics* 52, (2013):45–56.
- [56] R. A. Orozco, Y. M. Barbosa, “*Gerchberg-Saxton algorithm applied to a translational-variant optical setup,*” *Optics Express* Vol. 21, Issue 16, (2013)
: pp. 19128-19134,
- [57] Dholakia, K. “*Iterative Methods for Diffractive Optical Elements Computation,*” *Contemporary Physics*, 40(6), (1999):447.
- [58] J. R. Fienup and C. C. Wackerman, “*Phase-retrieval stagnation problems and solutions,*” *J. Opt. Soc. Am. A* 3(11), (1986):1897–1907.
- [59] F. Wyrowski and O. Bryndahl, “*Iterative Fourier transform algorithm applied to computer holography,*” *J. Opt. Soc. Am. A* 5(7), 1058 – 1065 (1988).

[60] F. Wyrowski, “*Iterative quantization of amplitude holograms,*” *Appl. Opt.* 28(18), 3864–3870 (1989).

[61] Neto, Yunlong Sheng, & Galmiche. (1997). “Speckle-free non-periodic Fresnel phase plates for beam shaping and optical interconnects,” *Microwave and Optoelectronics Conference, 1997. Linking to the Next Century. Proceedings. 1997 SBMO/IEEE MTT-S International*, 1, 82-86.

[62] Cong, W., Momose, A., & Wang, G. “*Fourier transform-based iterative method for differential phase-contrast computed tomography.*” *Optics Letters*, 37(11), (2012): 1784-6.

[63] Pang, H., Wang, J., Cao, A., & Deng, Q. “*High-accuracy method for holographic image projection with suppressed speckle noise,*” *Optics Express*, 24(20), (2016): 22766-22776.

[64] Z. Z. Yuan and S. H. Tao, “*Generation of phase-gradient optical beams with an iterative algorithm,*” *J. Opt.* 16(10), (2014): 105701.

[65] S. Tao and W. Yu, “*Beam shaping of complex amplitude with separate constraints on the output beam,*” *Opt. Express* 23(2), (2015): 1052–1062.

[66] L. Wu, S. Cheng, and S. Tao, “*Simultaneous shaping of amplitude and phase of light in the entire output plane with a phase-only hologram,*” *Sci. Rep.* 5, (2015): 15426.

[67] C. Chang, J. Xia, L. Yang, W. Lei, Z. Yang, and J. Chen, "Speckle-suppressed phase-only holographic three dimensional display based on double-constraint Gerchberg-Saxton algorithm," *Appl. Opt.* 54(23), (2015): 6994–7001.

[68] H. Aagedal, M. Schmid, T. Beth, S. Teiwes, and F. Wyrowski, "Theory of speckles in diffractive optics and its application to beam shaping," *J. Mod. Opt.* 43, (1996):1409 – 1421.

[69] J. Amako, H. Miura, and T. Sonehara, "Speckle-noise reduction on kinoform reconstruction using a phaseonly spatial light modulator," *Appl. Opt.* 34, (1995): 3165-3171.

[70] J. W. Goodman, "Some fundamental properties of speckle," *J. Opt. Soc. Am.* 66, (1976): 1145-1150.

[71] J. I. Trisnadi, "Hadamard speckle contrast reduction," *Opt. Lett.* 29, (2004):11-13.

[72] Pang, H., Wang, J., Cao, A., Zhang, M., Shi, L., & Deng, Q. "Accurate hologram generation using layer-based method and iterative Fourier transform algorithm," *IEEE Photonics Journal*, 9(1), (2016). 1.

[73] Banyasz, I., Kiss, G., & Varga, P. "Holographic image of a point source in the presence of misalignment," *Applied Optics*, 27(7), (1988): 1293-1297.

[74] Sherman, George C. "Holographic real image of a point source," *JOSA* 68.3 (1978): 423-424.

- [75] Adeyemi, A., & Darcie, T. “*Programmable Point-Source Digital In-Line Holographic Microscope with Enhanced Field of View*,” *Image and Signal Processing*, 2009. CISP '09. 2nd International Congress on, 1-4. (2009).
- [76] J.P. Waters, “*Holographic image synthesis utilizing theoretical methods*,” *Appl. Phys. Lett.* 9 (1966) 405–407.
- [77] Liu, Danjun, Yang, Zheng, Zheng, Qianying, Xia, Liangping, Yang, Ruofu, Du, Chunlei, & Yin, Shaoyun. “Calculation of surface plasmon holographic interferometry based on point light source,” *Optik*, 127(10), (2016): 4498-4501.
- [78] Fuster, J., Candelas, P., Rubio, C., Castiñeira-Ibáñez, S., & Tarrazó-Serrano, D. “*Frequency dependence of Fresnel zone plates focus*,” *The Journal of the Acoustical Society of America*, 141(5), (2017). 3959.
- [79] Brigham, E. *The Fast Fourier Transform*. Prentice-Hall. (1974).
- [80] Bracewell, R. (2000). *Fourier transform and its applications* (3rd ed.). Boston, Mass.: McGraw.
- [81] Davis, S., Abrams, M., & Brault, J. (2001). *Fourier Transform Spectrometry*.
- [82] Bernet, S., Harm, W., Jesacher, A., & Ritsch-Marte, M. “*Lensless digital holography with diffuse illumination through a pseudo-random phase mask*,” *Optics Express*, 19(25), (2011): 25113-24.
- [83] Poon, T., & Liu, J. *Introduction to Modern Digital Holography: With MATLAB*. (2014).

- [84] X.F. Meng, L.Z. Cai, Y.R. Wang, X.L. Yang, X.F. Xu, G.Y. Dong, X.X. Shen, and X.C. Cheng, "Wavefront reconstruction by two-step generalized phase-shifting interferometry," *Opt. Commun.* 281, (2008): 5701–5705
- [85] Z.Y. Wang and B.T. Han, "Advanced iterative algorithm for phase extraction of randomly phase-shifted interferograms," *Opt. Lett.* 29, (2004): 1671–1673.
- [86] Pavillon, N., Arfire, C., Bergoënd, I., & Depeursinge, C. "Iterative method for zero-order suppression in off-axis digital holography," *Optics Express*, 18(15), (2010): 15318-31.
- [87] Fiddy, M., & Shahid, U. "Legacies of the Gerchberg-Saxton algorithm," *Ultramicroscopy*, 134, (2013): 48-54.
- [88] Xia, Xinyi, Xia, Jun, & Zhang, Yuning. "19-4: Stereoscopic Hologram Calculation based on Gerchberg-Saxton (GS) Algorithm," *SID Symposium Digest of Technical Papers*, 47(1), (2016): 231-234.
- [89] Guo, C., Liu, S., & Sheridan, J. "Iterative phase retrieval algorithms. I: Optimization," *Applied Optics*, 54(15), (2015): 4698-70.
- [90] Moore, D., McGrane, S., Greenfield, M., Scharff, T., & Chalmers, R. "Use of the Gerchberg–Saxton algorithm in optimal coherent anti-Stokes Raman spectroscopy," *Analytical and Bioanalytical Chemistry*, 402(1), (2012): 423-428.
- [91] Mukherjee, S., & Seelamantula, C. "An iterative algorithm for phase retrieval with sparsity constraints: Application to frequency domain optical coherence tomography," *Acoustics, Speech and Signal Processing (ICASSP)*, 2012 IEEE International Conference on, (2012): 553-556.

[92] Meng, F., Zhang, D., Wu, X., & Liu, H. “*A comparison of iterative algorithms and a mixed approach for in-line x-ray phase retrieval,*” *Optics Communications*, 282(16), (2009):3392-3396.

[93] Avidor, G., & Gur, E. “An adaptive algorithm for phase retrieval from high intensity images,” *Image Processing Theory Tools and Applications (IPTA)*, 2010 2nd International Conference on, (2010). 225-228.

[94] Zhang, Y., Pedrini, G., Osten, W., & Tiziani, H. “*Whole optical wave field reconstruction from double or multi in-line holograms by phase retrieval algorithm,*” *Optics Express*, 11(24), (2003): 3234-3241.

[95] Hwang, H., Chang, H., & Lie, W. “*Multiple-image encryption and multiplexing using a modified Gerchberg-Saxton algorithm and phase modulation in Fresnel-transform domain,*” *Optics Letters*, 34(24), (2009): 3917-9.

[96] Sorzano, Vargas, Otón, De la Rosa-Trevín, Vilas, Kazemi, . Carazo. “*A Survey of the Use of Iterative Reconstruction Algorithms in Electron Microscopy,*” *BioMed Research International*, 2017, 17.

[97] Chen, Chien-Yu, Li, Wu-Chun, Chang, Hsuan-Ting, Chuang, Chih-Hao, & Chang, Tsung-Jan. “*3-D modified Gerchberg–Saxton algorithm developed for panoramic computer-generated phase-only holographic display,*” *Journal of the Optical Society of America B*, 34(5), (2017): B42-B48.

- [98] Zhang, C., & Wang, K. "A switching median–mean filter for removal of high-density impulse noise from digital images," *Optik - International Journal for Light and Electron Optics*, 126(9-10), (2015): 956-961.
- [99] Shrestha, S. Image Denoising using New Adaptive Based Median Filters. (2014).
- [100] Kim, Jong Man, Choi, Byung So, Kim, Sun II, Kim, Jong Min, Bjelkhagen, Hans I., & Phillips, Nicholas J. "Holographic optical elements recorded in silver halide sensitized gelatin emulsions, Part I. Transmission holographic optical elements," *Applied Optics*, 40(5), (2001): 622-32.
- [101] Wu, X., & GAO, W. "A general model for resolution of digital holographic microscopy," *Journal of Microscopy*, 260(2), (2015):152-162.
- [102] Abbasian, V., Akhlaghi, E., Charsooghi, M., Bazzar, M., & Moradi, A. "Digital holographic microscopy for 3D surface characterization of polymeric nanocomposites," *Ultramicroscopy*, 185, (2017): 72-80.
- [103] ROGERSGL: "Gabor diffraction microscopy: the holo gram as a generalized zone plate," *Nature* (London) 166: 237, 1950
- [104] N. O. Young, *Sky Telesc.* 25, 8 (1963). L. Mertz and N. O. Young in *Proc. Internat. Conf. on Optical Instruments* (Chapman and Hall, London, 1961), p. 305.
- [105] J. Garcia-Sucerquia, W. Xu, S. K. Jericho, M. H. Jericho, H. J. Kreuzer, "Digital in-line holography applied to microfluidic studies," *Proc. SPIE* 6112, pp. 175-184, 2006.

[106] Gardner, J.P., Mather, J.C., Clampin, M. et al. *Space Sci Rev* (2006) 123: 485. <https://doi.org/10.1007/s11214-006-8315-7>, [accessed Feb 01 2018].

[107] G. Zhou, Y. Chen, Z. Wang, and H. Song, “*Genetic local search algorithm for optimization design of diffractive optical elements,*” *Appl. Opt.* 38(20), 4281–4290 (1999).

[108] Charriere, F.; Marian, A.; Montfort, F.; Kuehn, J. and Colomb, T. (2006). “*Cell refractive index tomography by digital holographic microscopy,*” *Opt. Lett.*, Vol. 31, No. 2, (Jan. 2006) pp. 178-180.

APPENDICES

APPENDIX A

A.1 Fresnel Diffraction for a Circule Aperture

A.1.1 Diffraction

Diffraction refers to the behaviour of the optical wave when its lateral extent is confined by an aperture. This comes from the fact that the light rays not follow strictly rectilinear paths when the wave is disturbed on its boundaries.

The diffraction plays a role of most importance in branches of physics and engineering that deal with wave propagation.

A.1.2 Fresnel Diffraction

In this section we model diffraction due to a circular aperture. The phenomenon of diffraction usually can be classified into the two categories of Fraunhofer and Fresnel diffraction. Fraunhofer diffraction is an approximation where only plane waves which is valid in the limit of small Fresnel number $F \ll 1$.

Diffraction occurs if three factors are involved: a source; a diffracting element; and a screen. The diffracting element can be an aperture, a straight edge, an obstacle, a lens, a wire or any other object which comes in between the source and the screen. We can observe the intensity pattern on the screen due to the diffracting element. We keep the source and the diffracting element fixed and we move only the screen towards or away from the diffracting element (or we move the source keeping the screen fixed) and notice the change in the intensity pattern on the screen. If there is no qualitative change in the pattern apart from a slight scaling, the pattern is identified as Fraunhofer. On the other hand, the Fresnel diffraction occurs when there is a qualitative change in the pattern that is observed, such as the bright parts of the screen become dark and vice versa or even the shape of the pattern changes; then we call this a Fresnel diffraction.

So in the Fraunhofer limit when the screen and source both are effectively at a very large (infinite) distance from the diffracting element, the resultant wave is measured very far away from the place

where the wave-front was distorted. Whereas in the Fresnel case either or both (the source and the screen) are at finite distances from the diffracting element. Due to diffraction the image of a point source becomes fuzzy on the screen. Two nearby points on the object plane (source) may get merged in the image plane (screen) due to the finite size of the diffracting elements (such as lenses etc.) and hence we talk of spatial resolution. We are familiar with resolutions of microscopes and telescopes. When we view objects through microscopes and telescopes and see their images and each point of the object acts as a point source but we see its image as a little blurred. Thus due to diffraction we may not be able to distinguish or resolve two very close points on the object when we view it through an instrument like microscope or telescope.

The amplitude distribution for diffraction due to a circular aperture forms an intensity pattern with a bright central band surrounded by concentric circular bands of rapidly decreasing intensity (an Airy pattern).

A.1.3 Fresnel Zones

If we consider p_o as a point source of light which produces monochromatic spherical waves. The spherical wave is given by:

$$A/r_o \exp[-i(\omega t - kr_o)] \quad (\text{A.1})$$

where A is the amplitude of the wave at unit distance from the point source p_o , r_o is the radius, and t is time. Figure A.1 illustrates a point source p_o emitting spherical waves. After a while, the wave will pass through the observation point p . To understand the Fresnel zones, from the point of observation p , we draw spheres of radii $b, b + \lambda/2, b + 2\lambda/2, b + 3\lambda/2, \dots, b + j\lambda/2$, where b is the distance between the observation point p and the point C , and λ is the light wavelength. The term $b + j\lambda/2$ is used to mark the Fresnel zones and they are labelled as z_1, z_2, z_3 as shown in the Figure A.1. The term $b + j\lambda/2$ shows that the zone boundaries are successively half a wavelength away from the point of the observation p . We already know that each secondary source produces wavelets and are propagated to the point p . The resulting amplitude at the observation point p is the linear superposition of the contribution of all the wavelets. From Figure A.1,

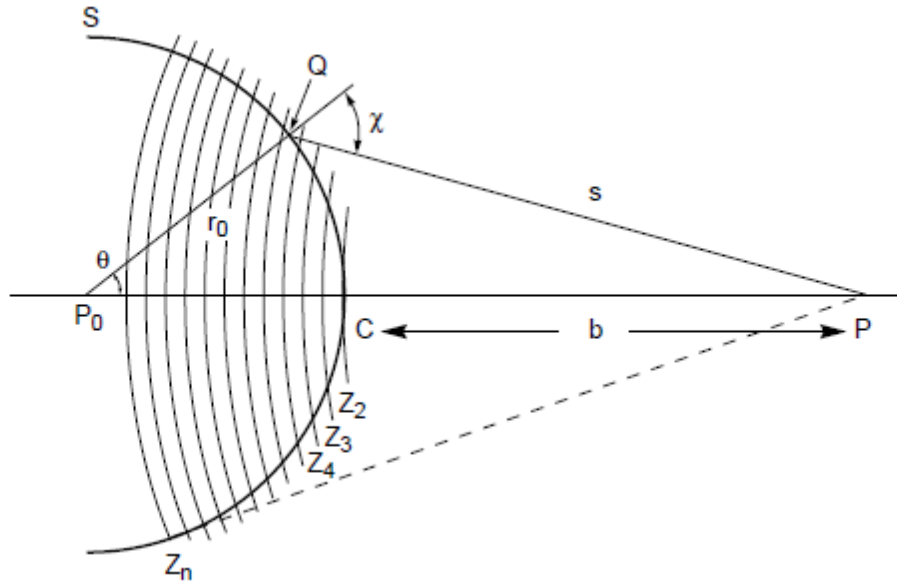


Figure A.1: Fresnel zone construction P_0 : point source. S : Wavefront. r_0 : radius of the wavefront. b : distance CP. s : distance QP

the wavelet at point C is in line with the point source p_o and the point of observation p . However, we can also consider the case the point Q where the observation point p which makes an angle χ with respect to the radius vector from the point source p_o . This variation between the point source p_o and the observation point p can be calculated by a term called the obliquity factor $k(\chi)$. The obliquity factor takes a unity value at point C where the angle $\chi = 0$. The $k(\chi)$ is very small and can be neglected for any two adjacent zones. Also the obliquity factor becomes very small and negligible for zones with high enough index j .

As we already discussed, that the distance of the successive zones from the observation point p differ by only $\lambda/2$, therefore the zones can be called half-period zones.

A.2 Rayleigh-Sommerfeld Solution

In studying monochromatic light propagation, consideration is given to two points, the first point at the source plane $U_1(\xi, \eta)$ and a point at a distant observation plane $U_2(x, y)$. By using the Rayleigh – Sommerfeld diffraction solution we can obtain $U_2(x, y)$ as the following:

$$U_2(x, y) = \iint U_1(\xi, \eta) h(x - \xi, y - \eta) d\xi d\eta \quad (\text{A.2})$$

where $h(x - \xi, y - \eta)$ is the Rayleigh – Sommerfeld impulse response and the general form is:

$$h(x, y) = \frac{z \exp(jkr)}{j\lambda r^2} \quad (\text{A.3})$$

Where k is the wave number ($k = \frac{2\pi}{\lambda}$), z is the distance between the centers of the source and the observation coordinate system, r is the distance between a position on the source plane and a position in the observation plane and:

$$r = \sqrt{z^2 + x^2 + y^2} \quad (\text{A.4})$$

We need to apply the Fourier convolution for the Eq. A.2 and re-label the source and observation plane variables as x and y . The Fourier convolution will be as follows:

$$U_2(x, y) = F^{-1}\{F\{U_1(x, y)\}H(f_x, f_y)\} \quad (\text{A.5})$$

where H is the Rayleigh – Sommerfeld transfer function and given by:

$$H(f_x, f_y) = \exp(jkz\sqrt{1 - (\lambda f_x)^2 - (\lambda f_y)^2}) \quad (\text{A.6})$$

From Eq. A.6 the Rayleigh–Sommerfeld condition requires that $r \gg \lambda$, i.e. the distance between the source and the observation position should be much greater than the wavelength.

A.3 Fresnel Approximation

The idea of the Fresnel approximation is to introduce approximations for the square root in the distance terms in Eq. A.4. The distance term will take the following form:

$$r_{12} \approx z \left[1 + \frac{1}{2} \left(\frac{x-\xi}{z} \right)^2 + \frac{1}{2} \left(\frac{y-\eta}{z} \right)^2 \right] \quad (\text{A.7})$$

Also we have to consider $r = z$ to arrive at the Fresnel diffraction expression as the following:

$$U_2(x, y) = \frac{e^{jkz}}{j\lambda z} \iint U_1(\xi, \eta) \exp \left\{ j \frac{k}{2z} [(x - \xi)^2 + (y - \eta)^2] \right\} d\xi d\eta \quad (\text{A.8})$$

To compare the Fresnel approximation with the Rayleigh-Sommerfeld, the impulse response now takes the following form:

$$h(x, y) = \frac{e^{jkz}}{j\lambda z} \exp \left[\frac{jk}{2z} (x^2 + y^2) \right] \quad (\text{A.9})$$

and the transfer function takes the following form:

$$H(f_x, f_y) = e^{jkz} \exp [j\pi\lambda z (f_x^2 + f_y^2)] \quad (\text{A.10})$$

The Fresnel number is the number we can use to make sure that the observation plane is in the Fresnel region. The Fresnel number is given by:

$$N_F = \frac{w^2}{\lambda z} \quad (\text{A.11})$$

Firstly, a square aperture was used with w is the half width of the aperture, λ is the wavelength and z is the distance to the observation plane. The observation plane is in the Fresnel region if N is less than one.

A.4 Fraunhofer Approximation

Fraunhofer diffraction refers to the diffraction patterns that are generated in the far field. The condition that needed for a far field propagation is given by:

$$z \gg \left(\frac{k(\xi^2 + \eta^2)}{2}\right)_{\max} \quad (\text{A.12})$$

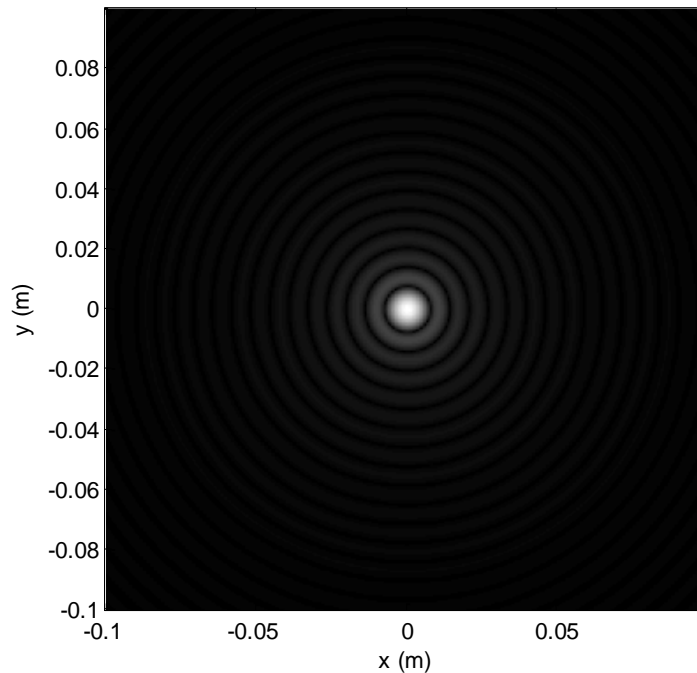
From the Eq. A.12, we can see that this condition requires very long propagation distances relative to the source support size. Regarding the Fresnel number, the commonly accepted requirement for Fraunhofer diffraction is $N \ll 1$.

A.4.1 Fraunhofer Diffraction Example

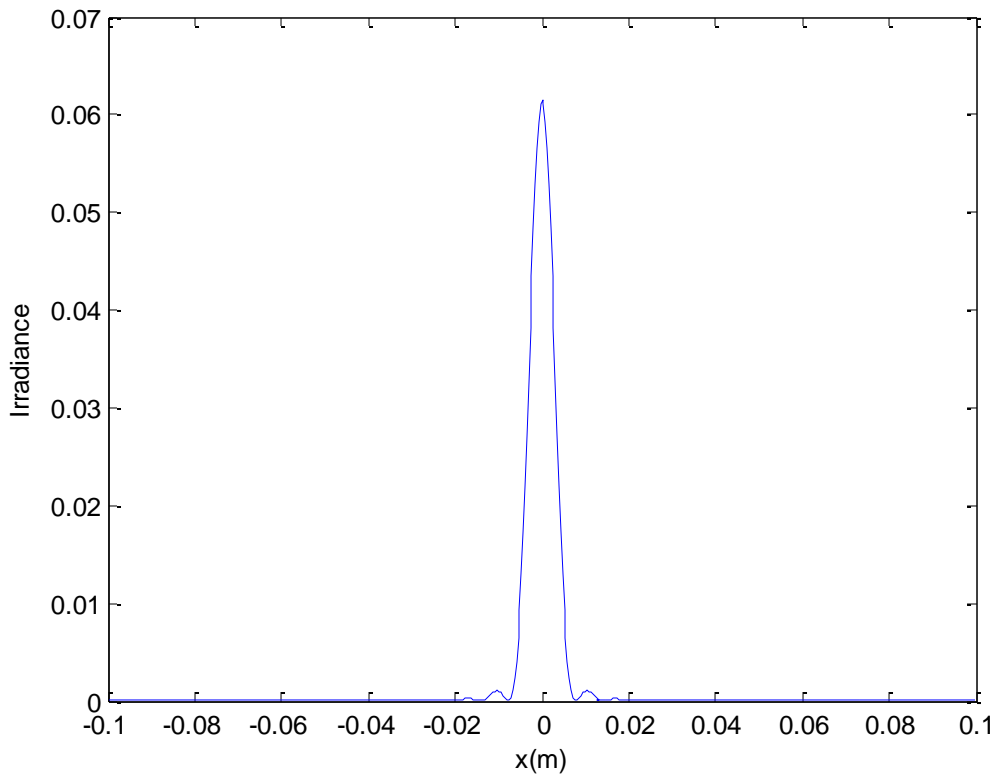
MATLAB™ code was employed to calculate the Fraunhofer diffraction (far-field diffraction) for a circular and rectangular aperture. The irradiance for each aperture is shown with the figures below, the Fraunhofer diffraction pattern for a circular aperture is shown in Figure A.2

The propagation distance: z_1

The side length: L



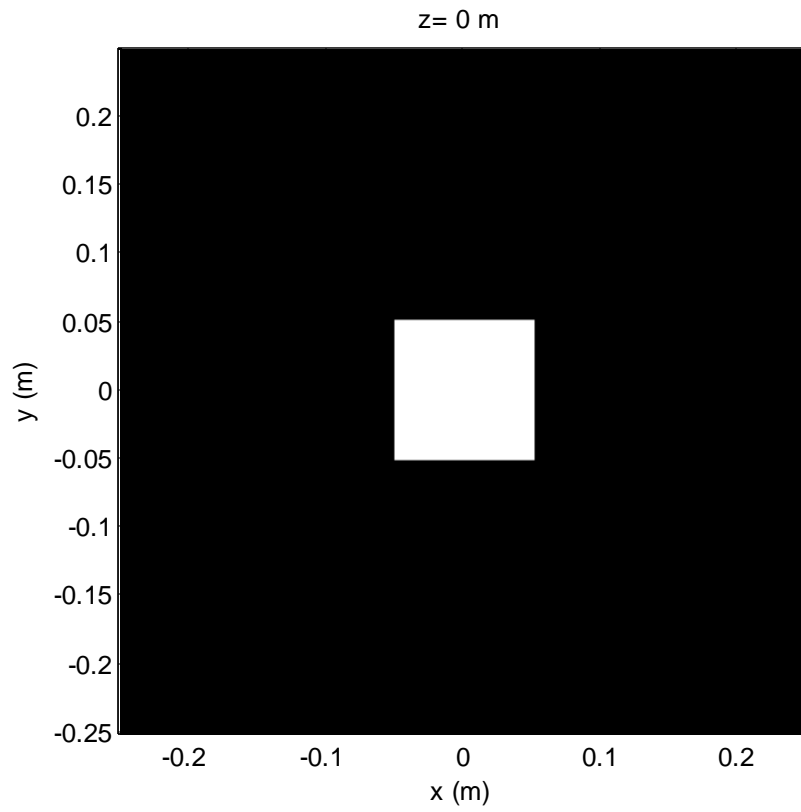
(a)



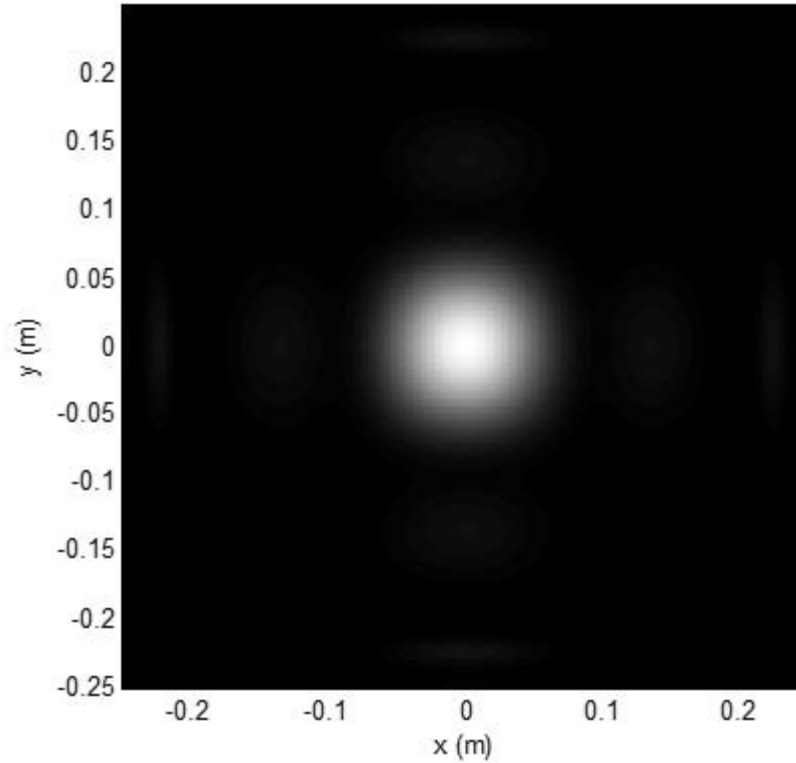
(b)

Figure A.2: Fraunhofer irradiance for a circular aperture: (a) image pattern and (b) x-axis profile.

The Fraunhofer pattern for a rectangular aperture with a (source) half width w and a propagation a distance z_2 is shown in Figure A.3.



(a)



(b)

Figure A.3: Fraunhofer irradiance for a rectangular aperture: (a) image pattern and (b) x-axis profile

A.5 Propagation Simulation

A.5.1 Fresnel Transfer Function Propagator

MATLABTM code was written to evaluate Eq. A.5 using the transfer function given in Eq. A.6 which represents the Fourier convolution interpretation for the source and observation planes. The benefit to using the Fresnel diffraction expression is that it applies to a wide range of propagation scenarios and is relatively straightforward to compute.

The MATLABTM code developed is based on the propagation Eq. A.8 and the transfer Eq. A.10, the M-file being given in Appendix B.

A.5.2 Circle Beam Example

Our work was to create a MATLAB™ code for the calculation of the Fresnel field (near-field) diffraction from a circular aperture.

The circle function is a symmetric 2D function, the circle function is scaled and is be given by the expression in Eq. A.13:

$$\text{circ}\left(\frac{\sqrt{x^2+y^2}}{a}\right) \quad (\text{A.13})$$

Where a is the circle radius. The Fourier transform is this is taken:

$$G(f_x, f_y) = \iint_{-\infty}^{\infty} g(x, y) \exp[-j2\pi(f_x x, f_y y)] dx dy \quad (\text{A.14})$$

Where g is a function of two variables x and y , in this case given by Eq. A.14.

The Fourier transform for the circle function is given by:

$$FT\left\{\text{circ}\left(\frac{\sqrt{x^2+y^2}}{a}\right)\right\} = a^2 \frac{J_1(2\pi a \sqrt{f_x^2+f_y^2})}{a \sqrt{f_x^2+f_y^2}} \quad (\text{A.15})$$

Where f_x and f_y are independent frequency variables associated with x and y , respectively, and $F(f_x, f_y)$ is a Bessel function of the first kind, order 1.

The Bessel function, cylinder function or cylindrical harmonics, of the first kind, are defined as the solutions to the Bessel differential equation.

A.5.3 Sample Interval

The function $g(x, y)$ is sampled as:

$$g(m\Delta x, n\Delta y) \quad (\text{A.16})$$

Where the sample interval is Δx in the x direction and Δy in the y direction, m and n are integers i.e. valued indices of the samples.

The sample rate is calculated in the x and y direction by $1/\Delta x$ and $1/\Delta y$ respectively. 512 samples in the x and y directions are used and m and n are given by:

$$m = -\frac{M}{2}, \dots, \frac{M}{2} - 1 \quad (\text{A.17})$$

$$n = -\frac{N}{2}, \dots, \frac{N}{2} - 1 \quad (\text{A.18})$$

Where $M = N = 512$ the sampling number in the x and y directions.

The side lengths (12.8 mm) are taken as L_x and L_y , where L_x is the length along x side of the sampled space and L_y is the length along the y side. The side lengths are related to the sampling parameters by:

$$L_x = M\Delta x, L_y = N\Delta y$$

The Shannon – Nyquist theorem is used to calculate the sample intervals Δx and Δy that are given by:

$$\Delta x < \frac{1}{2B_x} \quad (\text{A.19})$$

$$\Delta y < \frac{1}{2B_y} \quad (\text{A.20})$$

Where B_x is the bandwidth of the spectrum of the continuous function along the x direction and B_y is the bandwidth along the y direction.

The effective bandwidth is given by:

$$B \approx \frac{5}{w} \quad (\text{A.21})$$

Where w is the radius of the circle and which in this case is taken as 0.9 mm . Substituting Eq. A.21 into Eq. A.19 the sample interval is then given by:

$$\Delta x \leq \frac{w}{10} \quad (\text{A.22})$$

From A. 22 it can be seen that at least 10 samples across the radius of the circle function (20 across the full width) are needed to retain the effective bandwidth, which is indicated in Eq. A.21.

$\Delta x = \frac{L_x}{M}$, $\Delta y = \frac{L_y}{M}$ is used for the sample interval with $\Delta x = \Delta y$. In the code developed the sample interval is 0.025 mm

A.5.4 Coordinates

As mentioned previously $\Delta x = \Delta y$, $N = M$, $L_x = L_y = L$

Which simplifies the analysis and calculation. The coordinate range used is from $-L/2$ to $L/2$ in steps of Δx and MATLAB™ code is used to describe the coordinates of the samples along the x dimension by:

$$-\frac{L}{2} : \Delta x : \frac{L}{2} - \Delta x \quad (\text{A.23})$$

The same technique is used to calculate the samples along the y direction.

The Fourier transform shows the relationship between the spatial and spectral domain. The independent spatial frequency variables in the x and y directions, can be derived as:

$$-\frac{1}{2\Delta x} : \frac{1}{L} : \frac{1}{2\Delta x} - \frac{1}{L} \quad (\text{A.24})$$

Which means that the spatial frequency coordinates range from $-\frac{1}{2\Delta x}$ to $\frac{1}{2\Delta x} - \frac{1}{L}$

In steps of $\frac{1}{L}$.

A.5.5 Indexing, Centering and Shifting

The indices of the samples in the x and y directions are represented by Eq. A.23 and can be seen to take positive and negative values. However in the software application we use the positive integer values for vector or array indexing. In the MATLABTM code the indexing starts at 1.

For display purposes the circ function is centered by making the zero coordinate correspond to the first index position.

The centered vector values must also be shifted before applying the Fourier transform.

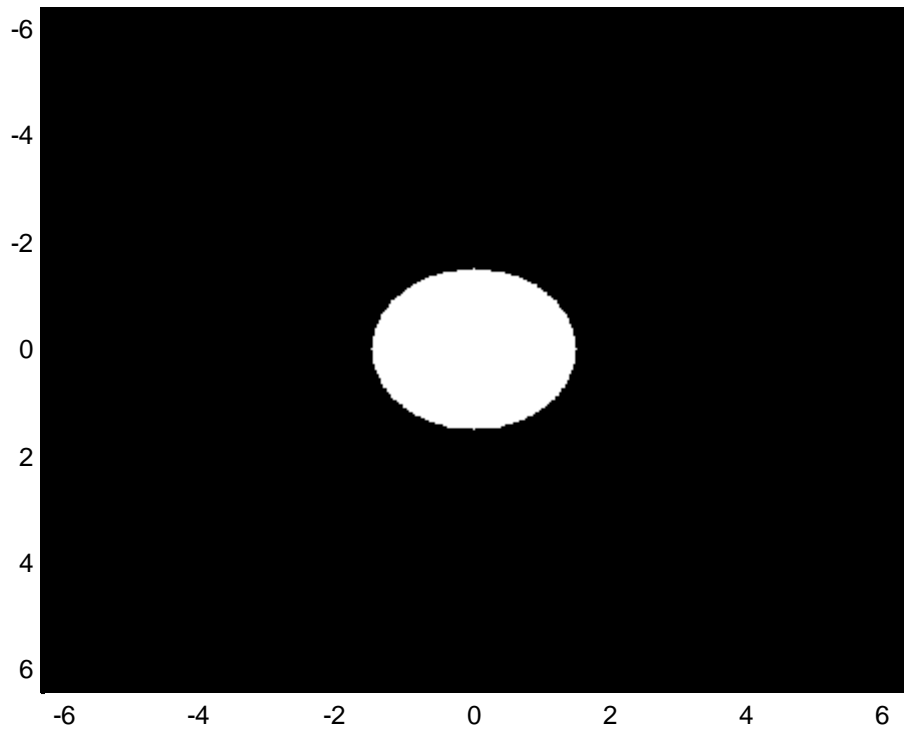
Next we present the MATLABTM simulation results for circular aperture propagation of a plane wave front using the Fourier transform and Bessel function.

The figures show the irradiance distributions and the field magnitude cross-sections for the circular aperture.

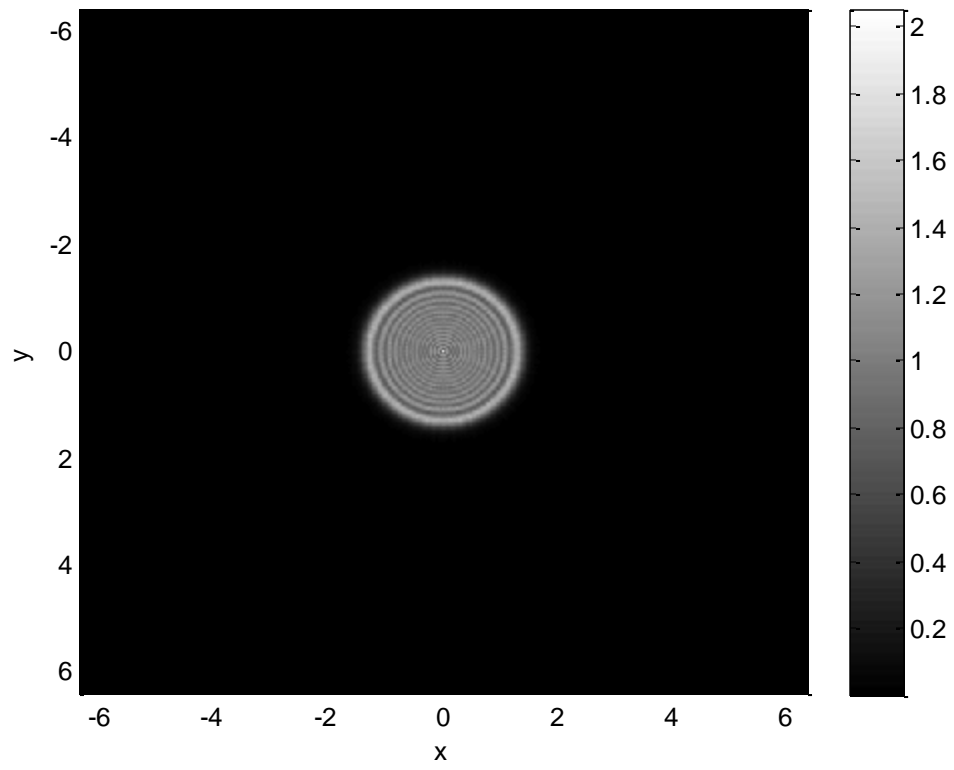
The propagation distance: z_1

The wavelength: $\lambda = 0.633 * 10^{-3} \text{mm}$;

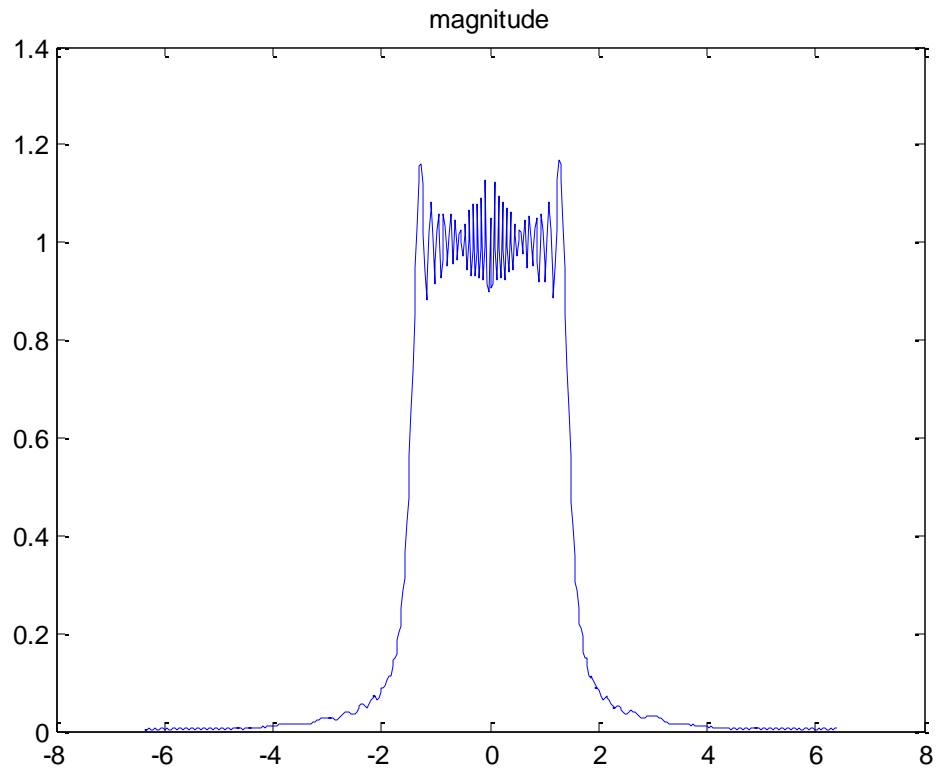
The radius of the circle: r_1



(a)



(b)



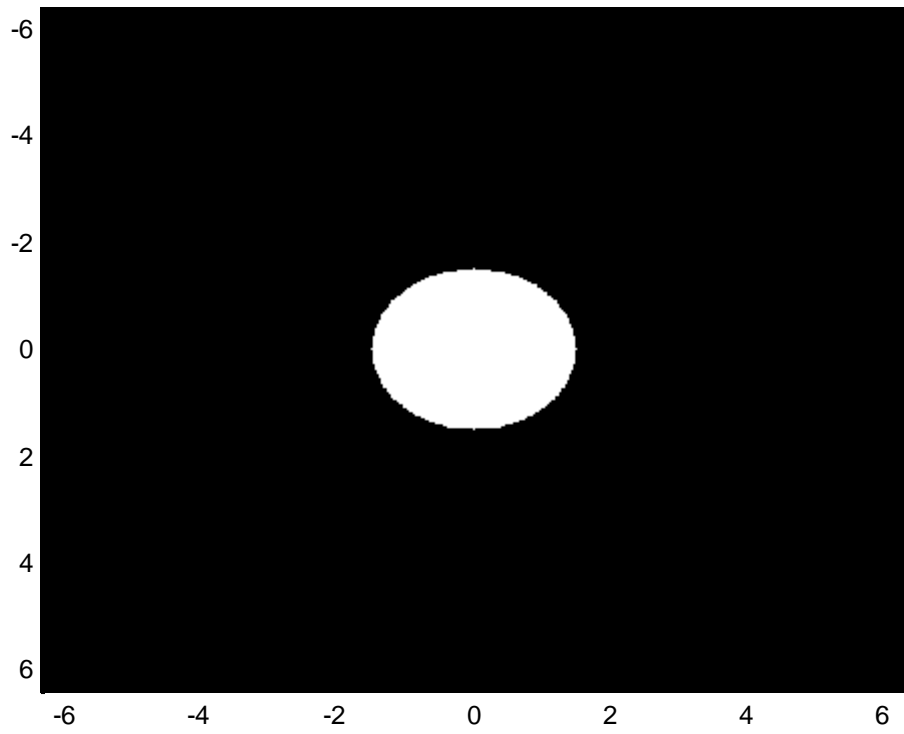
(c)

Figure A.4 : Fresnel diffraction. (a) circle aperture irradiance, (b) The Fresnel plane irradiance, (c) Fresnel plane magnitude cross-section

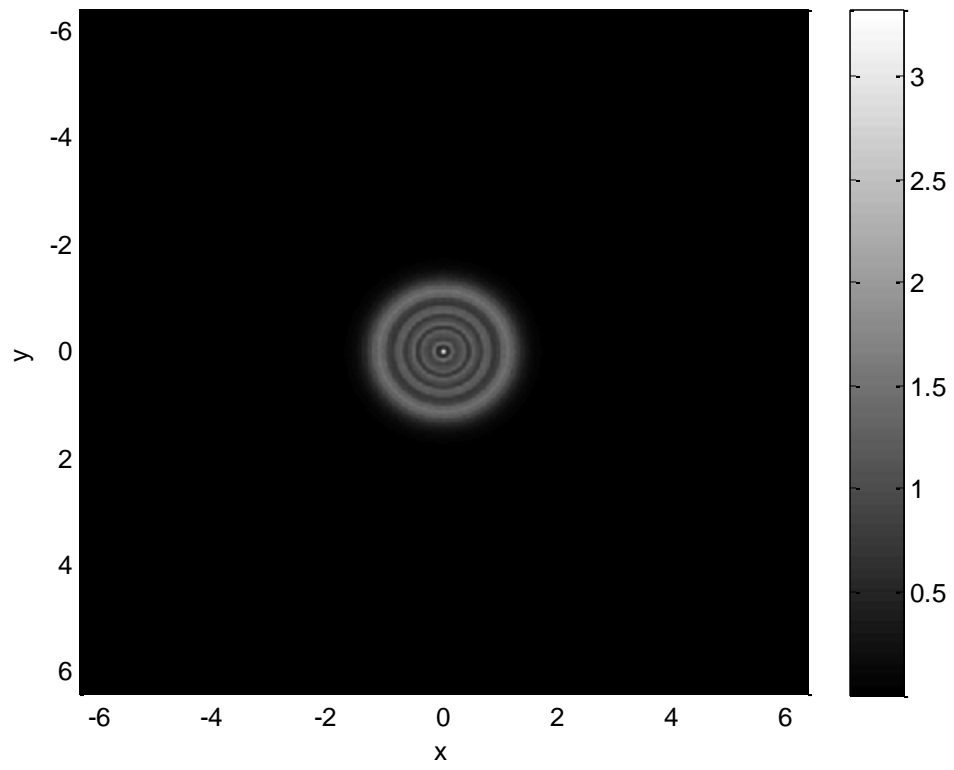
The propagation distance: z_2

The wavelength: $\lambda = 0.633 * 10^{-3} \text{mm}$;

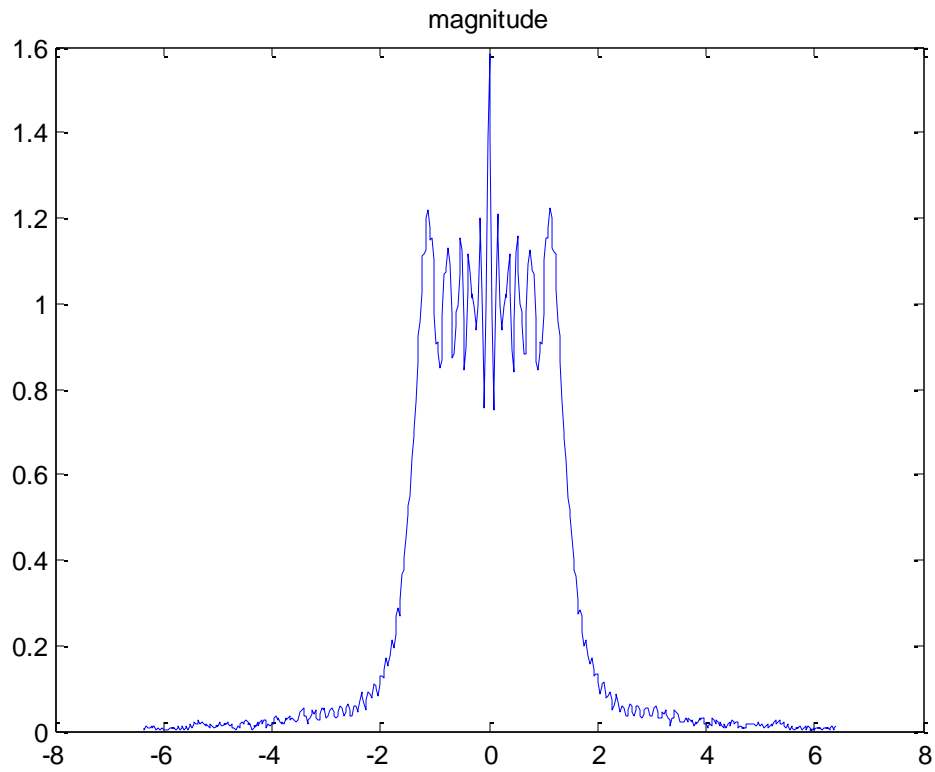
The radius of the circle: r_1



(a)



(b)



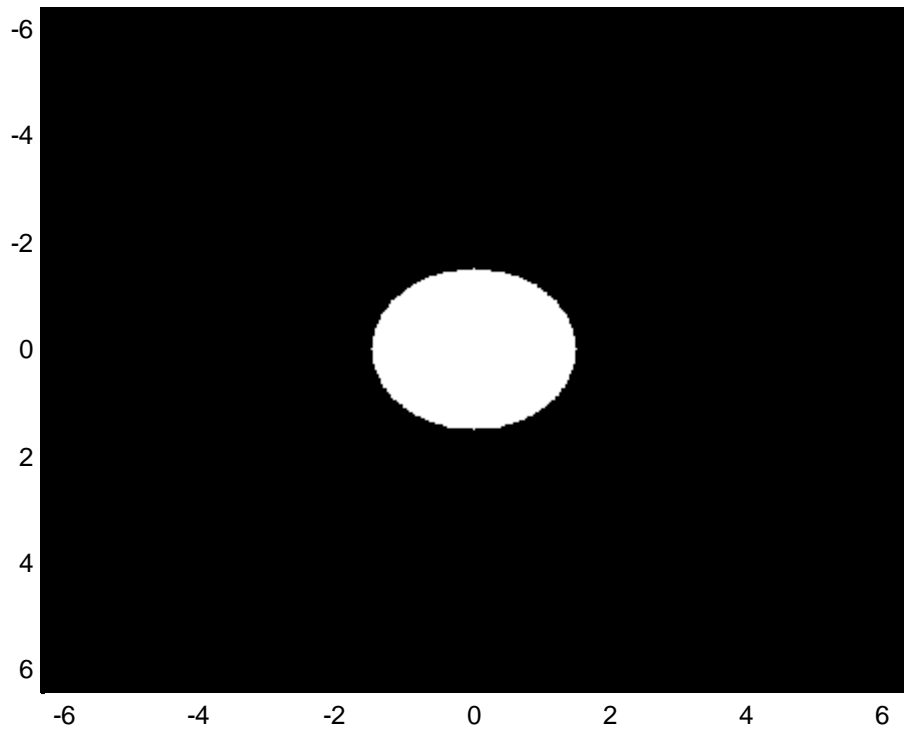
(c)

Figure A.5: Fresnel diffraction (a) the circle aperture, (b) the irradiance, (c) the magnitude cross-section

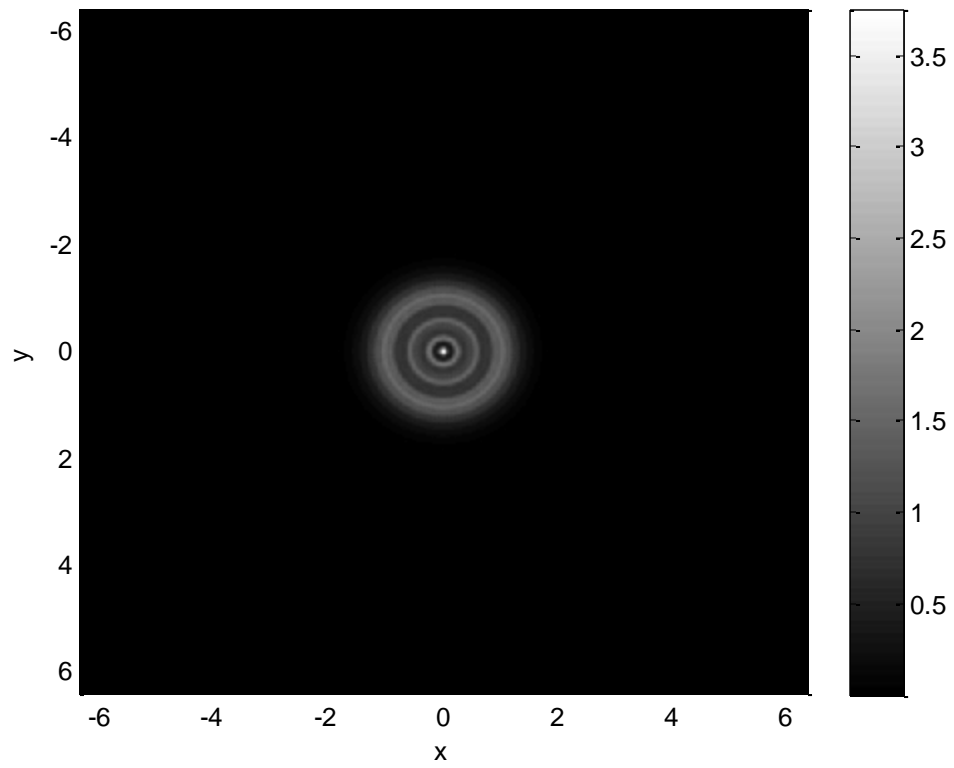
The propagation distance: z_3

The wavelength: $\lambda = 0.633 * 10^{-3}mm;$

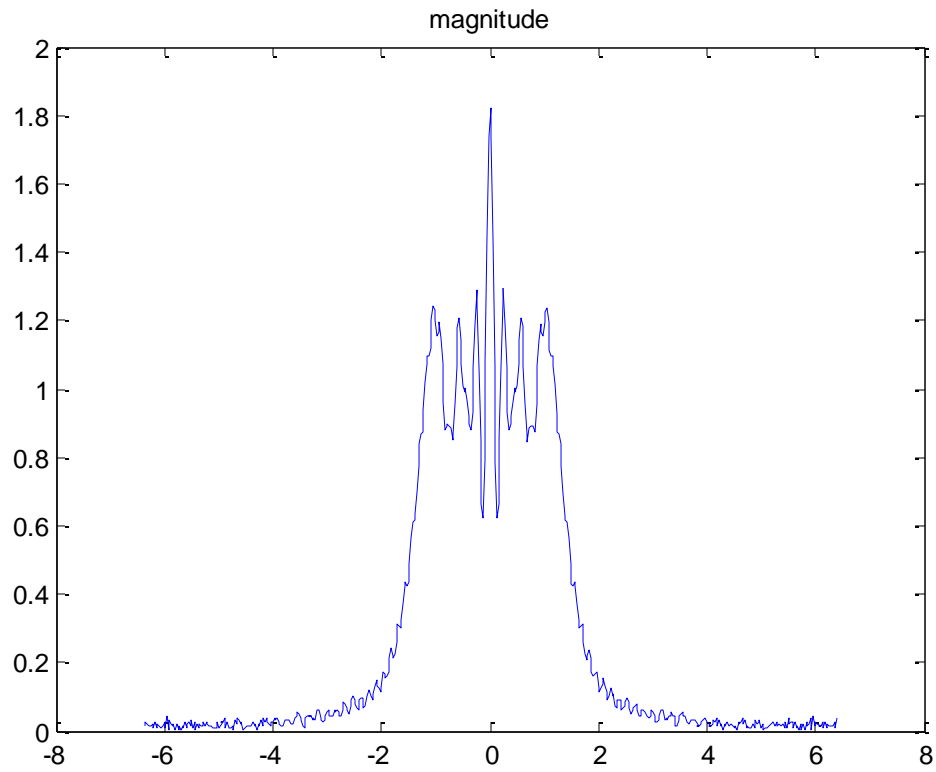
The radius of the circle: r_1



(a)



(b)



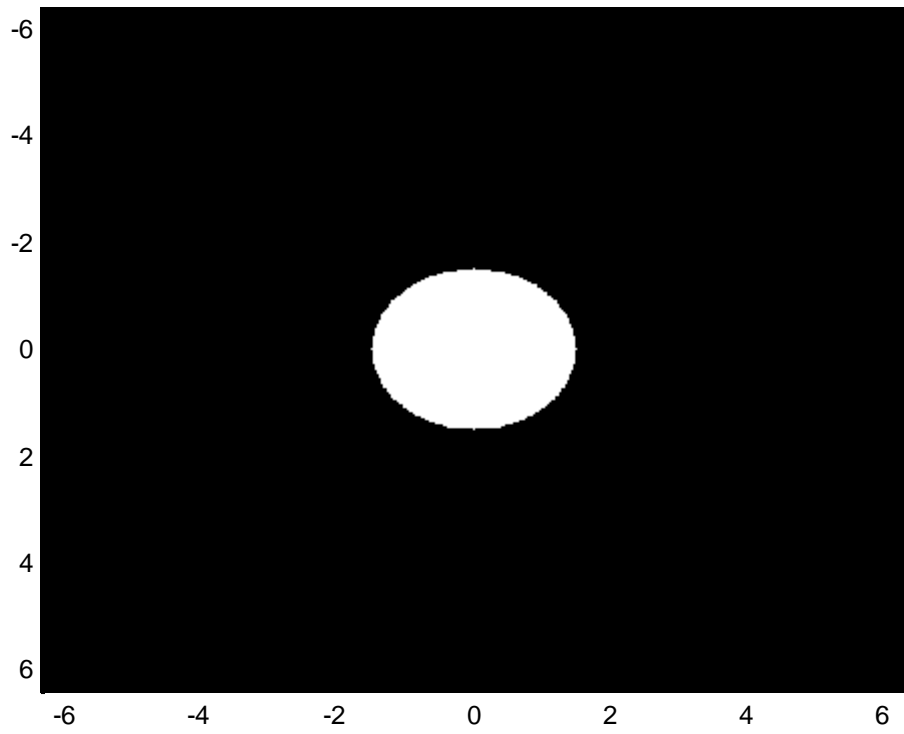
(c)

Figure A.6: Fresnel diffraction (a) the circle aperture, (b) the irradiance, (c) the magnitude cross-section

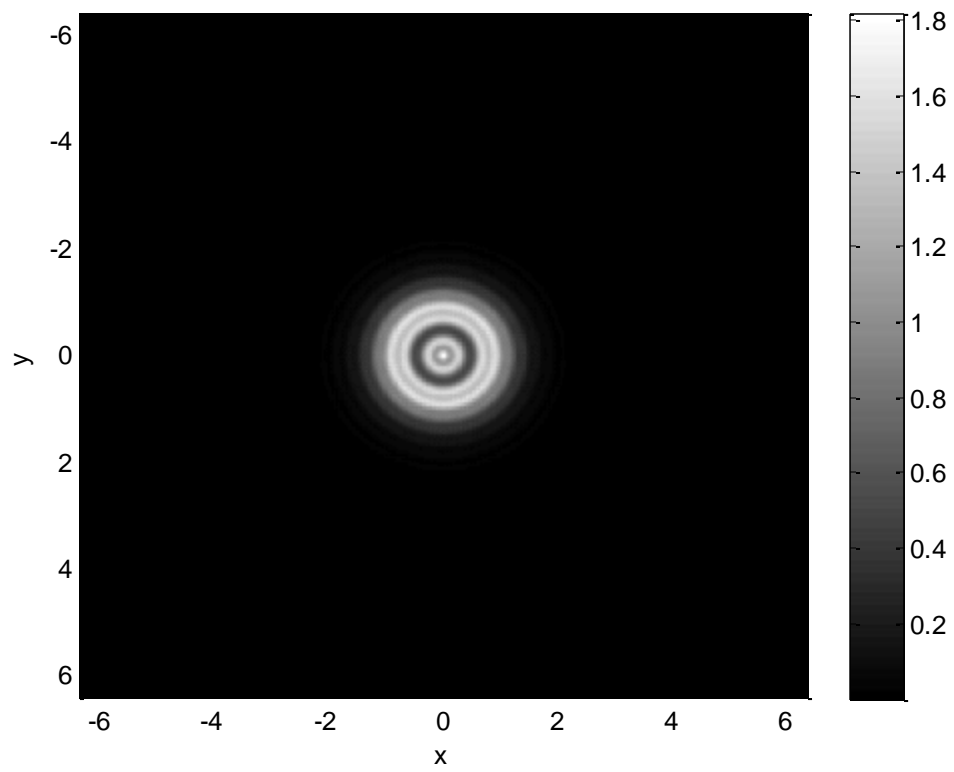
The propagation distance: z_3

The wavelength: $\lambda = 0.633 * 10^{-3}mm;$

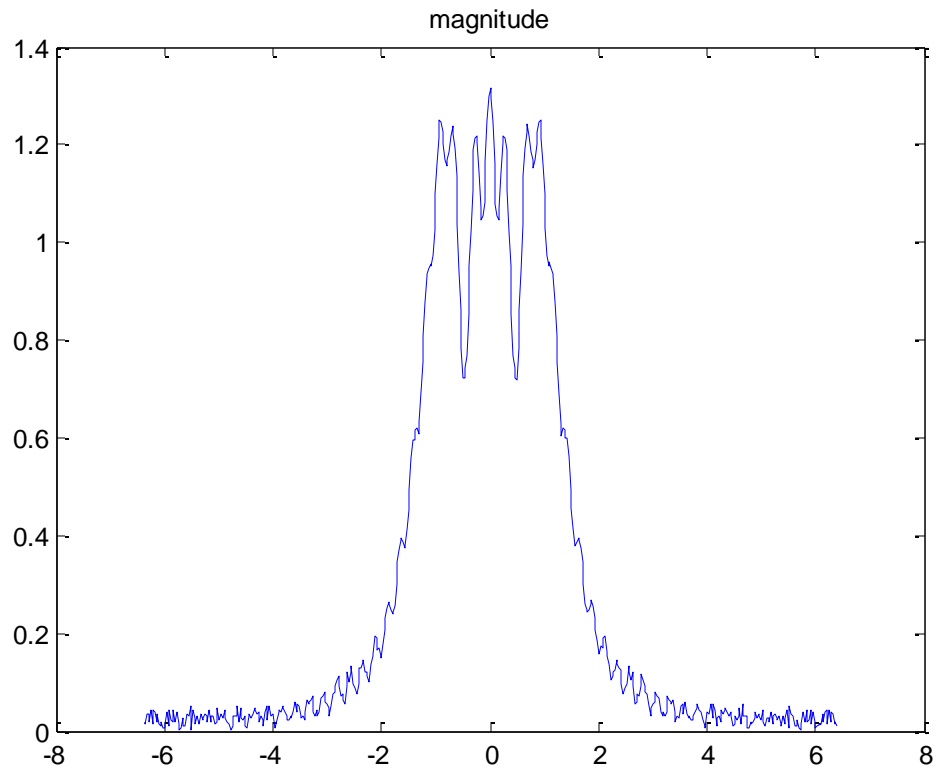
The radius of the circle: r_1



(a)



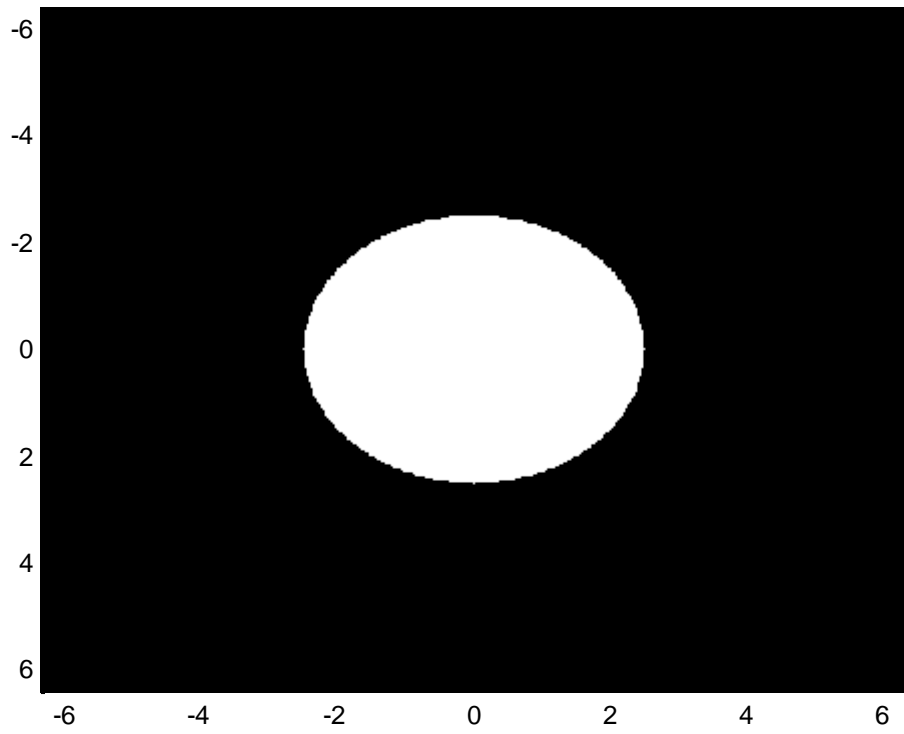
(b)



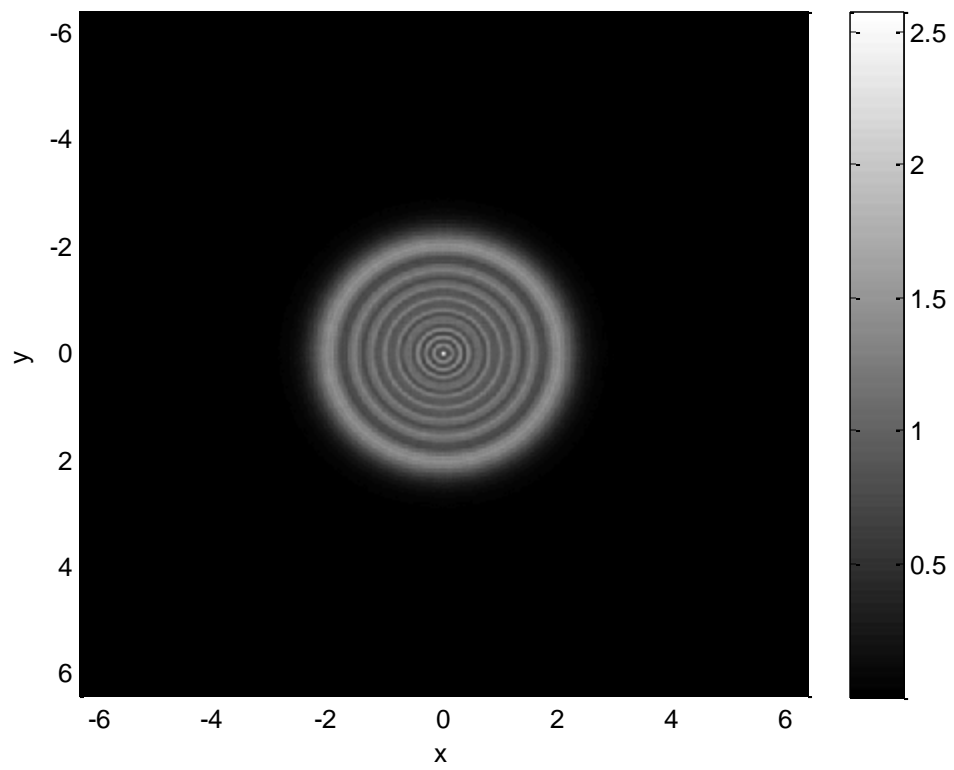
(c)

Figure A.7: Fresnel diffraction (a) the circle aperture, (b) the irradiance, (c) the magnitude

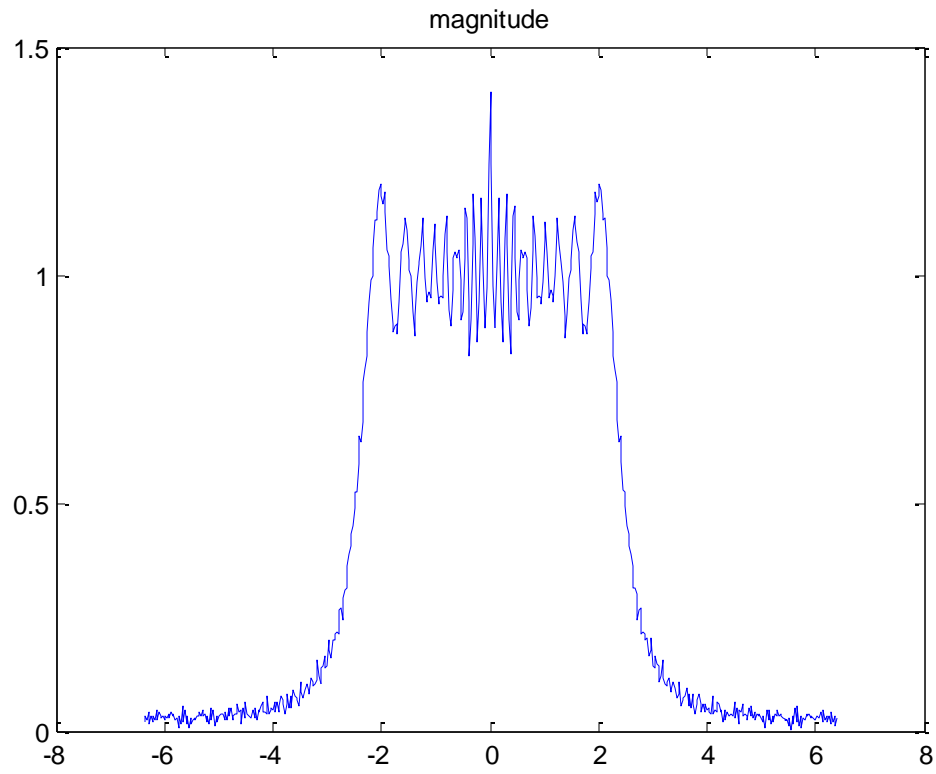
The radius of the circle is changed to a bigger diameter and the field is calculated for the z_3 propagation distance to generate the result shown in Figure A.8.



(a)



(b)



(c)

Figure A.8: Fresnel diffraction (a) the circle aperture, (b) the irradiance, (c) the magnitude

APPENDIX B

Matlab Code Developed to Model Beam Propagation

```
%%%%%%%% this is a MATLAB code to study the light propagation through a circle
%%%%%%%% aperture. We set-up the spatial axis and the frequency axis. We choose
%%%%%%%% the propagation distance and slit dimensions. The next step is to set
%%%%%%%% the transfer function and in this project we set the transfer function
%%%%%%%% to the size 512X512. The step after is making the circle aperture. To
%%%%%%%% make the circle aperture we need the centre and the radius of the
%%%%%%%% circle. We have tried different codes to construct the circle aperture
%%%%%%%% but this one is the as we validate it for different distances and size
%%%%%%%% of the aperture.
```

```
%%%%%%%% fft2 on Fourier transform of an impulse plane wave illuminating a
%%%%%%%% circular aperture with diameter d (a) circular input excitation
%%%%%%%% field, shft-input, (b) after applying a fftshift on shft-input to
%%%%%%%% produce input, ( c) after applying fft2 on input to produce F-input
%%%%%%%% and ( d) after applying a fftshift on F-input to produce the two-
%%%%%%%% dimensional spatial.
%%%%%%%% Appendix A showing the results of this code for different propagation
%%%%%%%% distances and different diameter.
```

```
ii=sqrt(-1);
lambda= 0.633*10^-3; % wavelength [mm]
%z=3; % distance [mm]
w=3; % width of slit is 2*w [mm]
z=2;
%z=w.^2/0.00005*lambda;
x=-6.375:0.025:6.4; % setup spatial axis [mm]
y=x;
freqx=-20:40/512:20-1/512; % setup frequency axis [1/mm]
freqy=freqx;
q=100;
%A=zeros(512);

fft_val=zeros(512);
fft_v=zeros(512);

u0=zeros(512); % field at z=0
a0=zeros(512); % angular spectrum at z=0
H=zeros(512); % transfer function
az=zeros(512); % angular spectrum at z=z
uz=zeros(512); % field at z=z

for nx=1:512 % setup transfer function
    for ny=1:512
        H(nx,ny)=exp(ii*2*pi*(z/(lambda*q))*...
            sqrt(1-((lambda*q)*freqx(nx))^2-((lambda*q)*freqy(ny))^2));
    end
end
```

```

%for nx=1:512      % setup transfer function
%  for ny=1:512
%    H(nx,ny)=exp(ii*2*pi*(z/(lambda*q))*...
%      sqrt(1-((lambda*q)*freqx(nx))^2-((lambda*q)*freqy(ny))^2));
%  end
%end

[nx,ny]=meshgrid(x,y);

A=y.'*x;
i_index=0;
for i=-12.75:0.05:12.8;
j_index=0;
i_index=i_index+1;
for j=-12.75:0.05:12.8;
j_index=j_index+1;
r=sqrt(i^2+j^2);
if r <=3% maybe r=5 better
A(i_index,j_index)=1;
else A(i_index,j_index)=0;
end
end
end

%radius=50;
%CenterX=257;
%CenterY=257;
%u0=rectangle('position',[CenterX-radius,CenterY-
radius,radius*2,radius*2],'Curvature',[1,1],'FaceColor','r');
%axis square
%plot(x,u0);

%u0(257-w*20:256+w*20,257-w*20:256+w*20)=1;      % setup aperture
%figure(1)
%imagesc(x,x,u0);colormap(gray);

%u0(57-w*20:256+w*20,100-w*20:256+w*20,w,w)=1;      % setup aperture
%fft_v=abs(fft2(A));
%a0=fftshift(fft_v);

a0=(fftshift(fft2(A)));      % fourier transform
az=a0.*H;      % multiply with transfer function
uz=ifft2(fftshift(az));      % inverse fourier transform
p=uz.*conj(uz);

```

```

%p= abs(uz.^2); %obs irrad

figure(1)
plot(x, p(:,256)); % plot of cross-section of intensity at z
xlabel('x'); ylabel('I');

figure(2)
imagesc(x, x, p); %diffraction pattern at z
xlabel('x'); ylabel('y'); colormap(gray);
colorbar;

figure(3) %diffraction pattern at z=0
imagesc(x,x,A);colormap(gray);

figure(4)
plot(x,unwrap(angle(uz(512/2+1,:))));
title('phase');

figure(5)
plot(x,abs(uz(512/2+1,:)));
title('magnitude')

```

APPENDIX C

Matlab Code Developed to Implement a Kinoform

```
%%%%%%%%%%%%%% A MATLAB code to record a kinoform hologram .
%%%%%%%%%%%%%% we use the Gerchberg Saxton algorithm to enhance the reconstructed
%%%%%%%%%%%%%% image. Firstly, we have the original image as the input of this
%%%%%%%%%%%%%% code. We use a logo image which its size is 256X256. In this code
%%%%%%%%%%%%%% we do not use a random phase. Number of iterations has a big
%%%%%%%%%%%%%% impact on the reconstructed image as we run the code with
%%%%%%%%%%%%%% different number of iterations and the quality of the
%%%%%%%%%%%%%% reconstructed image has changed. We use only 10 iterations first
%%%%%%%%%%%%%% and the reconstructed image suffers of with a big noise. The
%%%%%%%%%%%%%% second attempt was to increase the number of iterations and was a
%%%%%%%%%%%%%% 100 iterations, and the reconstructed image more clear and better
%%%%%%%%%%%%%% quality. Also, we include the code to construct the hologram and
%%%%%%%%%%%%%% to reconstruct the origin image either digitally ,as we done in
%%%%%%%%%%%%%% this project, or optically by printing the hologram using the
%%%%%%%%%%%%%% photographic process and illuminate the hologram by a coherent
%%%%%%%%%%%%%% light such as a laser light to reconstruct the origin image.
```

```
clear all;
close all;
I=imread('C:\Users\A\Documents\MATLAB\logo256.bmp');
%I = rgb2gray(I);
    I=double(I);
I=I./max(max(I));
avg1=mean(mean(I));
figure;imshow(mat2gray(I));
title('Original Object');
figure;
axis([0,101,0,1]);
xlabel('Number of iterations')
ylabel('RMSE')
hold on
I1=I;
for n=1:100;
    H=fftshift(fft2(fftshift(I1)));
    I2=fftshift(ifft2(fftshift(exp(1j.*angle(H)))));

    avg2=mean(mean(abs(I2)));

    I2=(I2./avg2).*avg1;
    rmse=(mean(mean((abs(I2)-I).^2)))^0.5;
    plot(n,rmse,'o');
    pause(0.3);
    I1=I.*exp(1j*angle(I2));
end
hold off
```

```

I2=I2./max(max(abs(I2)));
figure;
imshow(abs(I2));
title('Reconstructed image')

A=abs(I2);
A=A./max(max(A))*15;
A=round(A);
B=angle(conj(I2));
B=B-min(min(B));
B=B./max(max(B))*7;
B=round(B);

K=zeros(1024);
for m=1:64;
    for n=1:64;
        P=zeros(16);
        a=A(m,n);
        b=B(m,n);
        c=fix(a/2);
        d=rem(a,2);
        P(9-c:8+c+d,(1+b):(9+b))=1;
        L(16*(m-1)+1:16*(m-1)+16,16*(n-1)+1:16*(n-1)+16)=P;
    end
end
figure;imshow(L);
title('THE HOLOGRAM');

```

APPENDIX D

Matlab Code Developed for Iterative Phase Recovery

```
% MATLAB code to reconstruct a quadratic phase from modulus of the Fourier
% transform and is used to reconstruct a single point source.

clear;
ROWS=256;
COLS=256;
colormap(gray(255))
z=2;
sigm = 1/z;
y=-12.8;
for r=1 :COLS,
x=-12.8;
for c = 1 :ROWS, %compute Fresnel zone plate
FZP (r, c)=exp(j * sigm* (x- 0.0 )* (x- 0.0 )+j * sigm* (y+ 0.0)* (y+ 0.0 ));
x=x+0.1;
end
y=y+0.1;
end
%normalization
max1=max(FZP);
max2=max(max1);
scale=1/max2;
FZP=FZP.*scale;

figure(1);
h=figure(1);
saveas(h, 'C:\Users\A\Documents\MATLAB\FZP.png')
image( 127*( 1 +imag(FZP)));
title('Fresnel Zone Plate');
axis square on
axis off

%
%figure(2)
%imshow(g)

%imwrite(FZP, 'C:\Users\A\Documents\MATLAB\PT2.bmp');

%I = imread('C:\Users\A\Desktop\USB\USB ALL\MyImage-8.png');
%imwrite(I, 'C:\Users\A\Desktop\USB\USB ALL\MyImage-6.bmp');

%I = imread('C:\Users\A\Documents\MATLAB\PT2.bmp');

%a = imread('circlesBrightDark.png');
```

```

% CONVERT IMAGE TO BINARY
%bw = I < 20;
%imshow(bw)
%title('Image with Circles')

%title('Fresnel Zone Plate');
%I2= double(bw);
I=FZP;
I = imtranslate(I,[0,0]);
figure(100);
imshow(I);

figure(2);

imshow((mat2gray(abs(I))));

%imwrite(I2,'C:\Users\A\Desktop\USB\USB ALL\MyImage-12.bmp');

%clear
%close all

%I=imread('C:\Users\A\Desktop\USB\USB ALL\MyImage-12.bmp');
%I=double(I);
I=imresize(I,[256 256]);
figure(3);
imshow((mat2gray(abs(I))));
title('Fresnel Zone Plate');
I=fftshift(fft2(I));
sEF=angle(I);
%f=abs(I);
M0=256;
N=256; %matrix size
%T=512;

%generate some target points:
target=ones(N);
target(N/2-15,N/2-10:2:N/2+10)=1;
target(N/2+15,N/2-10:2:N/2+10)=1;

phaseF=rand(M0)*2*pi-pi; %initial random phase at target plane

sEF1=(exp(-1i.*phaseF)); %complex field of target points with random phase
figure(4);
sEF1=(mat2gray(abs(sEF1+pi)));
imshow(sEF1);

```

```

title('Random Phase');

%Example
%SEF1=rand(256,1);
%SEF=rand(256,1);
%----The code-----
%n=256;
%out=sEF1;
%out(1:n)=sEF1.*sEF(1:n);

sEF=sEF.*(sEF1);

A0=(nnz(target)/(N*N))*ones(N); %initial constanst amplitude distribution
Ad=target; %desired intensity distribution

%SEF=(exp(1i.*phaseF)); %complex field of target points with random phase

%fourier transform the field back to get a starting phase:
sEF=ifftshift(sEF);
sEinF=ifft2(sEF);

f=abs(sEinF);
phase1=angle(sEinF);

phase1=phase1./max(max(phase1));
avg1=mean(mean(abs(phase1)));

figure(5);
phase1=(mat2gray((phase1+pi)));
    %plot the phase as a grayscale image, [0,2pi]

    imshow(phase1)
    title('Phase Image of the Combination');

phaseF1=(N)*2*pi*0;

figure(6);
axis([-1,100,0,1]);
box on
xlabel('Number of iterations','FontSize',16,'Color','k');
title('Modified Gerchberg-Saxton Iterations','FontSize',16,'Color','k');
ylabel('RMSE','FontSize',16,'Color','k')

set(gca,'YTick',[0.0:0.2:1])% TO CHANGE THE Y-AXIS INCREMENT
set(gca,'XTick',[0.0:10:100])
flip(y);
hold on
f1=f;
T=(exp(1i.*phaseF1));

```

```

for i=0:10

    %complex field with the uniform amplitude distribution and starting
    %phase:
    I1=f1.*(exp(1i.*phaseF1));
    H=fftshift(fft2(fftshift(I1)));
    I2=fftshift(ifft2(fftshift(exp(1j.*angle(H)))));

    avg2=mean(mean(abs(I2)));
    %phase=(phase./avg2).*avg1;
    I2=(I2./avg2).*avg1;
    %rmse=((mean((conj(phase1)-(I2)).^2)).^0.5);
    rmse=abs(mean(mean((abs(I2)-f).^2)).^0.5);

    plot(i,rmse,'o');
    axis('ij');
    pause(0.5);
    f1=f.*exp(1j*angle(I2));

end

hold off
figure(7);
imshow(I2)
I2=I2-sEF1;
I2=(mat2gray(abs(I2+pi)));
figure(10000);
%plot the phase as a grayscale image, [0,2pi]
imshow(I2);
title('Phase Image after Iterations');

imwrite(I2,'C:\Users\A\Desktop\New folder (2)\USB\USB ALL\MyImage-
13.bmp');
figure(10000);
%plot the phase as a grayscale image, [0,2pi]
imshow(I2);
title('Phase Image after Iterations');
% rmse=((mean((abs(phase)-(abs(phase1)).^2)).^0.5);

    ii=sqrt(-1);
lambda= 0.633*10^-3; % wavelenght [mm]
%z=3; % distance [mm]
w=3; % width of slit is 2*w [mm]
z=5;
%z=w.^2/0.00005*lambda;
x=-6.375:0.025:6.4; % setup spatial axis [mm]
y=x;
freqx=-20:40/512:20-1/512; % setup frequency axis [1/mm]
freqy=freqx;
q=0.9;
%A=zeros(512);

fft_val=zeros(512);

```

```

fft_v=zeros(512);

u0=zeros(512);    % field at z=0
a0=zeros(512);    % angular spectrum at z=0
H=zeros(512);     % transfer function
az=zeros(512);    % angular spectrum at z=z
uz=zeros(512);    % field at z=z

for nx=1:256      % setup transfer function
    for ny=1:256
        H(nx,ny)=exp(ii*2*pi*(z/(lambda*q))*...
            sqrt(1-((lambda*q)*freqx(nx))^2-((lambda*q)*freqy(ny))^2));
    end
end

%for nx=1:512    % setup transfer function
% for ny=1:512
% H(nx,ny)=exp(ii*2*pi*(z/(lambda*q))*...
% sqrt(1-((lambda*q)*freqx(nx))^2-((lambda*q)*freqy(ny))^2));
%end
%end

[nx,ny]=meshgrid(x,y);

I=imread('C:\Users\A\Desktop\New folder (2)\USB\USB ALL\MyImage-13.bmp');
I=double(I);
I=imresize(I,[512 512]);
figure(8);
imshow(mat2gray(abs(I)));
title('Phase Image after Iterations');

%radius=50;
%CenterX=257;
%CenterY=257;
%u0=rectangle('position',[CenterX-radius,CenterY-
radius,radius*2,radius*2],'Curvature',[1,1],'FaceColor','r');
%axis square
%plot(x,u0);

%u0(257-w*20:256+w*20,257-w*20:256+w*20)=1;    % setup aperture
%figure(1)
%imagesc(x,x,u0);colormap(gray);

%u0(57-w*20:256+w*20,100-w*20:256+w*20,w,w)=1;    % setup aperture
%fft_v=abs(fft2(A));
%a0=fftshift(fft_v);

a0=(fftshift(fft2(I)));    % fourier transform

```

```

az=a0.*H;      % multiply with transfer function
uz=ifft2(fftshift(az));    % inverse fourier transform
p=uz.*conj(uz);

%p= abs(uz.^2); %obs irrads

figure(9)
plot(x, p(:,256));    % plot of cross-section of intensity at z
xlabel('x'); ylabel('p');
title('Intensity at z');

figure(10)
imagesc(x, x, p);    %diffraction pattern at z
xlabel('x'); ylabel('y'); colormap(gray);
colorbar;
title('Diffraction Pattern at z');
clim=get(gca, 'clim');

levels=255;
target=grayslice(p, linspace(clim(1), clim(2), levels));
map=jet(levels);
imwrite(target, map, 'C:\Users\A\Documents\MATLAB\I5.bmp');
I5 = imread('C:\Users\A\Documents\MATLAB\I5.bmp');
I5=fftshift((fftshift(fftshift(I5))));
figure(111);
imshow(I5)

imresize(I5, [256 256]);
imwrite(I5, 'C:\Users\A\Documents\MATLAB\Im.bmp');
figure(112);
surf(p)
colormap(jet);

%figure(222)
plot(x, I5(:,256));    % plot of cross-section of intensity at z
xlabel('x'); ylabel('p');
title('Intensity at z');

%figure(333);
%mesh(I5)
%colormap(jet);

I5 = imtranslate(I5, [0, 0]);
figure(333);
plot(I5);

figure(444)
plot(x, I5(:,256));    % plot of cross-section of intensity at z
xlabel('x'); ylabel('p');
title('Intensity at z');

```

APPENDIX E

Matlab Code Developed for Quadratic Phase Recovery

```
%%%%%%%%%%%%% MATLAB code to reconstruct the quadratic phase from the modulus
%%%%%%%%%%%%% of the Fourier transform for two Fresnel zone plates (FZPs). We
%%%%%%%%%%%%% first set a propagation distance
%%%%%%%%%%%%% and construct a Fresnel Zone plate which represent the hologram
%%%%%%%%%%%%% of a point source. Taking the Fourier transform to the FZP, the
%%%%%%%%%%%%% Fourier transform decomposes the signal into a phase and intensity
%%%%%%%%%%%%% and we are only interested on the phase. We need to use a known
%%%%%%%%%%%%% random phase to add it to the original phase, and we have to
%%%%%%%%%%%%% choose the best one from many of them we create them. We take the
%%%%%%%%%%%%% combination of the two phases
```

```
%%%%%%%%%%%%%%USING DIFFERENT CONSTRAINTS .. CHECK IN THE ITERATIONS LOOP
%%%%%%%%%%%%%%
%%%%%%%%%%%%%%
clear;
ROWS=256;
COLS=256;
colormap(gray(255))
z=5;
sigm = 1/z;
y=-12.8;

for r=1 :COLS,
x=-12.8;
for c = 1 :ROWS, %compute Fresnel zone plate
FZP1(r, c)=exp(j * sigm* (x- 0.0 )*( x- 0.0)+j * sigm* (y+ 50.0)* (y+ 50.0));
x=x+0.1;
end
y=y+0.1;
end

%normalization

max11=max(FZP1);
max22=max(max11);
```

```

scale=1/max22;
FZP1=FZP1.*scale;
figure(1);
colormap(gray(255));
image( 127*( 1 +imag(FZP1)));
axis square on
axis off

ROWS1=256;
COLS1=256;
colormap(gray(255))
z1=5;
sigm1 = 1/z1;
y1=-12.8;

for r1=1 :COLS1,
x1=-12.8;
for c1 = 1 :ROWS, %compute Fresnel zone plate
FZP (r1, c1)=exp(j * sigm1* (x1- 0.0 )* (x1- 0.0)+j * sigm1* (y1+ 10.0)* (y1+
10.0));
x1=x1+0.1;
end
y1=y1+0.1;
end

max1=max(FZP);
max2=max(max1);
scale=1/max2;
FZP=FZP.*scale;

figure(2);
colormap(gray(255));
image( 127*( 1 +imag(FZP)));
axis square on
axis off

ROWS3=256;
COLS3=256;
colormap(gray(255))
z3=5;
sigm3 = 1/z3;
y=-12.8;

for r=1 :COLS,
x=-12.8;
for c = 1 :ROWS, %compute Fresnel zone plate
FZP3(r, c)=exp(j * sigm3* (x- 0.0 )* (x- 0.0)+j * sigm3* (y+ 0.0)* (y+ 0.0));

```

```

x=x+0.1;
end
y=y+0.1;
end

%normalization

max111=max(FZP3);
max222=max(max111);
scale=1/max222;
FZP3=FZP3.*scale;
figure(33);
colormap(gray(255));
image(127*(1+imag(FZP3)));
axis square on
axis off

%FZP2=FZP+FZP1+FZP3;
FZP2=FZP+FZP1;
%FZP2=FZP;
figure(3);
colormap(gray(255));
image(127*(1+imag(FZP2)));

%normalization
%max1=max(FZP2);
%max2=max(max1);
%scale=1/max2;
%FZP2=FZP2.*scale;
%image(127*(1+imag(FZP2)));
%axis square on
%axis off

%
%figure(2)
%imshow(g)

%imwrite(FZP,'C:\Users\A\Documents\MATLAB\PT2.bmp');

%I = imread('C:\Users\A\Desktop\USB\USB ALL\MyImage-8.png');
%imwrite(I,'C:\Users\A\Desktop\USB\USB ALL\MyImage-6.bmp');

%I = imread('C:\Users\A\Documents\MATLAB\PT2.bmp');

%a = imread('circlesBrightDark.png');
% CONVERT IMAGE TO BINARY
%bw = I < 20;
%imshow(bw)
%title('Image with Circles')

```

```

%title('Fresnel Zone Plate');
%I2= double(bw);
I=FZP;
I = imtranslate(I,[0,0]);
figure(4);
colormap(gray(255));
image(127*(1+imag(I)));
imshow(I);

figure(2);

imshow((mat2gray(abs(I))));

%imwrite(I2,'C:\Users\A\Desktop\USB\USB ALL\MyImage-12.bmp');

%clear
%close all

%I=imread('C:\Users\A\Desktop\USB\USB ALL\MyImage-12.bmp');
%I=double(I);
I=imresize(I,[256 256]);
figure(5);
imshow((mat2gray(abs(I))));
title('Fresnel Zone Plate');
I=fftshift(fft2(I));
sEF=angle(I);
%f=abs(I);
M0=256;
N=256; %matrix size
%T=512;

%generate some target points:
target=ones(N);
target(N/2-15,N/2-10:2:N/2+10)=1;
target(N/2+15,N/2-10:2:N/2+10)=1;

phaseF=rand(M0)*2*pi-pi; %initial random phase at target plane

sEF1=(exp(-1i.*phaseF)); %complex field of target points with random phase
figure(6);
sEF1=(mat2gray(abs(sEF1+pi)));
imshow(sEF1);
title('Random Phase');

%Example
%sEF1=rand(256,1);
%sEF=rand(256,1);
%----The code-----
%n=256;

```

```

%out=sEF1;
%out(1:n)=sEF1.*sEF(1:n);

sEF=sEF.*(sEF1);

A0=(nnz(target)/(N*N))*ones(N); %initial constant amplitude distribution
Ad=target; %desired intensity distribution

%sEF=(exp(1i.*phaseF)); %complex field of target points with random phase

%fourier transform the field back to get a starting phase:
sEF=ifftshift(sEF);
sEinF=ifft2(sEF);

f=abs(sEinF);
phase1=angle(sEinF);

phase1=phase1./max(max(phase1));
avg1=mean(mean(abs(phase1)));

figure(7);
phase1=(mat2gray((phase1+pi)));
    %plot the phase as a grayscale image, [0,2pi]

    imshow(phase1)
    title('Phase Image of the Combination');

phaseF1=(N)*2*pi*0;

%sEF1=(exp(1i.*phaseF1));
figure(6);
axis([-1,100,0,1]);
box on
xlabel('Number of iterations','FontSize',16,'Color','k');
title('Modified Gerchberg-Saxton Iterations','FontSize',16,'Color','k');
ylabel('RMSE','FontSize',16,'Color','k')

set(gca,'YTick',[0.0:0.2:1])% TO CHANGE THE Y-AXIS INCREMENT
set(gca,'XTick',[0.0:10:100])
flip(y);
hold on
f1=f;
T=(exp(1i.*phaseF1));

for i=0:10

    %complex field with the uniform amplitude distribution and starting
    %phase:
    I1=f1.*(exp(1i.*phaseF1));

```

```

H=fftshift(fft2(fftshift(I1)));

% rmse=abs(mean(mean((abs(I1)-(f)).^2))).^0.5;

%k=(abs(mean((f).^2))).^0.5;
% rmse=rmse./k;

I2=fftshift(iff2(fftshift(exp(1j.*angle(H)))));

avg2=mean(mean(abs(I2)));
%phase=(phase./avg2).*avg1;
I2=(I2./avg2).*avg1;
%rmse=((mean((conj(phase1)-(I2)).^2)).^0.5;
%rmse=abs(mean(mean((abs(I2)-(f)).^2))).^0.5;
rmse=abs(mean(mean((abs(I2)-f).^2))).^0.5;

plot(i,rmse,'o');
axis('ij');
pause(0.5);
f1=f.*exp(1j*angle(I2));

end

hold off
figure(9);
imshow(I2)
I2=I2-sEF1;
I2=(mat2gray(abs(I2+pi)));
figure(10);
%plot the phase as a grayscale image, [0,2pi]
imshow(I2);
title('Phase Image after Iterations');

imwrite(I2,'C:\Users\A\Desktop\MyImage-13.bmp');
figure(11);
%plot the phase as a grayscale image, [0,2pi]
imshow(I2);
title('Phase Image after Iterations');
% rmse=((mean((abs(phase)-(abs(phase1))).^2))).^0.5;

ii=sqrt(-1);
lambda= 0.633*10^-3; % wavelenght [mm]
%z=3; % distance [mm]
w=3; % width of slit is 2*w [mm]
z=0.5;
%z=w.^2/0.00005*lambda;
x=-6.375:0.025:6.4; % setup spatial axis [mm]
y=x;
freqx=-20:40/512:20-1/512; % setup frequency axis [1/mm]
freqy=freqx;
q=0.9;

```

```

%A=zeros(512);

fft_val=zeros(512);
fft_v=zeros(512);

u0=zeros(512);    % field at z=0
a0=zeros(512);    % angular spectrum at z=0
H=zeros(512);     % transfer function
az=zeros(512);    % angular spectrum at z=z
uz=zeros(512);    % field at z=z

for nx=1:256      % setup transfer function
    for ny=1:256
        H(nx,ny)=exp(ii*2*pi*(z/(lambda*q))*...
            sqrt(1-((lambda*q)*freqx(nx))^2-((lambda*q)*freqy(ny))^2));
    end
end

%for nx=1:512    % setup transfer function
% for ny=1:512
% H(nx,ny)=exp(ii*2*pi*(z/(lambda*q))*...
% sqrt(1-((lambda*q)*freqx(nx))^2-((lambda*q)*freqy(ny))^2));
%end
%end

[nx,ny]=meshgrid(x,y);

I=imread('C:\Users\A\Desktop\MyImage-13.bmp');
I=double(I);
I=imresize(I,[512 512]);
figure(12);
imshow(mat2gray(abs(I)));
title('Phase Image after Iterations');

%radius=50;
%CenterX=257;
%CenterY=257;
%u0=rectangle('position',[CenterX-radius,CenterY-
radius,radius*2,radius*2],'Curvature',[1,1],'FaceColor','r');
%axis square
%plot(x,u0);

%u0(257-w*20:256+w*20,257-w*20:256+w*20)=1;    % setup aperture
%figure(1)
%imagesc(x,x,u0);colormap(gray);

%u0(57-w*20:256+w*20,100-w*20:256+w*20,w,w)=1;    % setup aperture
%fft_v=abs(fft2(A));

```

```

%a0=fftshift(fft_v);

a0=(fftshift(fft2(I)));    % fourier transform
az=a0.*H;    % multiply with transfer function
uz=ifft2(fftshift(az));    % inverse fourier transform
p=uz.*conj(uz);

%p= abs(uz.^2); %obs irrads

figure(13)
plot(x, p(:,256));    % plot of cross-section of intensity at z
xlabel('x'); ylabel('p');
title('Intensity at z');

figure(14)
imagesc(x, x, p);    %diffraction pattern at z
xlabel('x'); ylabel('y'); colormap(gray);
colorbar;
title('Diffraction Pattern at z');
clim=get(gca, 'clim');

levels=255;
target=grayslice(p,linspace(clim(1),clim(2),levels));
map=jet(levels);
imwrite(target,map,'C:\Users\A\Documents\MATLAB\I5.bmp');
I5 = imread('C:\Users\A\Documents\MATLAB\I5.bmp');
I5=fftshift((fftshift(fftshift(I5))));
figure(15);
imshow(I5)

```